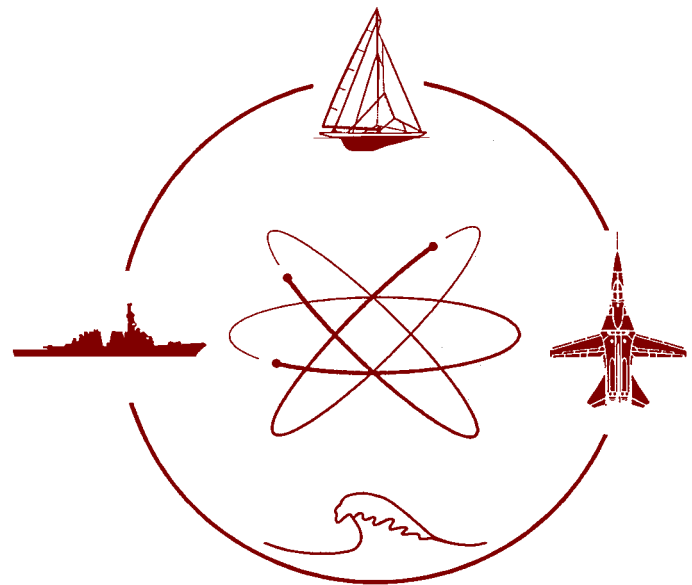


Davidson Laboratory

Marine Hydrodynamics,
Coastal & Ocean Engineering



TECHNICAL REPORT NO. 465

October, 1952

Effect of Forebody-Afterbody Proportions and Length-
Beam Ratio on the Hydrodynamic Characteristics of a
Series of Flying-Boat Models

by

Marvin I. Haar

Prepared For:

Bureau of Aeronautics, Department of the Navy
Under the Sponsorship of the Office of Naval Research

Contract No. N6onr-247

(Davidson Laboratory Project No. CD1046, CD1047,
CD1048)



Castle Point on Hudson,
Hoboken, NJ 07030

declassified by ONR letter dated 5 August 1957

EFFECT OF FOREBODY-AFTERBODY PROPORTIONS
AND LENGTH-BEAM RATIO
ON THE HYDRODYNAMIC CHARACTERISTICS OF
A SERIES OF FLYING-BOAT HULL MODELS

PREPARED FOR THE
BUREAU OF AERONAUTICS
DEPARTMENT OF THE NAVY

UNDER THE SPONSORSHIP OF THE
OFFICE OF NAVAL RESEARCH
CONTRACT NO. N6onr-247
PROJECT NO. NR062-015

REPORT NO. 465

(E.T.T. PROJECT NO. CD1046, CD1047, CD1048)

October 1952

Prepared by: Marvin I. Haar
Marvin I. Haar

Approved by: W.C. Hugli
W.C. Hugli, Jr.

EXPERIMENTAL TOWING TANK
STEVENS INSTITUTE OF TECHNOLOGY
HOBOKEN, NEW JERSEY

TABLE OF CONTENTS

	Page
Summary	1
Introduction	2
Definition of Terms	4
Description of Models	7
Loading Criteria	7
Over-all Design	7
Hull Design	8
Apparatus and Procedure	11
Results	14
General Test Data	14
Comparative Test Data	14
Forebody-Afterbody Load Distribution	14
Discussion	15
General Test Data	15
Length-Beam Ratio Comparisons of Parent Hulls	15
Effect of Forebody-Afterbody Proportions	16
Constant Over-all $K_{3/2}$ Comparison	17
Constant Over-all K_2 Comparison	18
Planing Resistance and Longitudinal Stability	18
Forebody-Afterbody Loading	19
Concluding Remarks	20
References	21
Appendix: Determination of Spray, Load, and Moment Contour Charts ..	23
Table I: Model Dimensions	25
Figures 1 through 44	

SUMMARY

An investigation to determine the influence of forebody-to-afterbody length ratio on the hydrodynamic characteristics of flying-boat hulls with over-all length-beam ratios ranging from 7 to 24 was conducted at the Experimental Towing Tank, Stevens Institute of Technology, Hoboken, New Jersey. Forebody length-beam ratios ranged from 4 to 8 and afterbody length-beam ratios from 3 to 16. Tests were run at load coefficients from 0.90 to 7.50 and with sternpost angles of 6° and 10° . Resistance, trim, spray, and some longitudinal stability data were obtained.

All of the data are presented in collapsed form in summary charts. Contour charts showing the relations between forebody wetted length, load, moment, and trim, and the height of the location of the main spray blister are included and should be of assistance to preliminary design engineers. Comparative data on the effect of length-beam ratio or forebody-afterbody proportions on the hydrodynamic characteristics result in different trends depending upon the loading criterion (constant load, planform area or $length^2 \cdot beam$ product) used.

The constant planform area ($K_{3/2}$) criterion used in the design of the parent hulls indicated an increase in hump resistance as the length-beam ratio (L/b) was increased. The height of the main spray was lowest at the intermediate value of L/b . No consistent effect of forebody-afterbody proportions on hump resistance was indicated. At the higher values of L/b , the hump resistance increased as the afterbody length was increased, while at the lower values of L/b , an optimum forebody-afterbody length ratio was obtained. The shortest afterbody always yielded the lowest spray.

The planing resistance and longitudinal stability characteristics were generally satisfactory.

INTRODUCTION

Although the effect of an over-all increase in length-beam ratio on the hydrodynamic characteristics of flying boats has been fairly well established in current literature (see References 1,2,3), the more detailed relationship of forebody-to-afterbody proportion has not been as fully pursued. Such an investigation, to determine the influence of forebody-to-afterbody length ratio on the hydrodynamic characteristics of flying-boat hulls with over-all length-beam ratios ranging from 7 to 24, was undertaken by the Experimental Towing Tank, Stevens Institute of Technology, Hoboken, New Jersey. This project was part of a research program for the Bureau of Aeronautics, Department of the Navy, and was sponsored by the Office of Naval Research under Task Order III, Contract No. N6onr-247, Section A, Item 1a.

The relationship of forebody-afterbody proportion as determined from tests with a given forebody and afterbodies of varying length, sternpost angle, etc. has been investigated for configurations having relatively low length-beam ratios, below 10 (see References 4 through 7). Although a given forebody-afterbody proportion of a low length-beam ratio hull may be established to give optimum hydrodynamic performance, it does not necessarily follow that if the over-all length-beam ratio is doubled, for instance, the same relative forebody-afterbody proportions will still yield the best possible hydrodynamic performance. As few as five years ago, an over-all length-beam ratio of 9 or 10 was considered high. Since then, length-beam ratio hulls of 20 and 30 have been projected and model tests performed (see References 8 and 9). However, these very high length-beam ratio hulls were usually achieved by taking a good-performing, low length-beam ratio hull and expanding the length (and usually decreasing the beam simultaneously) in a manner that kept the forebody-afterbody proportions constant.

Inasmuch as the forebody and the afterbody each has different functions in the over-all planing process, it is evident that an increase in length-beam ratio could affect the separate functions disproportionately. Consequently, the investigation described herein was undertaken. An effort was made to make the scope of the project as broad as possible. In all, nine different models were tested, each run at two sternpost angles and three loads. The models were divided into three groups -- each group being represented by a particular forebody and three afterbodies. The forebody length-beam ratios varied from 4 to 8, and the afterbody length-beam ratios ranged from 3 to 16.

The test program was run over a wide range of loadings in order to permit comparisons, wherever possible, at constant load, constant load coefficient, constant planform area, and constant length²-beam product. Each model was tested for displacement resistance and main spray. The models exhibiting the best characteristics were then investigated for high-speed planing resistance and longitudinal stability.

An attempt has been made to present the data in a form that will be of maximum benefit to the preliminary design engineer. The dimensions for the over-all length and beam of a projected conventional hull configuration are usually pre-determined by the primary purpose of the design, which includes load, speed, range, etc. The next decision is that of locating the step so that the forebody-afterbody proportions will yield the most satisfactory hydrodynamic characteristics. It is hoped that the charts included herein will, within the limitations imposed by the lines of the models used, aid materially in producing a configuration with good spray, resistance, and stability characteristics.

DEFINITION OF TERMS

The terms and symbols used in this report are defined as follows:

Load coefficient	$C_{\Delta} = \Delta/wb^3$
Forebody load coefficient	$C_{\Delta_f} = \Delta_f/wb^3$
Speed coefficient	$C_V = V/\sqrt{gb}$
Getaway speed coefficient	$C_{V_g} = V_g/\sqrt{gb}$
Resistance coefficient	$C_R = R/wb^3$
Trimming moment coefficient	$C_M = M/wb^4$
Forebody trimming moment coefficient	$C_{M_f} = M_f/wb^4$
Longitudinal spray coefficient	$C_X = X/b$
Vertical spray coefficient	$C_Z = Z/b$
Chine wetted length coefficient	$C_{WL_c} = W.L.(chine)/beam$
Over-all length-beam ratio	L/b
Forebody length-beam ratio	L_f/b
Afterbody length-beam ratio	L_a/b
Aerodynamic pitch damping constant	$M_q/V \frac{\rho}{2} b^4$

where

Δ = load on water, lb.
 Δ_f = forebody load on water, lb.
 w = specific weight of water, lb./ft.³ (62.3 for these tests)
 b = maximum beam of hull at chine, ft.
 V = speed, ft./sec.
 g = acceleration of gravity (32.2 ft./sec.²)
 V_g = getaway speed, ft./sec.
 R = resistance, lb.
 M = trimming moment, lb.ft.
 M_f = forebody trimming moment, lb.ft.
 X = longitudinal position of main spray point of tangency, measured fore (positive) or aft (negative) of the step centroid, ft.
 Z = vertical position of main spray point of tangency, measured from the tangent to the forebody keel at the main step, ft.
 WL_c = length of chine that is wetted, measured forward from step, ft.
 L = over-all length (forebody plus afterbody), ft.
 L_f = forebody length, measured from the intersection of chine and keel to the step centroid along a line parallel to the tangent to the forebody keel at the main step, ft.

L_a = afterbody length, measured along the baseline from the step centroid to the sternpost, ft.
 M_q = aerodynamic tail damping derivative (see APPARATUS AND PROCEDURE for complete definition)
 ρ = mass density of water, lb.sec.²/ft.⁴

Also,

h = step height at the main step keel, % of maximum beam
 γ = local angle of attack at the chine, deg.
 β_f = forebody deadrise at keel and main step, deg.
 σ = sternpost angle, the angle between the tangent to the forebody keel at the main step and a line joining the tip of the step and the sternpost, deg.

Trim (τ) is the angle between the tangent to the forebody keel at the main step and the free water surface.

Moment data are referred to the center of gravity, and water trimming moments which tend to raise the bow are considered positive.

The coordinates of the center of gravity are measured above the tangent to the forebody keel at the main step and forward of a plane perpendicular to the keel and passing through the step centroid.

The following combinations of the coefficients defined above are used:

Planing range

Lift coefficient	$\sqrt{C_\Delta}/C_v$	(Reference 10)
Resistance coefficient	$\sqrt{C_R}/C_v$	(Reference 11)

Displacement range

Speed coefficient	$C_v^2/C_\Delta^{1/3}$	(Reference 11)
Resistance coefficient	$C_R/C_v^2 C_\Delta^{2/3}$	(Reference 11)
Longitudinal spray coefficient	$C_x/C_\Delta^{1/3}$	(Reference 12)
Vertical spray coefficient	C_z/C_Δ	(Reference 12)

The numerical designation of each model (shown on the summary charts) describes the principal hull proportions. Thus, if a chart has the designation

4 - 3 - 1.18 - 22

it means

$$L_f/b = L_a/b = h/\sigma = \beta_f$$

The basis for the above numerical model designation is explained in Reference 13. It has been modified herein by the addition of the L_a/b term.

DESCRIPTION OF MODELS

LOADING CRITERIA

In any investigation involving changes in the size of flying-boat hulls, it is obvious that some kind of criterion for load-carrying ability must be established (Reference 1). It is quite apparent that if the length-beam ratio is increased by holding the beam constant and increasing the length, the higher length-beam ratio hull will be able to carry a greater load than the lower length-beam ratio hull and still maintain, roughly, equivalent hydrodynamic characteristics. In order to set up a suitable size relationship between varying length-beam ratio hulls, the use of a constant length²-beam product (K_2) (Reference 3) and a constant length-beam product or planform area ($K_{3/2}$) (References 1 and 14) has been proposed as a method of achieving hulls with equivalent load-carrying ability.* While no definition or criterion of size is absolute, it is believed that maintaining a constant planform area of the hull minimizes the size effects at least as well as any other criterion. Also, the constant planform area criterion is the more conservative. Consequently, the parent hulls in each group for the current investigation were laid out on the basis of a constant length-beam product. All hulls were placed under a single airplane superstructure.

OVER-ALL DESIGN

As a starting point, a hull having a length-beam ratio of 10, and a beam of 5.50 in. was assigned a gross load coefficient (C_{Δ_0}) of 2.00 and a getaway speed coefficient (C_{Vg}) of 9.00 on the basis of current design practice. These assigned values resulted in a $K_{3/2}$ value of 0.0633, which was left constant for the design loadings of the other parent hulls in the series as shown in Figure 1.

* A brief description of the K factors is herewith presented. The conventional expression for hydrodynamic load coefficient is defined as

$$C_{\Delta} = \Delta/\omega b^3$$

If it is considered that this expression, based only on the beam, is insufficient for a satisfactory representation of the loading, then the inclusion of the hull length can be expressed by an equation of the following type:

$$C_{\Delta} = K(L/b)^n$$

Combining the above equations will yield the expression

$$K = \Delta/\omega L^n b^{3-n}$$

if the following values of n are considered: $0 < n < 3$.

$$\text{For } n = 2, K_2 = \Delta/\omega L^2 b \quad (\text{constant } L^2 b).$$

$$\text{For } n = 3/2, K_{3/2} = \Delta/\omega L^{3/2} b^{3/2} \quad (\text{constant planform area}).$$

The models were divided into three groups, each group consisting of a forebody with three afterbodies of different length:

Group No.	Over-all Length-Beam Ratio, L/b	Forebody Length-Beam Ratio, L_f/b	Afterbody Length-Beam Ratio, L_a/b
I	7.0 - 10.0	4.0	3.0 4.0 6.0
II	10.0 - 16.0	6.0	4.0 6.0 10.0
III	14.0 - 24.0	8.0	6.0 10.0 16.0

As can be seen from the above tabulation, a wide range of over-all length-beam ratios was included together with what was considered to be a satisfactory overlapping of afterbody length-beam ratios in order to make the test program as comprehensive as possible. The pertinent dimensions of each model are given in Table I, and the lines are shown in Figures 2 through 4.

In each group, the hull with the intermediate afterbody length was designated the "parent" of the group, with the long and short afterbody considered as modifications of the parent.

HULL DESIGN

A detailed description of the hull design of the models in Group I is presented in Reference 15. A similar procedure was used for the design of the models in Groups II and III. Briefly, an attempt was made, insofar as possible, to design these hulls analytically. The available planing surface data plus the results of previous model tests on flying-boat hulls were used as much as possible. For example, on the basis of previous experience, values of hump speed, hump trim, and load on the water at hump speed were established for the "parent" of each group. With the aid of available empirical planing surface relationships (References 16 through 19), the estimated forebody wetted length, center of pressure, and hydrodynamic pitching moment were obtained. The use of forebody wake profile data made it possible to determine the center of pressure of the afterbody, and by trial and error, the afterbody moment required to balance the hydrodynamic moment on the forebody was obtained by varying the sternpost angle. Reference 15 is included as an addendum.

In order to simplify the scaling of the hull lines, they were laid out from readily computable curves, with minor variations being made wherever necessary. The "forebody flat" region (linear increase in deadrise with forebody

length) immediately forward of the step ranged from $1\frac{1}{2}$ beams on the shortest forebody to almost $2\frac{1}{2}$ beams on the longest forebody. The length of the forebody flat was a compromise between a length long enough to provide adequate planing area at the hump, and short enough to permit easy fairing of the buttock lines. The deadrise increased from 22° at the step to $26\frac{1}{2}^\circ$ at the forward end of the forebody flat. An approximately elliptical keel curvature was used forward of the forebody flat, with the variation of deadrise in this region varying parabolically to a maximum of 70° at the bow. Care was taken at the bow sections to keep the local angles of attack (γ) at the chine below 16° in order to permit easy entry into head waves and to control the bow spray.

Although the afterbody is required for static buoyancy and trim control at low speeds, excessive afterbody area at high speeds results in excessive resistance from the impingement of the forebody spray jet. Consequently, the afterbodies were warped from a deadrise of approximately 26° at the step to a maximum of 45° at the midpoint, and back to 22° at the sternpost. The high afterbody deadrise was incorporated also to reduce the impact loads in rough water. The deadrise at the sternpost was reduced in order to provide a more effective planing surface for low-speed trim control.

A 50° Vee-planform step was used on all models so that the junction of the forebody, with lower deadrise, and the afterbody, with higher deadrise, could be made without obtaining an excessive step depth at the chines. The depth of the step at the keel was 6% of the beam. This step depth, in conjunction with a warped afterbody, was considered adequate for satisfactory high-speed resistance characteristics and landing stability.

The beam dimensions for the three parent hulls were determined, in part, as a result of compromises between the hull length and weight of the extreme (highest and lowest) length-beam ratio configurations. Since the hulls were designed on the basis of a constant $L \times b$, it was obvious that the beam dimension would have to vary. The variation was, in a sense, dependent upon the maximum beam that could be handled conveniently in the E.T.T. apparatus and the minimum beam at which no appreciable scale effect would be introduced. The beams for the three parent hulls ($L_f/b = 4, 6, \text{ and } 8$) were 6.15, 5.02, and 4.10 in., respectively.

It had been felt at the E.T.T. and by other researchers that tests with models having a beam substantially less than 6 in. would result in water

adhering to the sides of the model at low planing speeds. The consequent increase in the resistance and spray height would thereby produce errors when scaled up to full-size. In order to prevent any scale effect due to side wetting on the small-beam models used in this investigation, metal-relieved chines were incorporated into the models. The metal edges were inlaid into the planing surface bottom at the chine, so as to yield a sharp discontinuity. The hull side was indented immediately above the chine edge to prevent any water from clinging to the sides.

APPARATUS AND PROCEDURE

The tests were conducted in Tank No. 3 of the Experimental Towing Tank (Reference 20), using the regular seaplane apparatus. All tests were run in smooth water at constant speeds.

In the planing speed range, the models were unloaded according to the parabolic unloading curves shown in Figure 5. These curves were based on a gross load coefficient (C_{Δ_0}) which was varied from model to model on the basis of constant planform area ($K_{3/2}$) (Figure 1).

In the displacement speed range, constant loadings were chosen in a manner to bracket the unloading curve for the respective model. These loadings varied about the C_{Δ_0} value shown in the unloading curves in such a manner as to permit comparison of the data on the basis of various loading criteria: constant load (Δ_0), constant load coefficient (C_{Δ_0}), constant planform area ($K_{3/2}$), and constant length²-beam product (K_2).

Displacement resistance and main spray data were obtained on all of the configurations in the series. These tests were run free-to-trim. The resistance investigation was made with an 0.040-in. diameter strut towed ahead of the model to induce turbulence in the model boundary layer. The resistance data presented herein include the air drag of the model, but do not include the air drag of the apparatus. The main spray characteristics were analyzed from records of the dimensions of the main spray blister obtained from three-view photographs. A camera mounted above the model simultaneously recorded the top view and side views of the spray blister with the aid of mirrors. This photographic technique is described in detail in Reference 21.

The following loading schedule was used for the displacement resistance and main spray tests:

Group No.	Model No.	L_f/b	L_a/b	C_{Δ}				
I	1067-02	4	3	0.90	1.20			
	1067-01	4	4	0.90		1.50		
	1067-03	4	6	0.90		1.50	2.00	
II	1068-02	6	4		1.50	2.00		
	1068-01	6	6		2.00	2.50	3.00	
	1068-03	6	10		2.00		3.00	4.00
III	1069-02	8	6			3.00	4.00	5.00
	1069-01	8	10			4.00	5.00	6.00
	1069-03	8	16			5.00	6.00	7.50

Tests at each of the above loadings were made at two sternpost angles, 6° and 10°, and two moment conditions: zero moment and a constant bow-down (thrust) moment of 20.6 in.-lb. Inasmuch as the beam decreased with increase in length-beam ratio from Group I to Group III, the pitching moment coefficient (C_M) value increased accordingly from +0.4 to +0.9 to +2.0. It is obvious from this test schedule that a prohibitive number of photographs would be required for a complete main spray analysis. Consequently, the number of photographs was reduced appreciably by the method outlined in the APPENDIX.

With respect to the loading criteria ($K_{3/2}$ and K_2) mentioned above, it should be pointed out, for example, that approximately equivalent hydrodynamic characteristics would be expected of model 1067-02 at a C_Δ of 1.20 and model 1069-03 at a C_Δ of 7.50 on the basis of a constant $K_{3/2}$. Similarly, if a constant K_2 criterion is used, model 1067-02 at a C_Δ of 0.90 should have comparable hydrodynamic characteristics with model 1069-01 at a C_Δ of 6.00.

The high-speed planing resistance and the longitudinal stability (porpoising) characteristics were obtained on the four configurations which were found to have the most desirable displacement resistance and spray characteristics: models 1067-03-10, 1068-02-06, 1068-03-10, and 1069-02-06, where the last two digits indicate the sternpost angle (summary chart designations 4-6-0.71-22, 6-4-1.33-22, 6-10-0.80-22, and 8-6-1.12-22, respectively).

The resistance in the planing speed range was determined at speed intervals from hump speed to getaway at loads bracketing the unloading curve so that data could be obtained over a complete range of values of the coefficient ratio $\sqrt{C_\Delta}/C_V$. At each load-speed combination, the resistance was measured at various fixed trim angles in order to determine the "best trim."

Longitudinal stability was determined by means of the specific porpoising apparatus described in Reference 22. For the present general tests, the hydrofoil, which supplies the lift force and its derivatives in specific tests, was removed from the apparatus. The porpoising limits were obtained by applying moments at the load-speed combinations described above for the planing resistance. A calibrated dashpot provided for the aerodynamic tail damping rate in pitch (M_q) which was determined from the following equation:

$$M_q = 1.43 \times 10^{-2} V_m \text{ lb.ft.sec./radian}$$

A definition of the aerodynamic derivatives, together with a method for obtaining the required constants, is presented in Reference 10.

RESULTS

GENERAL TEST DATA

All of the data obtained on each configuration are presented in the collapsed form of one-sheet summary charts shown in Figures 6 through 23. Each summary chart is divided into three sections. The top shows the model body plans and main spray data. In the center section, the free-to-trim and resistance data are given for the displacement speed range, and in the bottom section are shown the resistance data for the planing range and longitudinal stability limits.

The spray data are plotted in the form of nondimensional coefficients describing the spray blister envelope in accordance with the method presented in Reference 12. Displacement speed resistance and trim data are plotted in the form of $C_R/C_v^2 C_\Delta^{2/3}$ and τ against $C_v^2/C_\Delta^{1/3}$. The resistance data in the planing speed range are presented in the form of $\sqrt{C_R}/C_v$ contours plotted on a grid of τ vs. $\sqrt{C_\Delta}/C_v$. These contours show the variation with τ when $\sqrt{C_\Delta}/C_v$ is fixed, as well as the values of τ and $\sqrt{C_R}/C_v$ for minimum resistance at a particular value of $\sqrt{C_\Delta}/C_v$. The upper and lower trim limits of longitudinal stability are superimposed on the resistance contours.

COMPARATIVE TEST DATA

The effect of length-beam ratio on the resistance, trim, and spray is shown in Figures 24 through 34 for the various loading criteria.

FOREBODY-AFTERBODY LOAD DISTRIBUTION

The proportion of the total load sustained by the forebody in the displacement speed range is shown in Figures 35 through 37. These charts were obtained from the data presented in Figures 38 through 43, by the method outlined in the APPENDIX.

DISCUSSION

GENERAL TEST DATA

The general test data have been presented in the form of summary charts so as to permit direct comparison with previous E.T.T. data which were presented similarly. It will be noted that the displacement resistance has been plotted in the form of $C_R/C_V^2 C_\Delta^{2/3}$ vs. $C_V^2/C_\Delta^{1/3}$. These combinations of coefficients were originally conceived as a method for eliminating the load parameter from the resistance curves. Although previous tests have indicated that these coefficients do collapse the resistance curves, it was found that the resistance data obtained during the present investigation did not collapse very well for all modifications (e.g., model 1068-02-10, Figure 13). However, on some configurations (model 1068-03-06, Figure 16), the resistance curves collapsed perfectly with load. Observation of the data does not indicate any clear-cut trend with respect to the effect of length-beam ratio, afterbody length, and sternpost angle on the collapsing of the resistance data. In general, the shorter forebody group (1067) does not collapse as well as the other two forebody groups (1068 and 1069).

LENGTH-BEAM RATIO COMPARISONS OF PARENT HULLS

Inasmuch as the hull series used in this investigation was designed on the assumption that constant planform area ($K_{3/2}$) would yield equivalent hydrodynamic characteristics, the major comparisons have been made on the basis of a constant $K_{3/2}$. The constant $K_{3/2}$ value of 0.0633 used in the design of the hulls holds true for only the parent model of each group. Thus, on the basis of this criterion, and using the appropriate loading obtained from Figure 1, the effect of length-beam ratio can be determined by comparing the hydrodynamic characteristics of the three parent hulls. By maintaining this load constant within each group, the effect of afterbody length can be obtained. These effects can then be compared for the three groups and the trends noted. It is believed that this type of analysis is the most desirable for the series investigated herein.

The hump resistance, height of the tangent to the main spray blister at the estimated propeller disc location, and hump trim are shown in Figures 24, 25, and 26, respectively. These data are presented for two sternpost angles, 6° and 10° , and the parent hulls for each group are indicated. The

parent hulls, designed on the basis of a constant $K_{3/2}$, are compared for the corresponding constant load value which yields a $K_{3/2} = 0.0633$. Each hull therefore has the same load per unit planform area. Since the forebody-afterbody proportions of the three parents are the same (except for a slight variation in the longest forebody group), the forebody-afterbody loading should also be the same.

It can be seen that, despite the use of the constant $K_{3/2}$ criterion, there is an increase in the hump resistance as the length-beam ratio is increased from parent to parent. The hump trims for parents I and II are essentially the same, while the hump trims for parent III are approximately 2° lower. The forebody-afterbody ratio for parent III is slightly lower than for the other parents. The longer afterbody would expectedly produce a lower trim.

The C_v at which the hump trim occurred is shown in Figure 27. The scatter of the data is such that a single curve represents the over-all trend of linearly increasing C_v with increasing L/b . No attempt was made to isolate any effects within each L/b group.

Figure 25 indicates that the height of the main spray is lower at the intermediate L/b 's than at the extremes. The spray height (Z) is somewhat lower for parent II than for either parent I or III. Parent III spray is slightly higher than the parent I spray. No consistent effect of sternpost angle is indicated at the lower L/b 's. A plot of the spray height coefficient (C_z) vs. L/b shows exactly the same trends (Figure 28).

The effect of length-beam ratio on the speed when spray enters the propellers is shown in Figure 29, and, in general, indicates the same trend as the effect of L/b on hump speed (Figure 27).

EFFECT OF FOREBODY-AFTERBODY PROPORTIONS

Reference to the plots just mentioned reveals the effect of varying the afterbody length for each of the three groups of forebodies on the resistance, trim, and spray. In Group I, the hump resistance for a constant sternpost angle is a minimum when $L_f/b:L_a/b = 4:4$ (Figure 24), while in Group II, the hump resistance remains approximately constant as $L_f/b:L_a/b$ is varied from 6:4 to 6:10. Group III shows a definite increase in hump resistance as the afterbody length is increased. As is known, the hump trim decreases as the afterbody length is increased (Figure 26). In

all three groups, the higher sternpost angle produces higher resistances. It is highly probable that in the consideration of any design calling for an afterbody of increased length, the sternpost angle would be increased simultaneously in order to provide less afterbody interference for planing resistance and longitudinal stability.

All three groups indicate an identical trend with respect to the height of the main spray. Figure 25 shows that the shortest afterbody always yields the lowest spray. However, there is a small increase in spray height as the afterbody length is increased beyond that of each parent.

CONSTANT OVER-ALL $K_{3/2}$ COMPARISON

It was pointed out before that only the parent hulls were designed on the basis of a constant $K_{3/2}$ (planform area). Therefore the hydrodynamic characteristics of the parent configurations were previously compared for a constant load. The other models in each group, although not designed to the constant $K_{3/2}$ value of 0.0633, can be compared on the basis of a constant $K_{3/2}$ by a proper adjustment of the test loadings. A plot of this nature for the hump resistance is shown in Figure 30 at a $K_{3/2} = 0.05$. This value was chosen because it provides a maximum overlapping of the loads actually tested. Caution must be exercised in any conclusions obtained from this chart. For example, these contours indicate that, at an over-all length-beam ratio of 10, the model having an $L_f:L_a$ of 6:4 (1068-02) has approximately 50% of the resistance of the model having an $L_f:L_a$ of 4:6 (1067-03). However, at $K_{3/2} = 0.05$, the actual load on the water for model 1067-03 was approximately twice the load for model 1068-02.

Since only the parent configurations were actually designed to a constant $K_{3/2}$ criterion, the forebody-afterbody load distribution of models other than the parents is not constant (see Figures 35 through 37). In the displacement speed range, the forebody carries a major portion of the load. Consequently, any changes in the relative forebody-afterbody loading would invalidate the basic assumption of the constant $K_{3/2}$ criterion: constant load per unit planform area. It is interesting to note that these same data converted to resistance coefficient (C_R) and plotted against length-beam ratio for an over-all constant $K_{3/2}$ indicate an exponential relationship (Figure 31).

The plot of hump trim vs. L/b in Figure 32 shows an approximate linear variation in hump trim with change in length-beam ratio. A comparison of

this plot with Figure 26 also indicates the effect of the different loading criteria.

The actual height of the tangent to the main spray blister at the estimated propeller disc location is shown in Figure 33 for a constant over-all value of $K_{3/2}$. The pattern of this plot is almost exactly comparable to that of Figure 30 for the hump resistance. Again, it should be pointed out that while at a given value of L/b there appears to be an appreciable difference in the height of the main spray blister depending upon the relative forebody-afterbody length-beam ratios, the actual loads on the water were different when compared on this $K_{3/2}$ criterion.

CONSTANT OVER-ALL K_2 COMPARISON

The constant K_2 criterion has also been proposed as a method for obtaining equivalent hydrodynamic characteristics regardless of length-beam ratio. This criterion maintains a constant L^2b , thus emphasizing the effect of length as compared with the constant planform area criterion of $K_{3/2}$. Although no plots are shown herein for a constant K_2 , analysis of the data will indicate exactly the same trends and order of magnitude variation as were shown in the previous section for the constant over-all $K_{3/2}$ comparison.

PLANING RESISTANCE AND LONGITUDINAL STABILITY

Fixed-trim planing resistance and trim limits of stability were obtained on four configurations -- 1067-03-10, 1068-02-06, 1068-03-10, and 1069-02-06 (Figures 11, 12, 17, and 18, respectively) -- ranging in length-beam ratio from 10 to 16. These modifications were thought to be the most representative of the series. Models 1068-02-06 ($L_f:L_a = 6:4$) and 1069-02-06 ($L_f:L_a = 8:6$) were chosen because, within their respective groups, they have the most satisfactory displacement resistance and main spray characteristics. Model 1068-03-10 ($L_f:L_a = 6:10$) is the most satisfactory of the long afterbody configurations, while model 1067-03-10 ($L_f:L_a = 4:6$) combined with model 1068-02-06 ($L_f:L_a = 6:4$) offers a comparison of the effects of forebody-afterbody proportions (Figures 11 and 12). A comparison of models 1068-02-06 and 1068-03-10 (Figures 12 and 17) indicates the effect of afterbody length for a given forebody length.

In general, the resistance contours are approximately the same for all the models, but at high speeds (low values of $\sqrt{C_\Delta}/C_v$), some variation will

be noted. A comparative plot of C_R/C_Δ vs. $\sqrt{C_\Delta}/C_V$ is shown in Figure 34 for the free-to-trim (zero moment) resistance and the resistance at best trim. No consistent effect of length-beam ratio on the planing resistance is evident, especially at the higher speeds.

An attempt to compare the trim limits of the four models does not indicate any definite trends with respect to the effect of length-beam ratio. As would be expected for all forebodies having the same angles of deadrise, the lower limit of stability is essentially the same for all the models. Those configurations that have a short afterbody result in a lower limit with a high hump at the low-speed end. Consequently, the free-to-trim curve cuts through the lower limit. Those configurations with a long afterbody (and high sternpost angle) yield a free-to-trim curve that is in the neighborhood of the upper trim limit at high speeds. In the design of any long afterbody configuration, care must be exercised to include adequate warping and sternpost angle to eliminate any possible interference instability that might result in suction due to entrained air under the afterbody. The spread between the upper and lower limits appears satisfactory except for model 1067-03-10 (Figure 11), in which the upper limit hooks down sharply at high speeds.

FOREBODY-AFTERBODY LOADING

While no definite effects of length-beam ratio on the forebody load can be deduced from the data shown in Figures 35 through 37, the forebody appears to carry between 80% and 95% of the gross load at hump speed (maximum resistance). As would be expected, the high percentages of forebody load are those resulting from the lowest gross load tested for a particular configuration. The modifications that fall noticeably outside of the percentage range mentioned above are those with the longest afterbody and low sternpost angle. Models 1067-03-06, 1068-03-06, and 1069-03-06, at their respective heavy test loads have between 60% and 65% of the gross load supported by the forebody.

CONCLUDING REMARKS

The length-beam ratio data presented herein are wide in scope: over-all length-beam ratios ranging from 7 to 24, forebody length-beam ratios ranging from 4 to 8, afterbody length-beam ratios ranging from 3 to 16, and load coefficients from 0.90 to 7.50. The effect of length-beam ratio and forebody-afterbody proportions on the hydrodynamic characteristics varied to some degree depending upon the loading criterion used.

A comparison of the parent hulls on the basis of the constant plan-form area ($K_{3/2} = 0.0633$) hull design criterion indicated that as the length-beam ratio was increased from 8 to 18, the hump resistance increased slightly, the hump trim decreased at the highest L/b , and the height of the main spray was a minimum at the intermediate L/b .

Use of the same $K_{3/2}$ value of 0.0633 did not indicate a consistent trend on the resistance for the relation of afterbody to forebody proportions as the over-all length-beam ratio was increased. At the high length-beam ratios, the hump resistance increased with an increase in afterbody length, while at the low length-beam ratios, an optimum value of forebody-to-afterbody length was obtained. The height of the main spray was always lowest for the shortest-afterbody configuration.

All of the data obtained during the investigation are presented in collapsed form in the summary charts. Since the lines of the models used conform to those in current use, the contour charts showing the relation between forebody wetted length, load, moment, trim, and height and location of the main spray blister should be of use to the primary designer.

REFERENCES

1. Davidson, K.S.M. and Locke, F.W.S., Jr. *General Tank Tests on the Hydrodynamic Characteristics of Four Flying-Boat Hull Models of Differing Length-Beam Ratios.* NACA ARR No. 4F15, June 1944.
2. Carter, Arthur W. and Haar, Marvin I. *Hydrodynamic Qualities of a Hypothetical Flying Boat with a Low-Drag Hull Having a Length-Beam Ratio of 15.* NACA TN No. 1570, April 1948.
3. Parkinson, John B. *Design Criterions for the Dimensions of the Forebody of a Long-Range Flying Boat.* NACA ARR No. 3K08, November 1943.
4. Hugli, W.C., Jr.; Strümpf, Albert; and Axt, W.C. *An Investigation of the Effects of Hull Proportion and Step Depth on the Hydrodynamic Characteristics of Flying-Boat Hull Models with Varying Length-Beam Ratios.* E.T.T. Report No. 312, February 1947.
5. Haar, Marvin I. *Tank Tests of a 1/10-Size Model of a Hypothetical Flying Boat with a Hull Length-Beam Ratio of 9.0.* NACA TN No. 1648, July 1948.
6. Olson, Roland E. and Land, Norman S. *Effect of Afterbody Length and Keel Angle on Minimum Depth of Step for Landing Stability and on Take-Off Stability of a Flying Boat.* NACA TN No. 1571, September 1948.
7. Schnaubelt, F.J. and Hopkins, R.M. *The Effect of Varying Hull Proportion, Step Depth, and Length-Beam Ratio on the Hydrodynamic Characteristics of Flying Boat Hull Models.* CVAC Report No. ZH-032, August 1946.
8. Riebe, John M. *Aerodynamic Characteristics of Flying-Boat Hulls Having Length-Beam Ratios of 20 and 30.* NACA RM No. L8H11, November 10, 1948.
9. Carter, Arthur W. and Whitaker, Walter E., Jr. *Effect of Increase in Hull Length-Beam Ratio from 15 to 20 on the Hydrodynamic Characteristics of Flying Boats.* NACA RM No. L9G05, August 24, 1949.
10. Locke, F.W.S., Jr. *General Porpoising Tests of Flying-Boat Hull Models.* NACA ARR No. 3I17, December 1942.
11. Locke, F.W.S., Jr. *General Resistance Tests on Flying-Boat Hull Models.* NACA ARR No. 4B19, February 1944.
12. Locke, F.W.S., Jr. *General Main Spray Tests of Flying-Boat Models in the Displacement Range.* NACA ARR No. 5A02, March 1944.

13. Locke, F.W.S., Jr. *A Collection of the Collapsed Results of General Tank Tests of Miscellaneous Flying-Boat Hull Models.* NACA TN No. 1182, March 1947.
14. Davidson, K.S.M. *Notes on Flying Boat Landings.* E.T.T. Note No. 5, May 1, 1944.
15. Hugli, W.C., Jr. *Description of the Lines of the Proposed Flying-Boat Hull Models with Forebody Length-Beam Ratio of 4.0.* E.T.T. Note No. 90, October 1948.
16. Korvin-Kroukovsky, B.V.; Savitsky, Daniel; and Lehman, William F. *Wetted Area and Center of Pressure of Planing Surfaces.* E.T.T. Report No. 360, August 1949. Sherman M. Fairchild Publication Fund Paper No. 244, Institute of the Aeronautical Sciences, New York.
17. Siler, William. *Lift and Moment of Flat Rectangular Low Aspect Ratio Lifting Surfaces.* A Thesis submitted in partial fulfillment of the requirements for the Degree of Master of Science, Stevens Institute of Technology, 1949.
18. Locke, F.W.S., Jr. *Tests of a Flat Bottom Planing Surface to Determine the Inception of Planing.* Navy Department, Bureau of Aeronautics, Research Division DR Report No. 1096, December 1948.
19. Locke, F.W.S., Jr. *An Empirical Study of Low Aspect Ratio Lifting Surfaces with Particular Regard to Planing Craft.* Navy Department, Bureau of Aeronautics, Research Division DR Report No. 1043, January 1948.
20. Fried, W. *The No. 3 Tank for Model Seaplane Tests.* E.T.T. Report No. 289, October 1945.
21. Locke, F.W.S., Jr. and Bott, H.L. *A Method for Making Quantitative Studies of the Main Spray Characteristics of Flying-Boat Hull Models.* NACA ARR No. 3K11, June 1943.
22. Davidson, K.S.M. and Locke, F.W.S., Jr. *Some Systematic Model Experiments on the Porpoising Characteristics of Flying Boat Hulls.* NACA ARR No. 3F12, June 1943.

APPENDIX

DETERMINATION OF SPRAY, LOAD, AND MOMENT CONTOUR CHARTS

The method of obtaining the spray curves shown in the usual coefficient form on the summary charts (Figures 6 through 23) was a departure from the standard procedure used at the E.T.T., wherein spray photographs are normally taken for each complete configuration. The number of spray photographs required for the eighteen modifications plus numerous loading and moment conditions of this investigation was considered prohibitive. It was therefore assumed that the main spray pattern of a flying-boat configuration could be uniquely determined by the speed, trim angle, and wetted length of the forebody alone. Spray photographs could then be taken of merely the three different forebodies over the pre-determined range of parameters obtained from the various afterbody configurations and loading conditions.

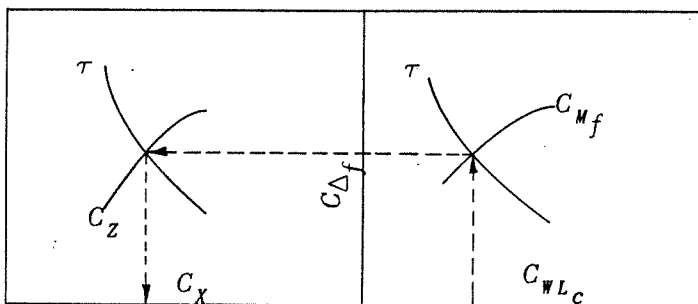
To outline the scope of testing necessary to cover all possible combinations of trim angle and forebody wetting that might be encountered during a test of a complete model, a preliminary investigation was conducted in which the forebody of each group was tested in combination with the shortest afterbody at 10° sternpost angle and the longest afterbody at 6° sternpost angle, at appropriate loading conditions. The forebody chine wetted lengths and trim angles measured during these tests supplied the limits required for the tests of the three forebodies alone.

Spray photographs were then taken of each of the three forebodies (without any afterbody attached) at regular speed intervals throughout the displacement range and at sufficient loads and moments to fill the requirements of the preliminary tests described above. From these photographs, C_x and C_z dimensions of the spray blister and the distance along the forebody chine wet by spray (C_{wLc}) were measured and trim angle was read from the trim scale on the model. The nose-down moment has been recorded on the data sheets. At each speed, individual charts of C_w vs. τ , C_x vs. τ , C_z vs. τ , and C_{wLc} vs. τ were plotted at constant forebody load. The curves from these charts were cross-plotted in order to construct the contour charts on Figures 38 through 43. These charts, in addition to providing spray locations, supply the means of determining the load and moment on the forebody.

Each complete model was subsequently tested for free-to-trim resistance according to the standard test schedule. The program for these tests

stipulated that the speeds match those used when testing the forebody alone and that, in addition to the usual trim angle and drag measurements, a record should be made of the forebody chine wetted length (C_{WLc}) at each run. This information -- speed, trim angle, and C_{WLc} -- is needed to use the contour charts.

The technique involved in using these charts is as follows:



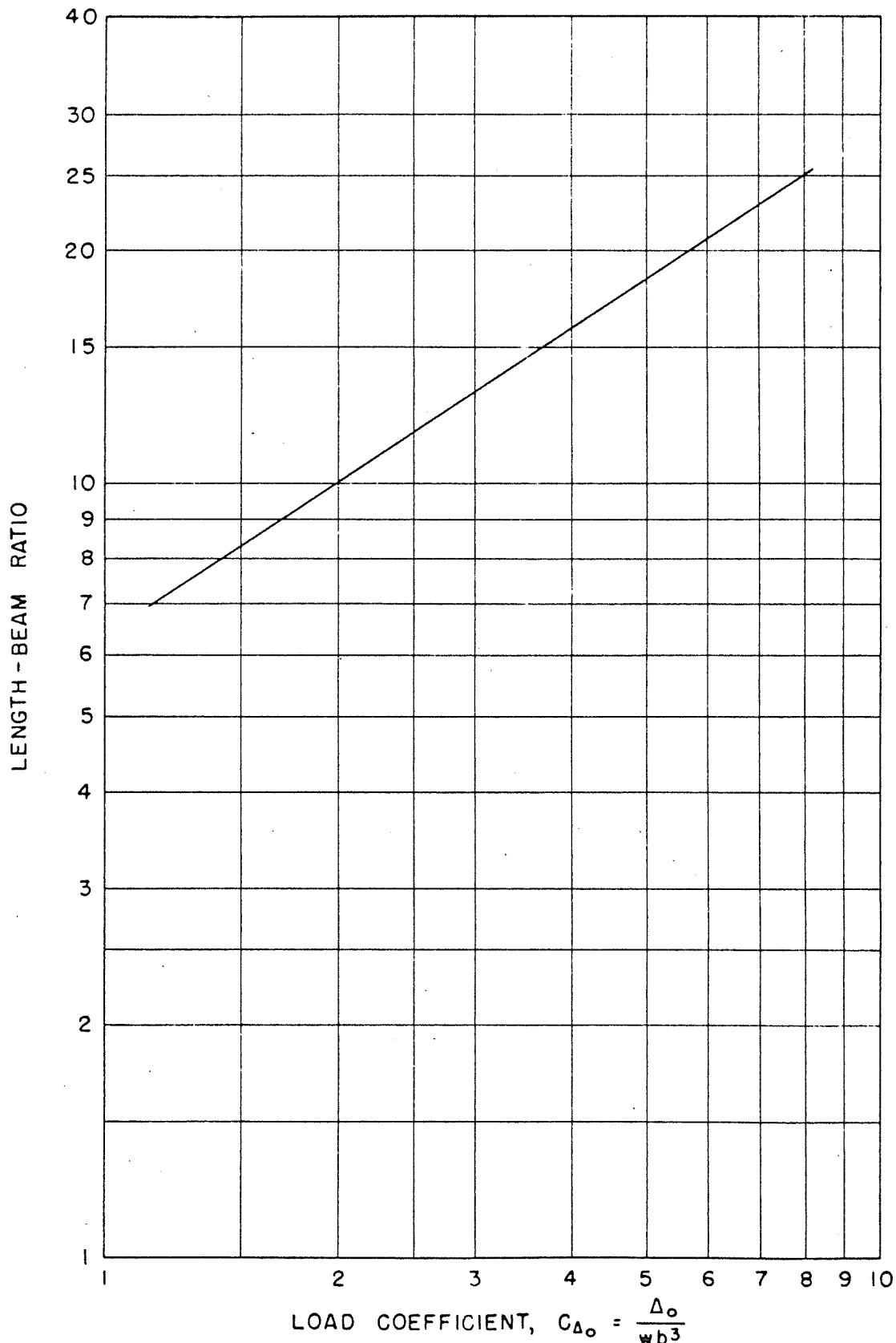
1. Select the contour chart for the desired speed.
2. Enter the base scale of the right-hand section of the chart with the value of C_{WLc} obtained during the free-to-trim resistance test. The intersection of this C_{WLc} value and the corresponding trim angle provides the point from which to read the $C_{\Delta f}$ on the forebody from the ordinate scale and the C_{Mf} on the forebody from the contour curves of forebody moment.
3. Move to the left section of the chart along the specified line of $C_{\Delta f}$ until it intersects the desired trim curve. This intersection provides the spray locations C_x from the abscissa and C_z from the contour curves.

As a check on the spray measurements read from the contour charts, two complete models were tested and spray photographs taken. These were analyzed in the usual manner and found to be in good agreement with the predicted curves (Figure 44).

TABLE I
MODEL DIMENSIONS

		1067-02	1067-01	1067-03	1068-02	1068-01	1068-03	1069-02	1069-01	1069-03	Model No.
Forebody Designation	short	short	short	medium	medium	medium	medium	long	long	long	
Afterbody Designation	short	medium	long	short	medium	medium	long	short	medium	medium	
Overall Length-Beam Ratio	7.0	8.0	10.0	10.0	12.0	16.0	14.0	18.0	18.0	24.0	
Beam, Maximum, in.	6.15	6.15	6.15	5.02	5.02	5.02	4.10	4.10	4.10	4.10	
Forebody Length-Beam Ratio	4.0	4.0	4.0	6.0	6.0	6.0	8.0	8.0	8.0	8.0	
Forebody Length (to Step Centroid), in.	24.60	24.60	24.60	30.12	30.12	30.12	32.80	32.80	32.80	32.80	
Afterbody Length-Beam Ratio	3.0	4.0	6.0	4.0	6.0	10.0	6.0	10.0	10.0	16.0	
Afterbody Length (from Step Centroid), in.	18.45	24.60	36.90	20.08	30.12	50.20	24.60	41.00	41.00	65.60	
Step Depth (at Keel), in.	0.37	0.37	0.37	0.30	0.30	0.30	0.25	0.25	0.25	0.25	
Distance from Step Centroid to Step Apex, in.	2.43	2.43	2.43	2.00	2.00	2.00	1.63	1.63	1.63	1.63	

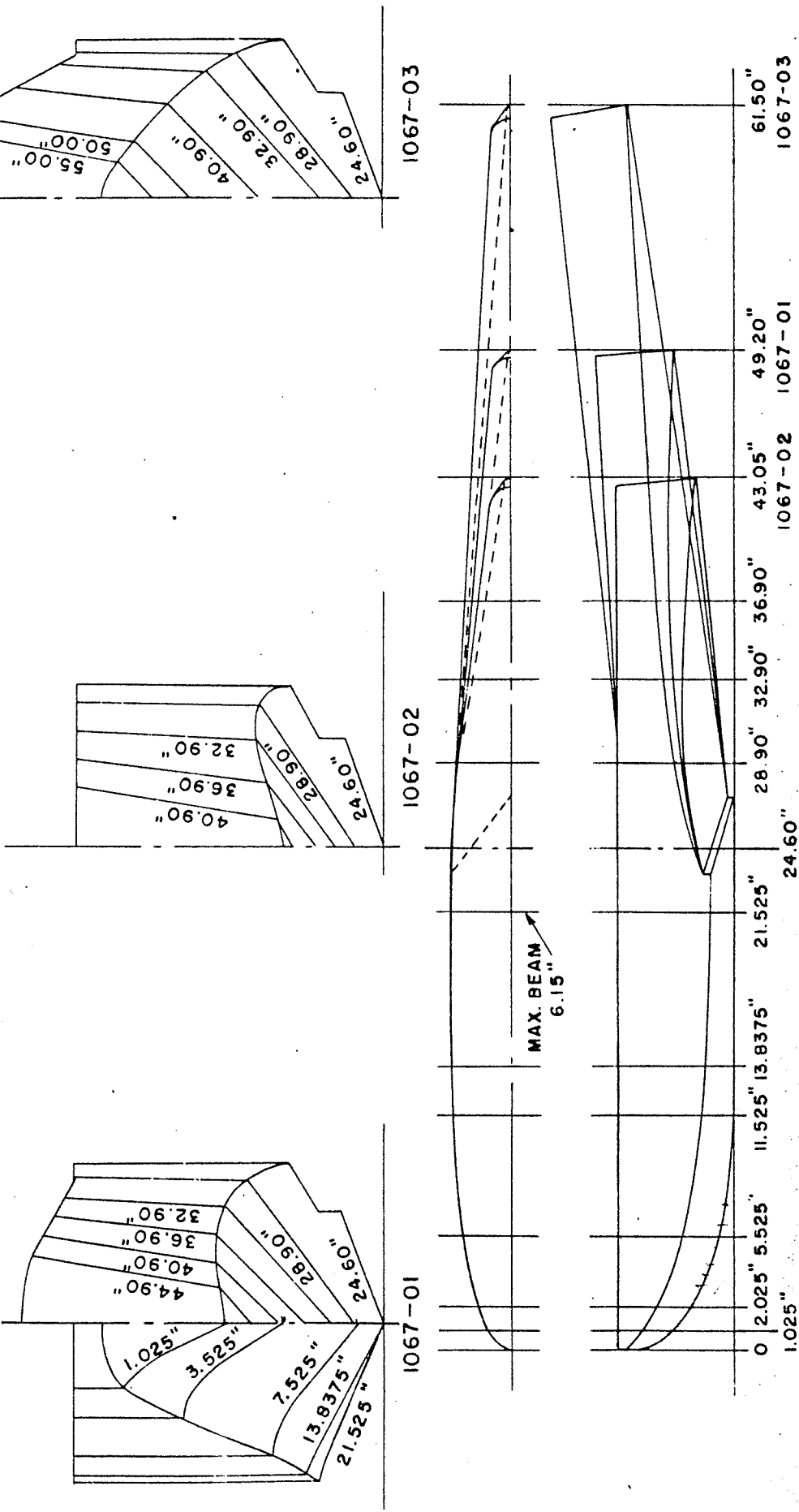
LENGTH-BEAM RATIO VS. LOAD COEFFICIENT
FOR $K_{3/2} = .0633$



HULL MODELS

GROUP I MAX. BEAM = 6.15" ; $L_f / b = 4$

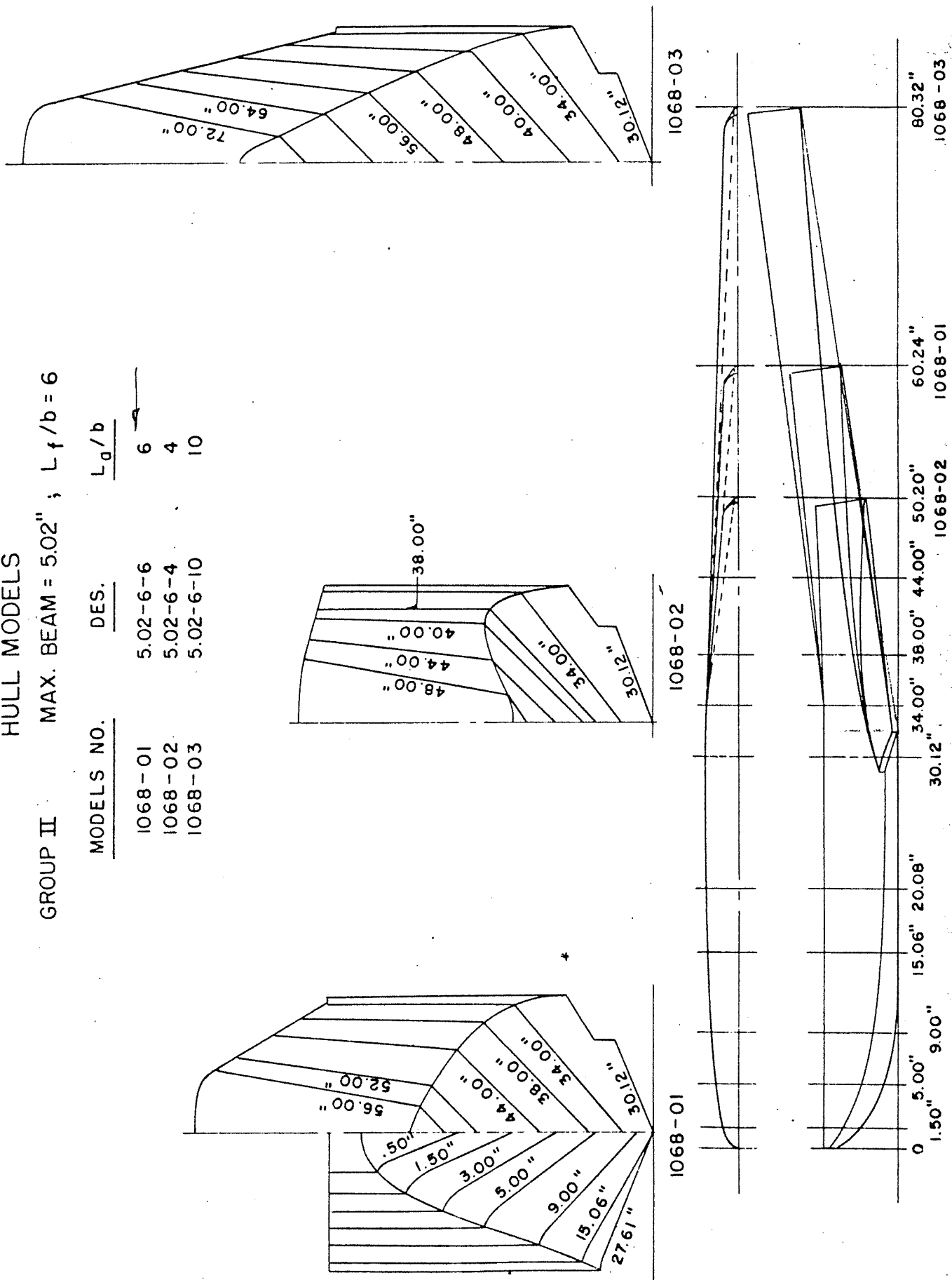
MODELS NO.	DES.	L_d / b
1067-01	6.15-4-4	4
1067-02	6.15-4-3	3
1067-03	6.15-4-6	6



HULL MODELS

GROUP II MAX. BEAM = 5.02" ; $L_f/b = 6$

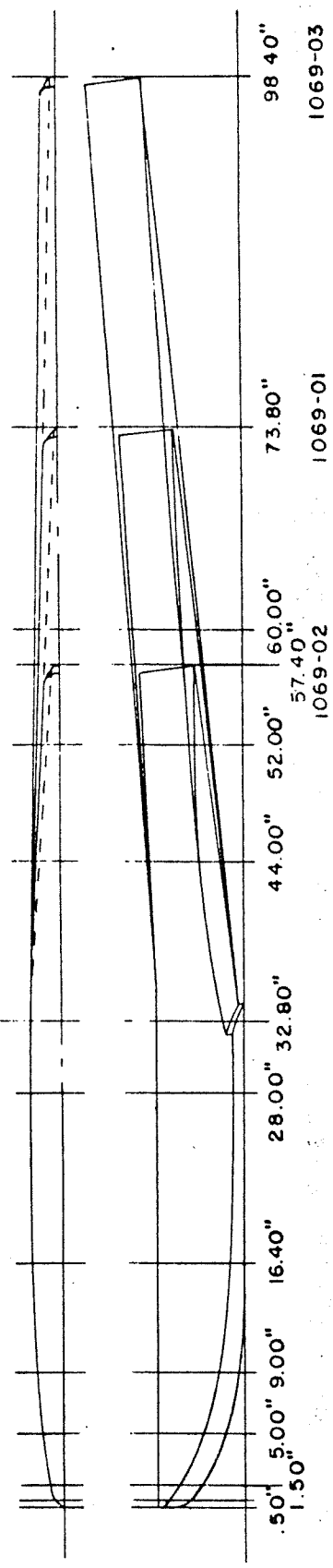
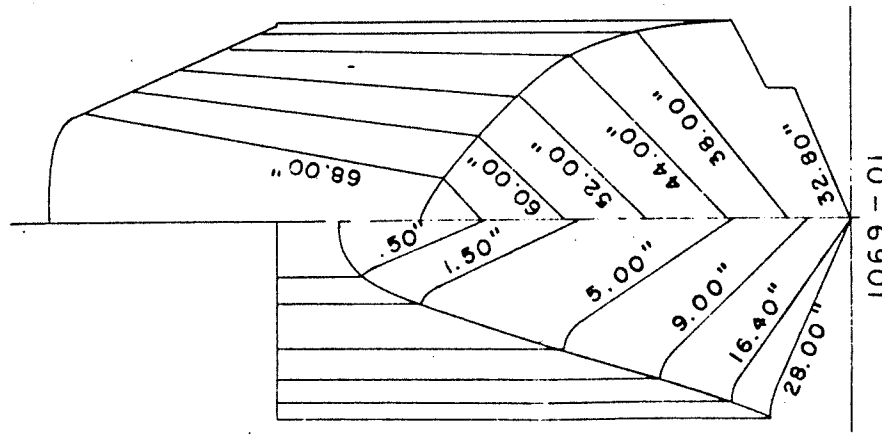
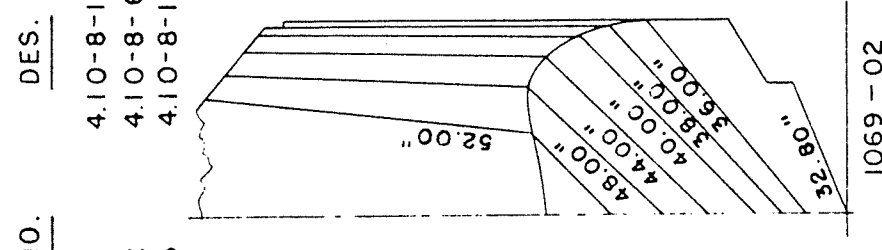
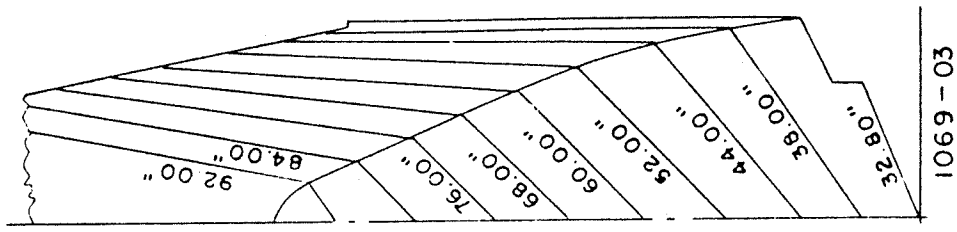
<u>MODELS NO.</u>	<u>DES.</u>	<u>L_a/b</u>
1068-01	5.02-6-6	6
1068-02	5.02-6-4	4
1068-03	5.02-6-10	10

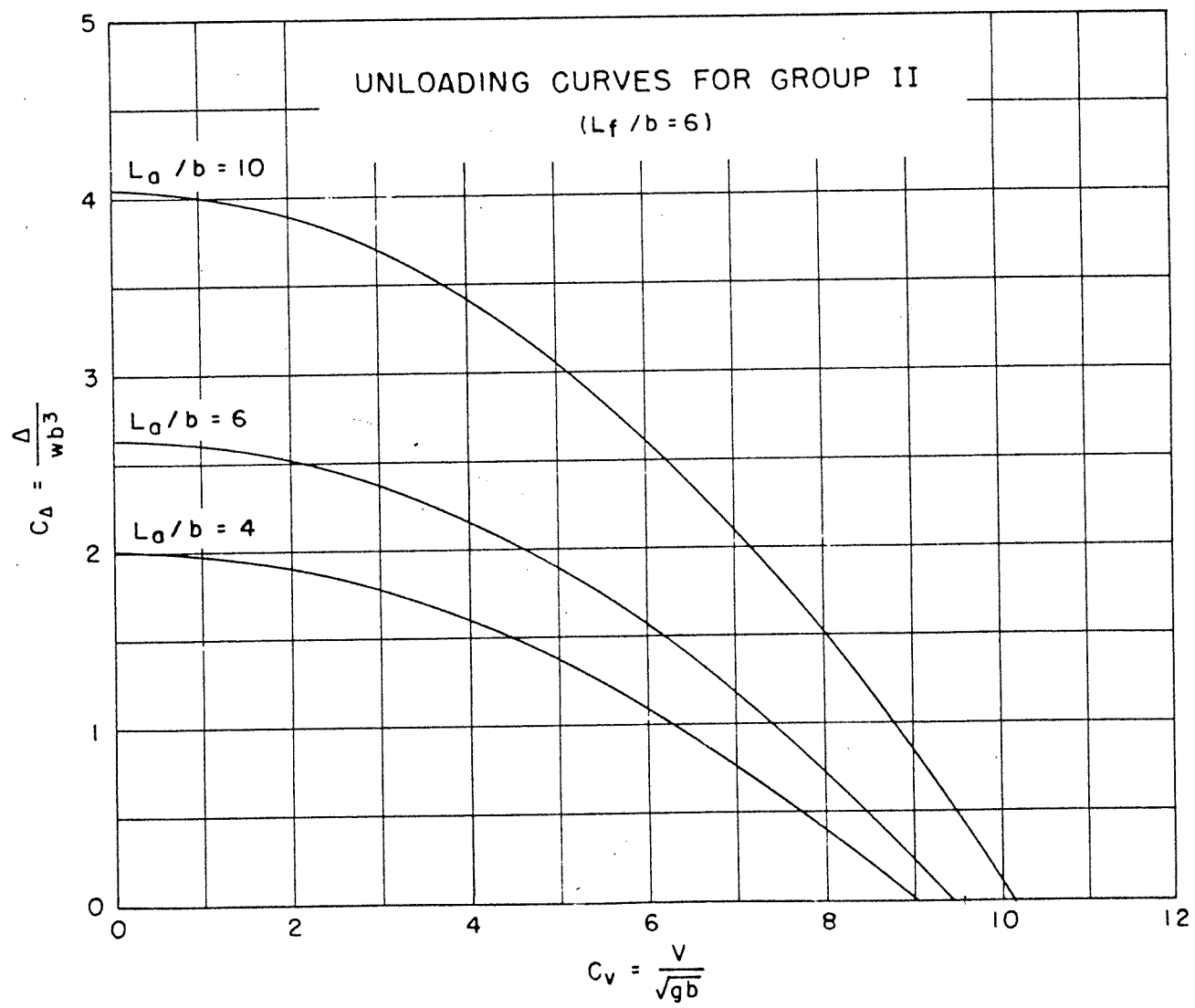
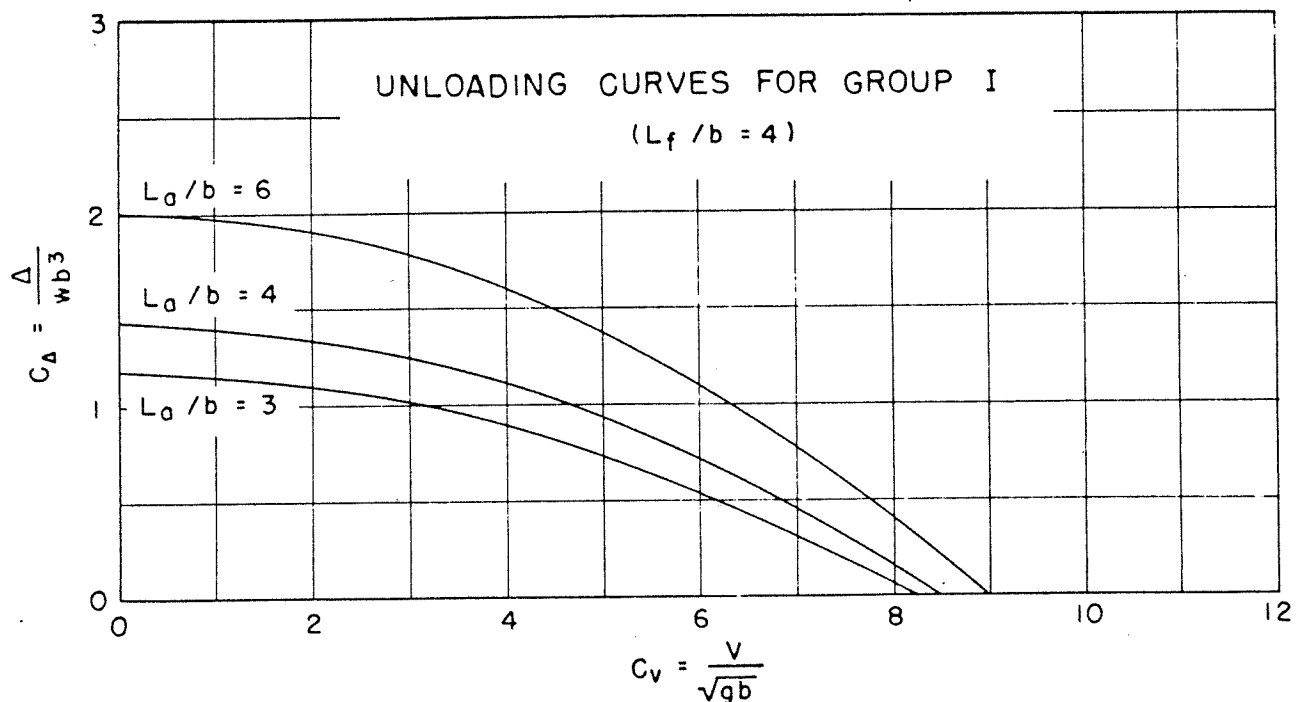


HULL MODELS

GROUP III MAX. BEAM = 4.10" ; $L_f/b = 8$

MODELS NO.	DES.	L_a/b
1069-01	4.10-8-10	10
1069-02	4.10-8-6	6
1069-03	4.10-8-16	16





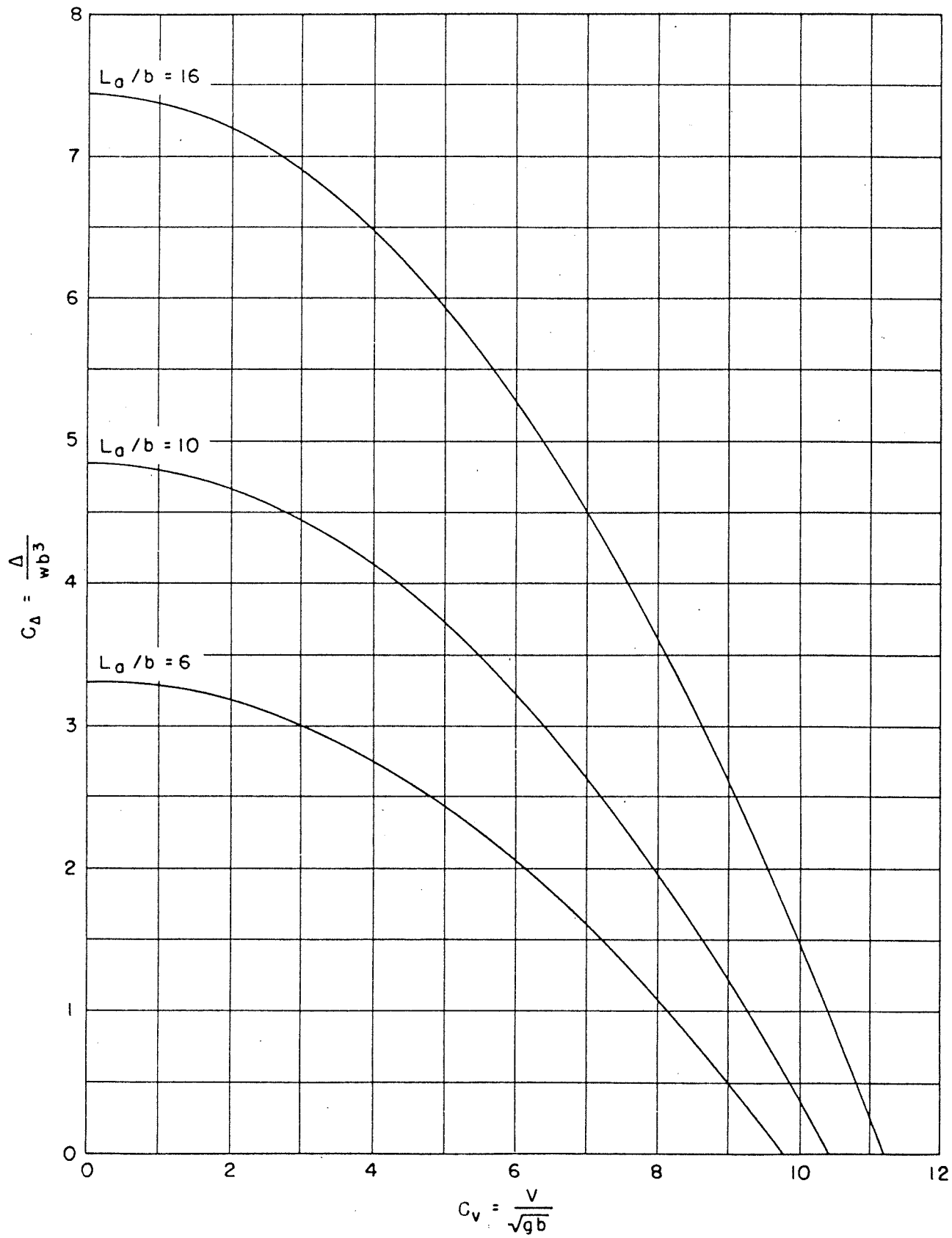
UNLOADING CURVES FOR GROUP III
($L_f/b = 8$)

FIGURE 6

DESIGNATION: 4-3-1.18-22

MODEL NO. 1067-02-06 C.G. = 0.27 b FWD. OF CENTROID $C_{\Delta_0} = 1.17$ (NOMINAL)
 MODEL BEAM: 6.15" $C_{\Delta} = 1.06$ b ABOVE KEEL $k/L =$ TESTED AT E.T.T. NO. 3 TANK
 DATE: SEPT. 19, 1951

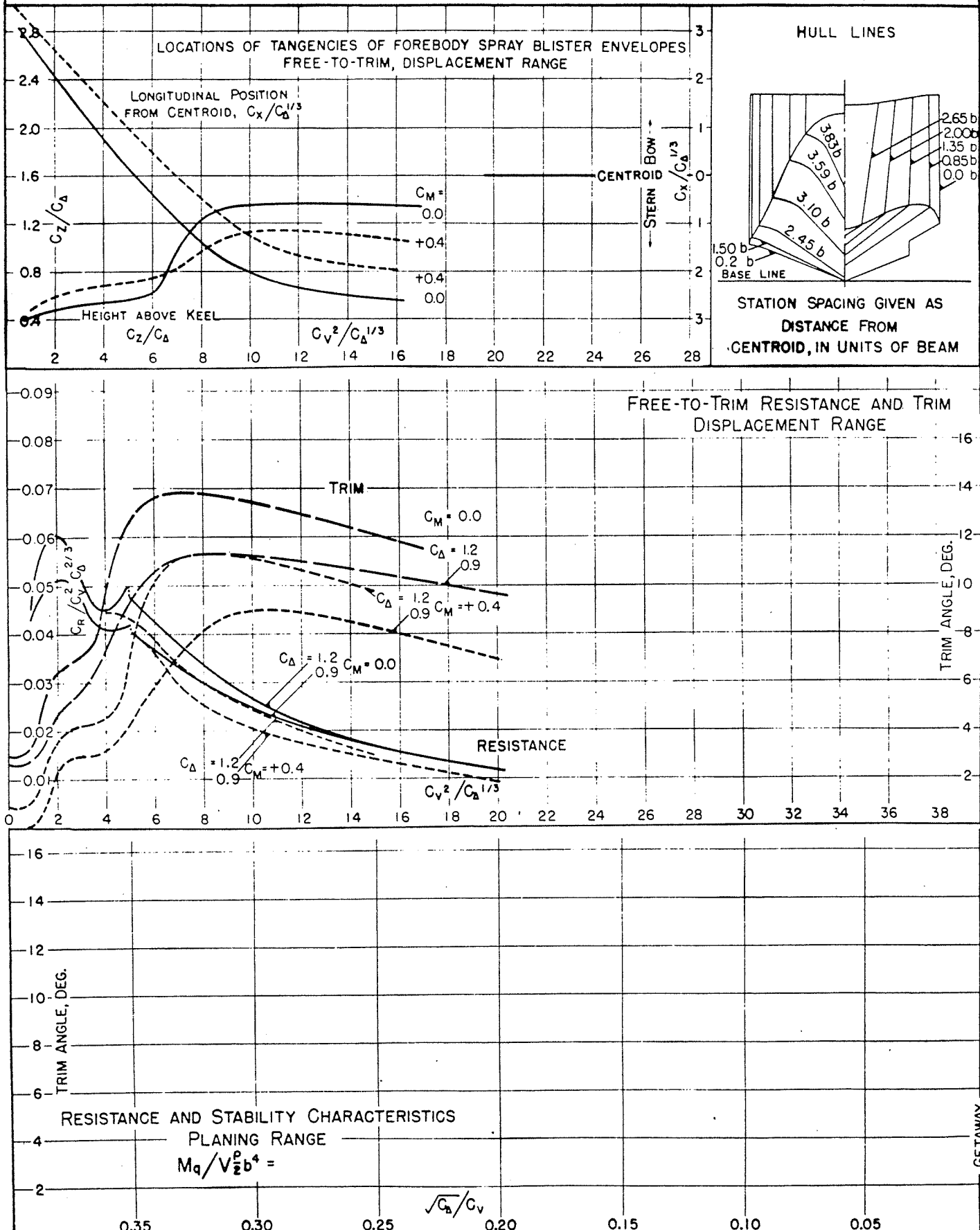


FIGURE 7

DESIGNATION: 4-3-0.71-22

MODEL NO. 1067-02-10 C.G. = 0.27 b FWD. OF CENTROID $C_{b_0} = 1.17$ (NOMINAL)
 MODEL BEAM: 6.15 " C.G. = 1.06 b ABOVE KEEL $k/L =$ TESTED AT E.T.T. No. 3 TANK
 DATE: SEPT. 24, 1951

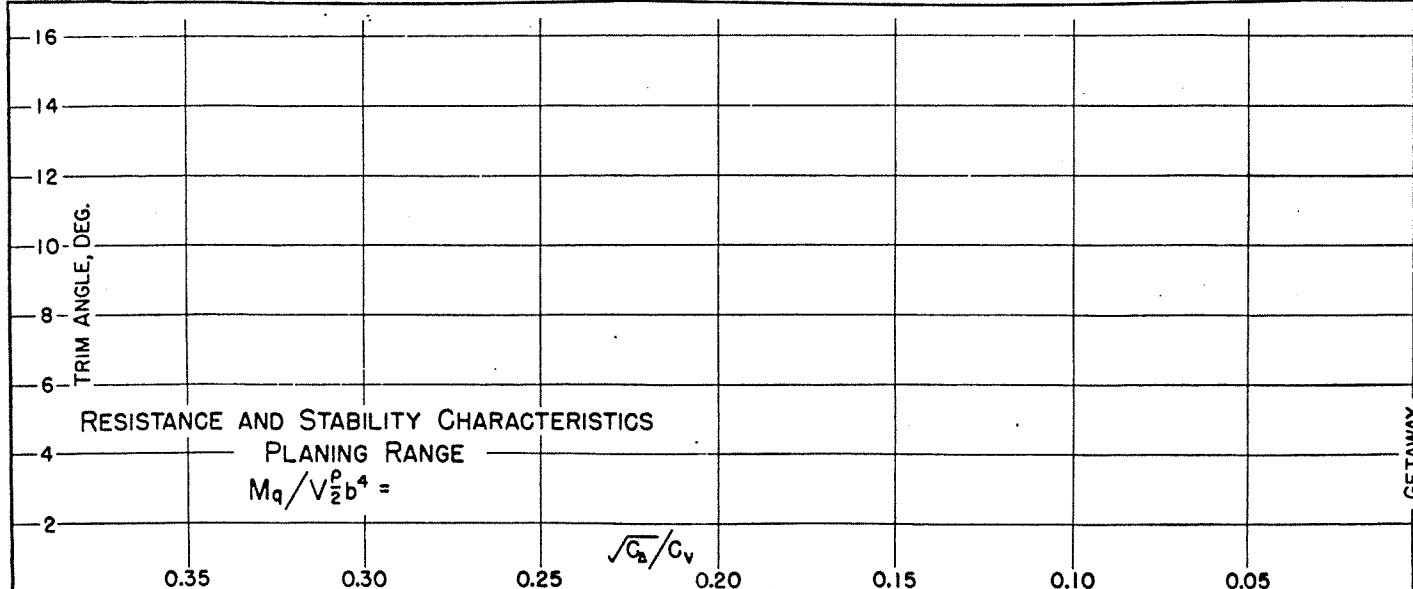
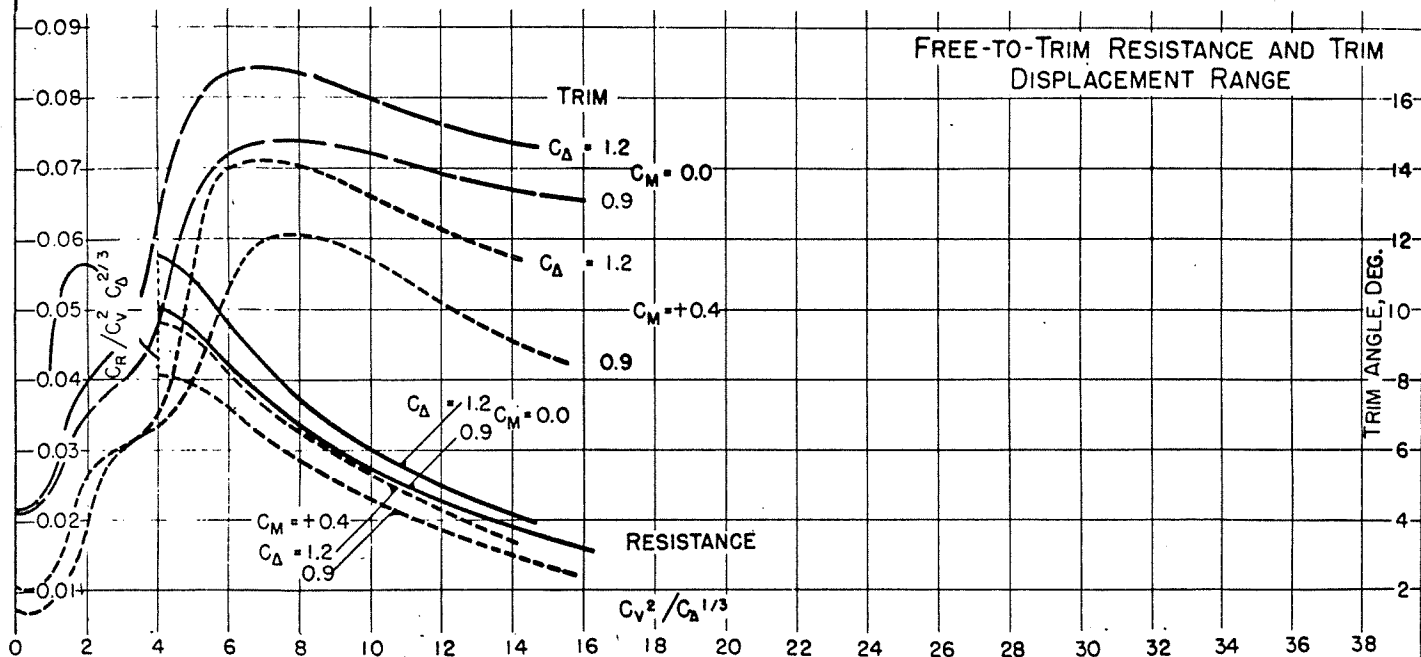
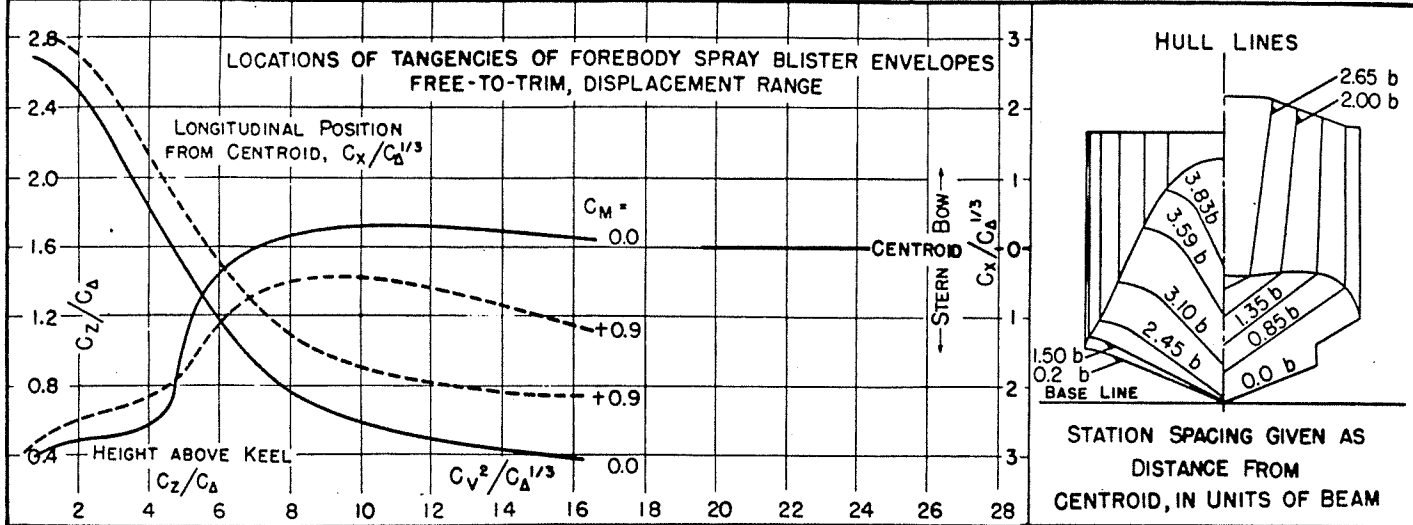


FIGURE 8

DESIGNATION: 4-4-1.18-22

MODEL NO. 1067-01-06 C.G. = 0.27 b FWD. OF CENTROID $C_{\Delta} = 1.43$ (NOMINAL)
 MODEL BEAM: 6.15" 1.06 b ABOVE KEEL $k/L =$ TESTED AT E.T.T. NO. 3 TANK
 DATE: SEPT. 6, 1951

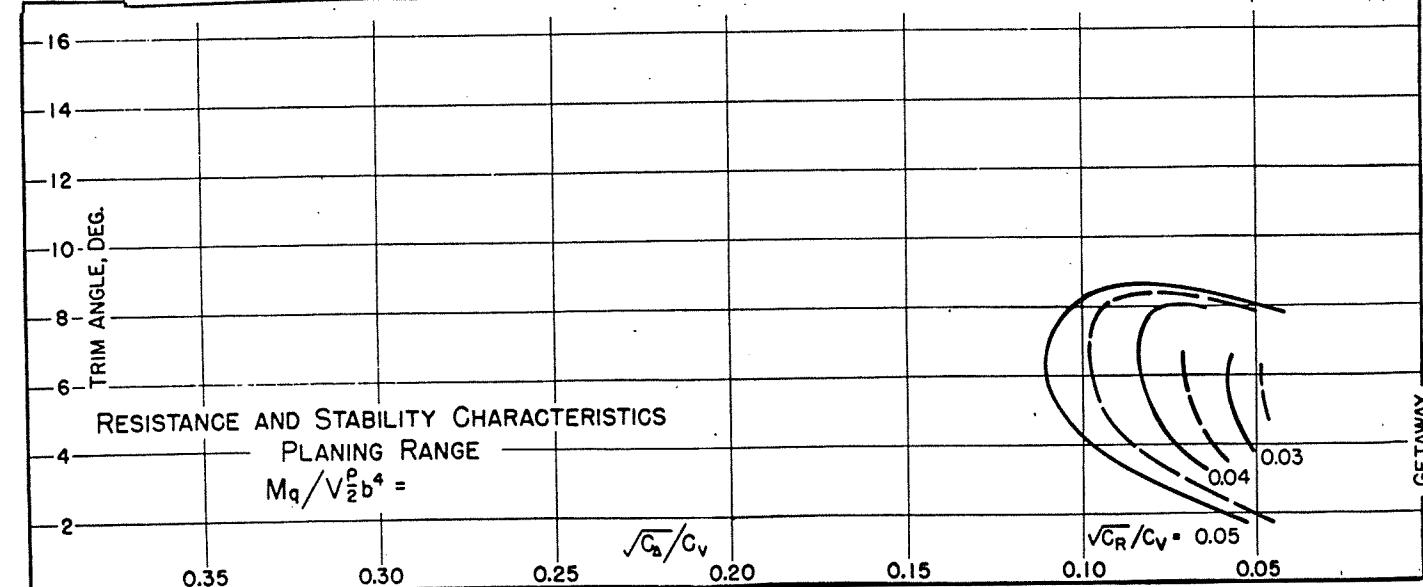
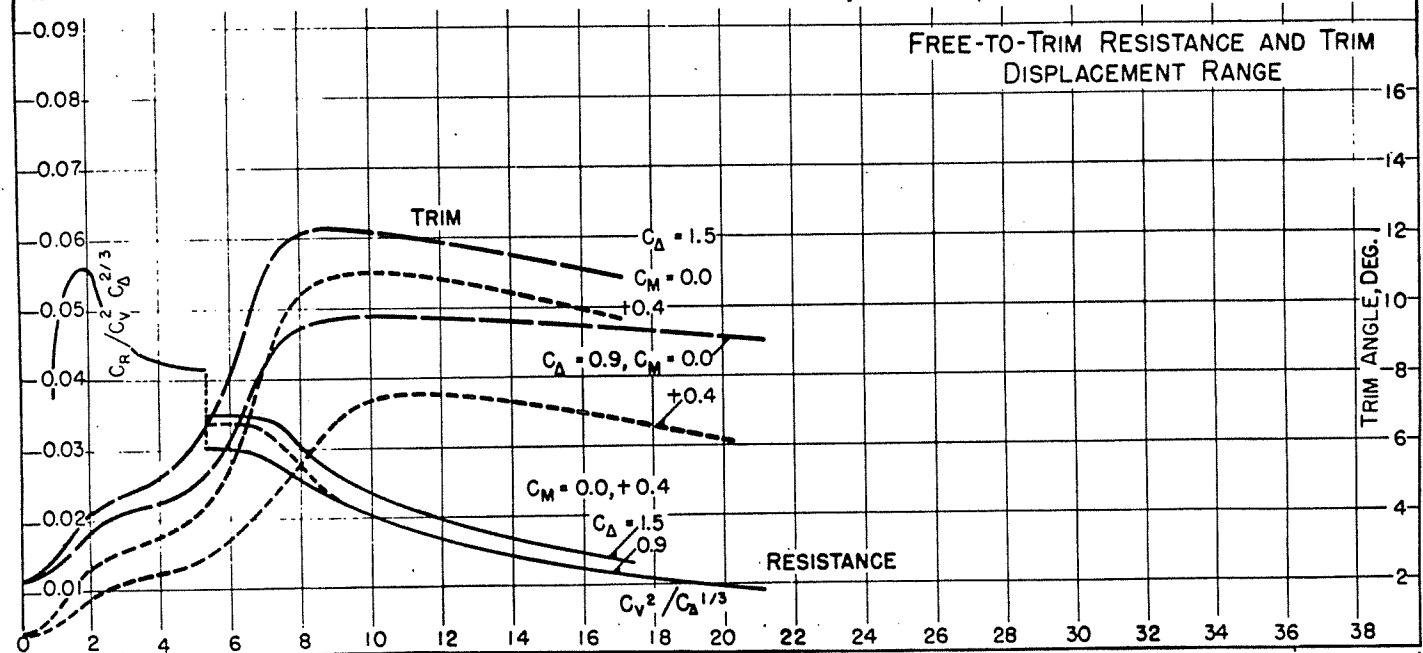
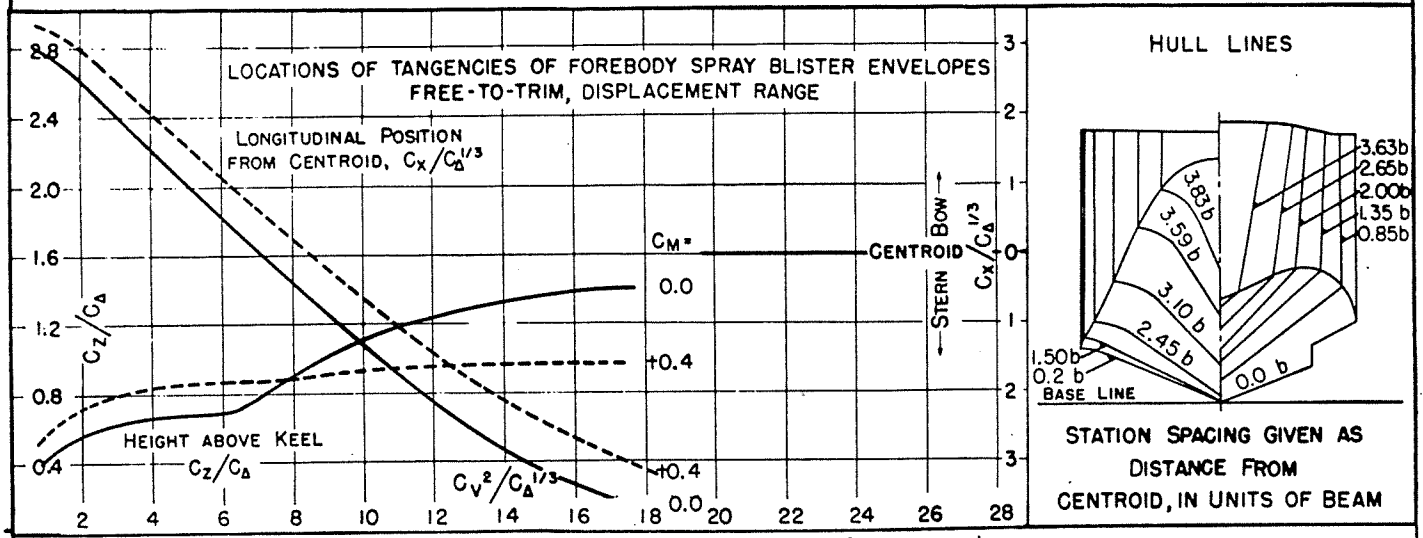


FIGURE 9

DESIGNATION: 4-4-071-22

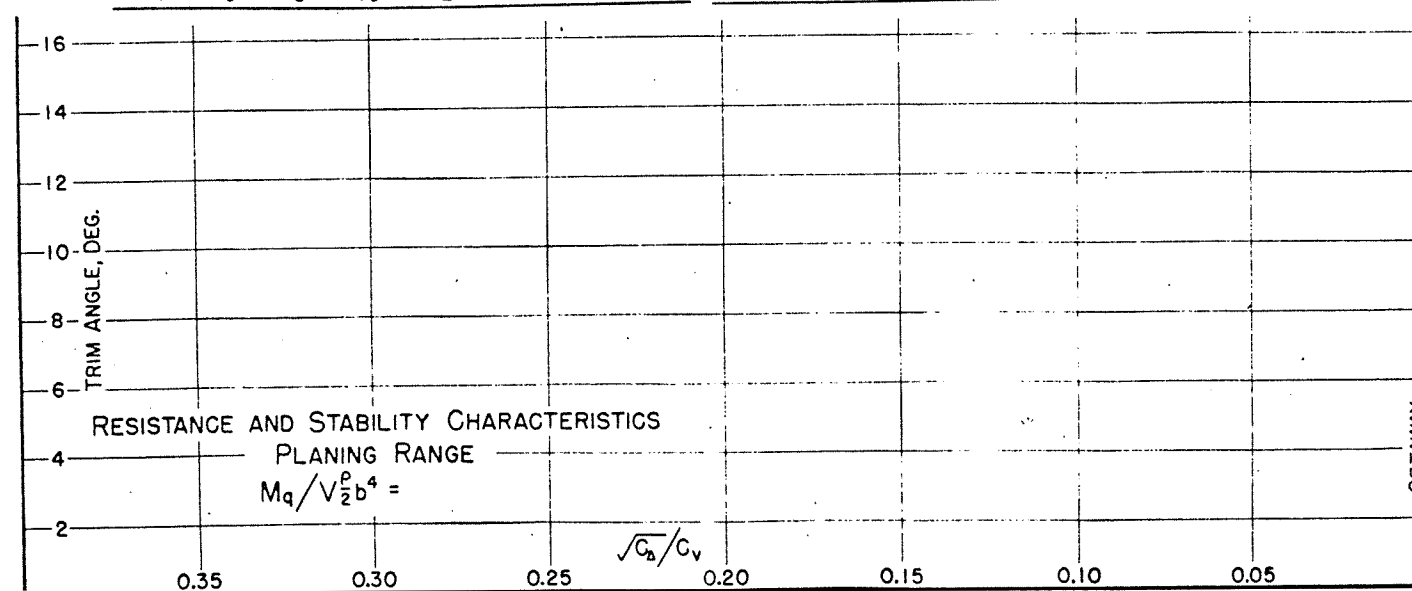
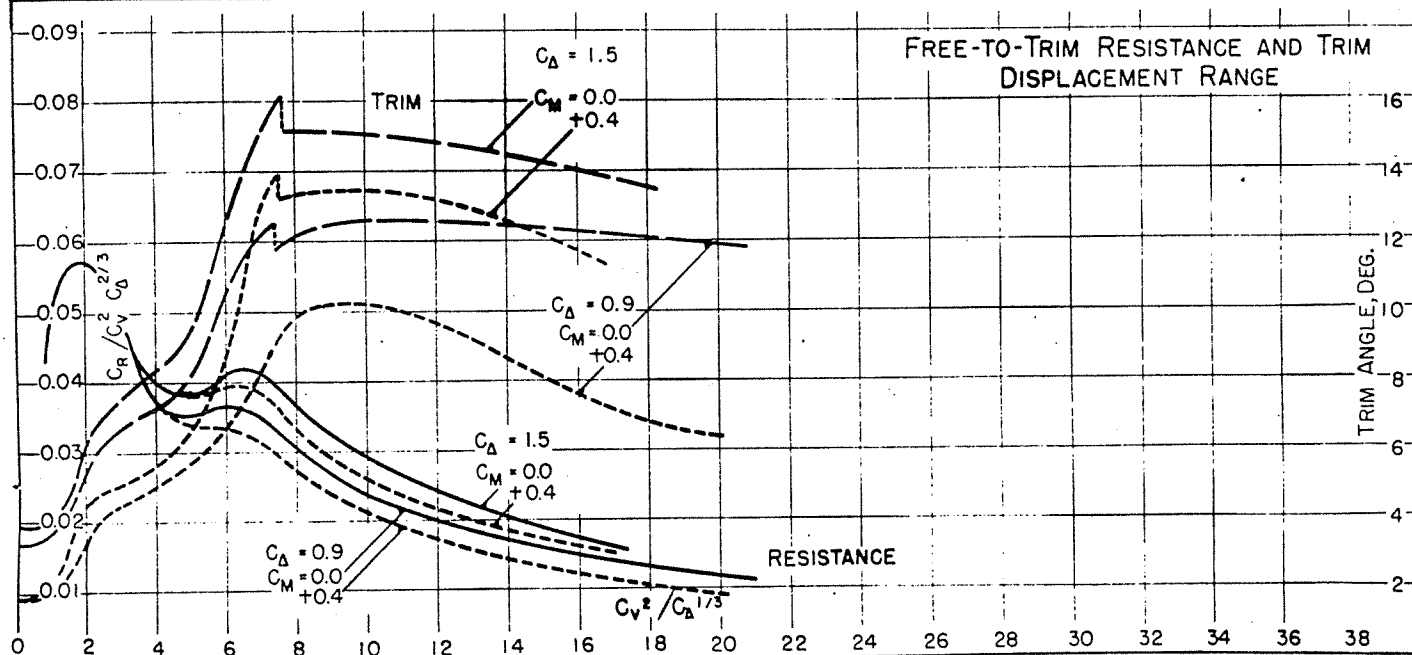
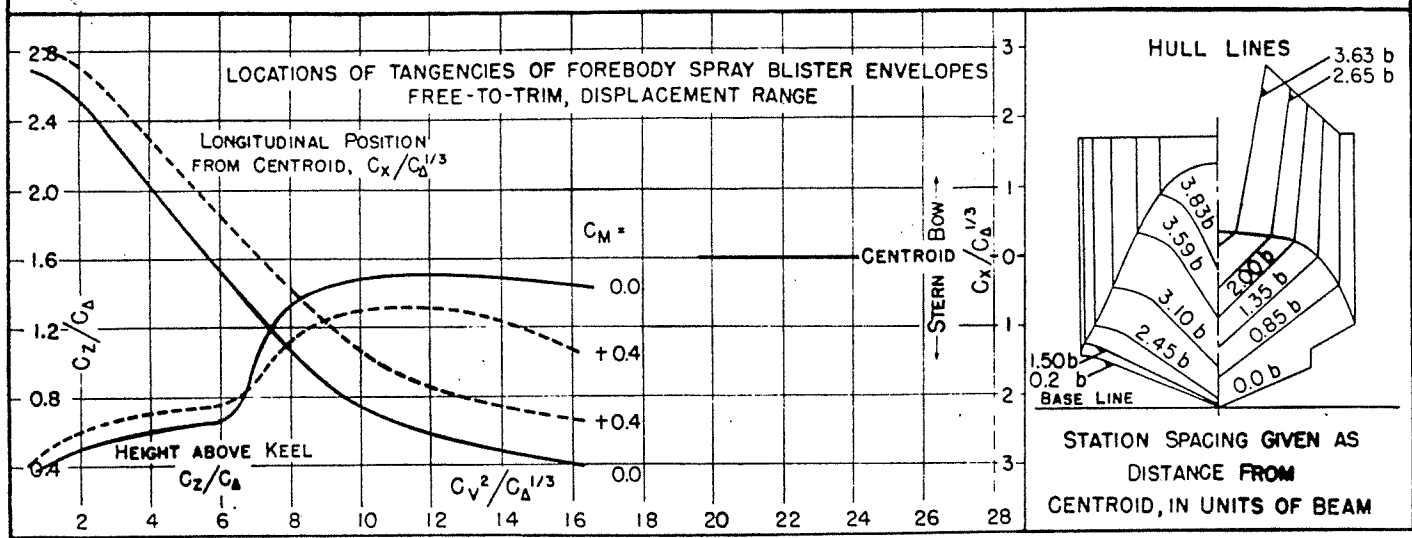
MODEL NO. 1067-01-10 C.G. = 0.27 b FWD. OF CENTROID $C_{\Delta} = 1.43$ (NOMINAL)
MODEL BEAM: 6.15" 1.06 b ABOVE KEEL $k/L =$ TESTED AT E.T.T. NO. 3 TANK
DATE: SEPT. 11, 1951

FIGURE 10

DESIGNATION: 4-6-1.18-22

MODEL NO. 1067-03-06 C.G. = 0.27 b FWD. OF CENTROID $C_{b0} = 2.00$ (NOMINAL)
 MODEL BEAM: 6.15" $C_{b0} = 1.06$ b ABOVE KEEL $k/L =$ TESTED AT E.T.T. No. 3 TANK
 DATE: SEPT. 14, 1951

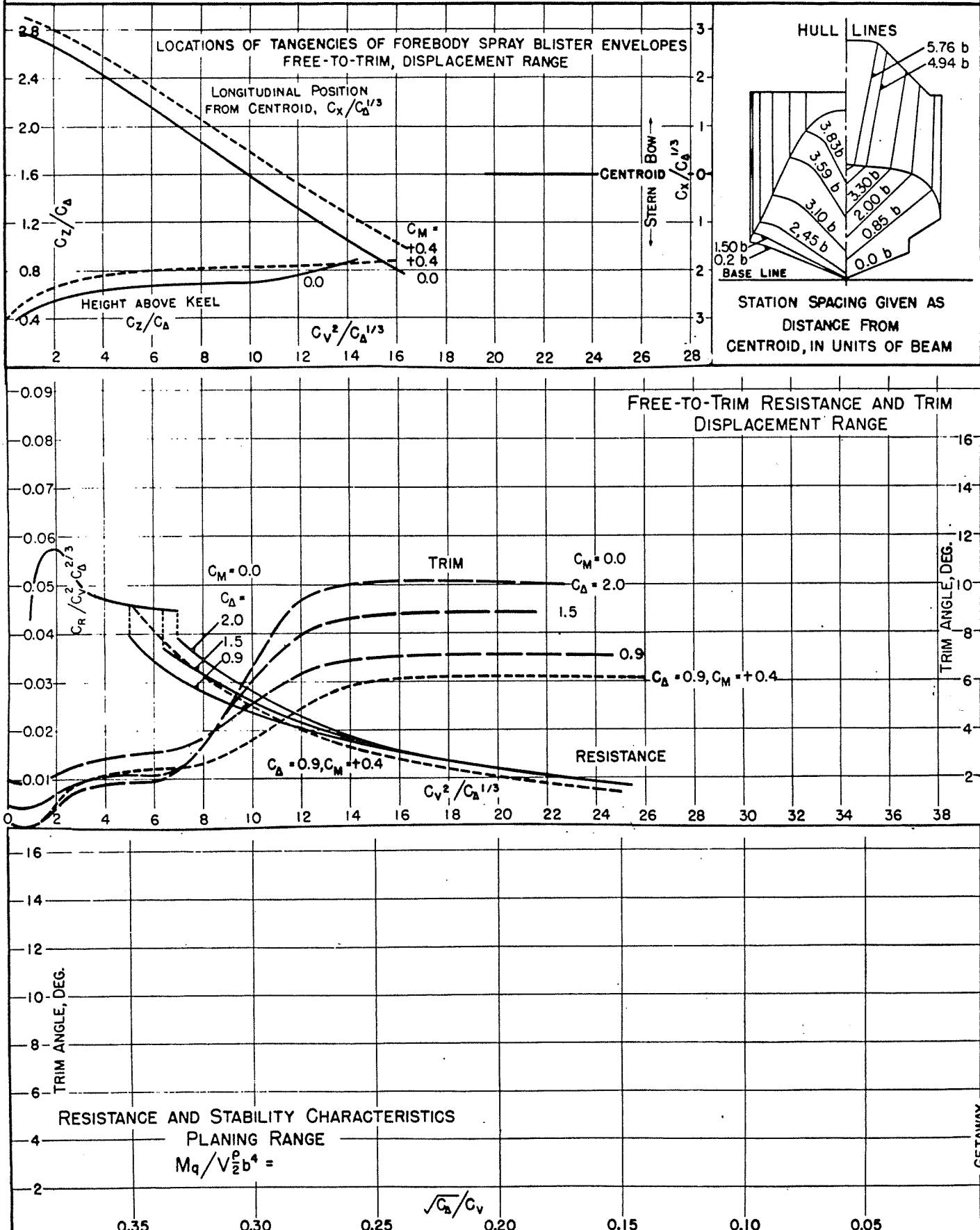


FIGURE II

DESIGNATION: 4-6-071-22

MODEL NO. 1067-03-10 C.G. = 0.27 b FWD. OF CENTROID $C_d = 2.00$ (NOMINAL)
MODEL BEAM: 6.15" 1.06" ABOVE KEEL $k/L =$

TESTED AT E.T.T. No. 3 TANK
DATE: SEPT. 25, 1951

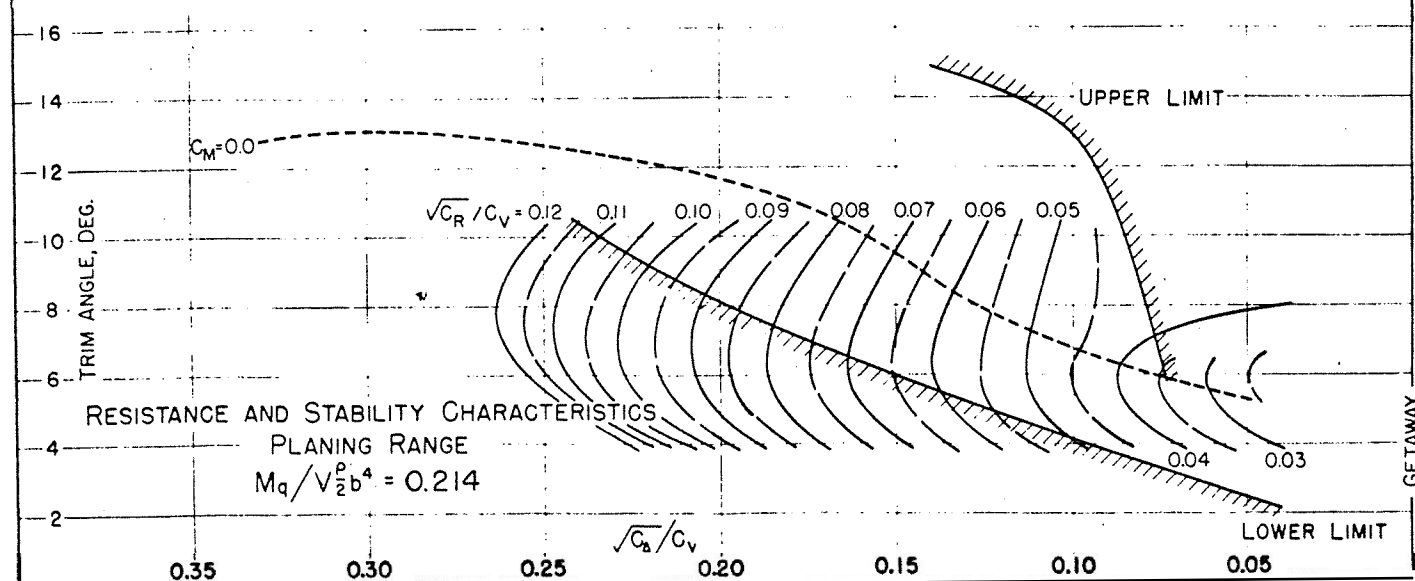
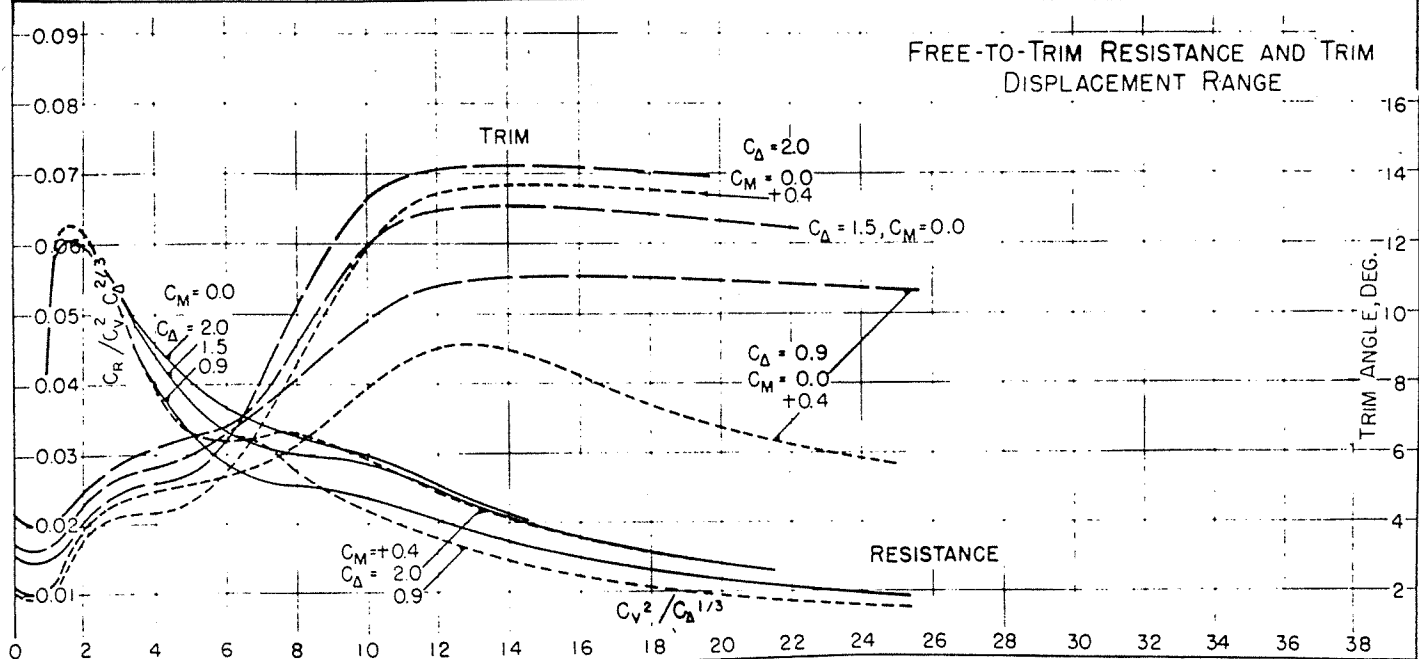
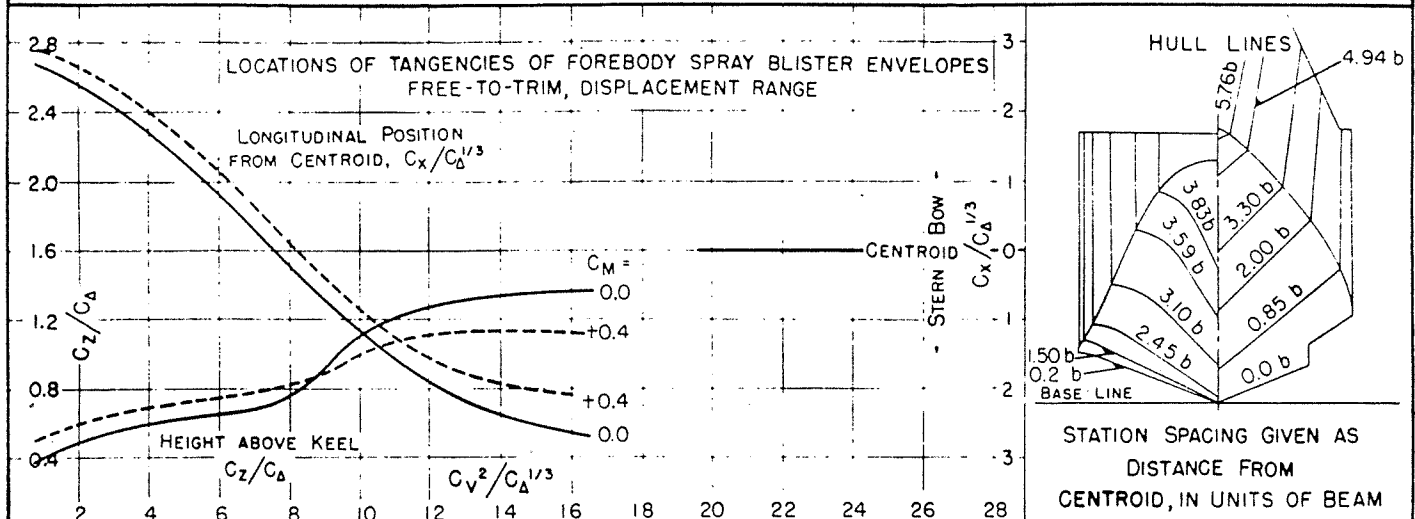


FIGURE 12

DESIGNATION: 6-4-1.33-22

MODEL NO. 1068-02-06 C.G. = 0.32 b FWD. OF CENTROID $C_{b_0} = 2.00$ (NOMINAL) TESTED AT E.T.T. No.3 TANK
 MODEL BEAM: 5.02" 1.29 b ABOVE KEEL $k/L =$ DATE: Oct. 23, 1951

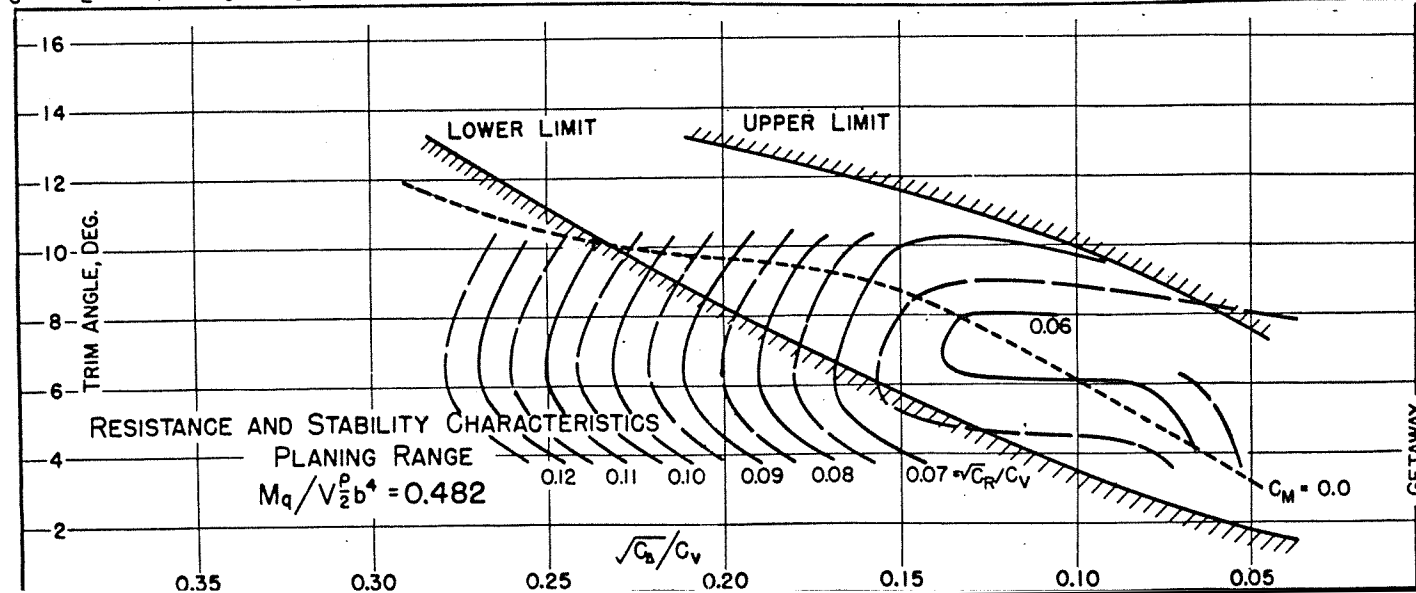
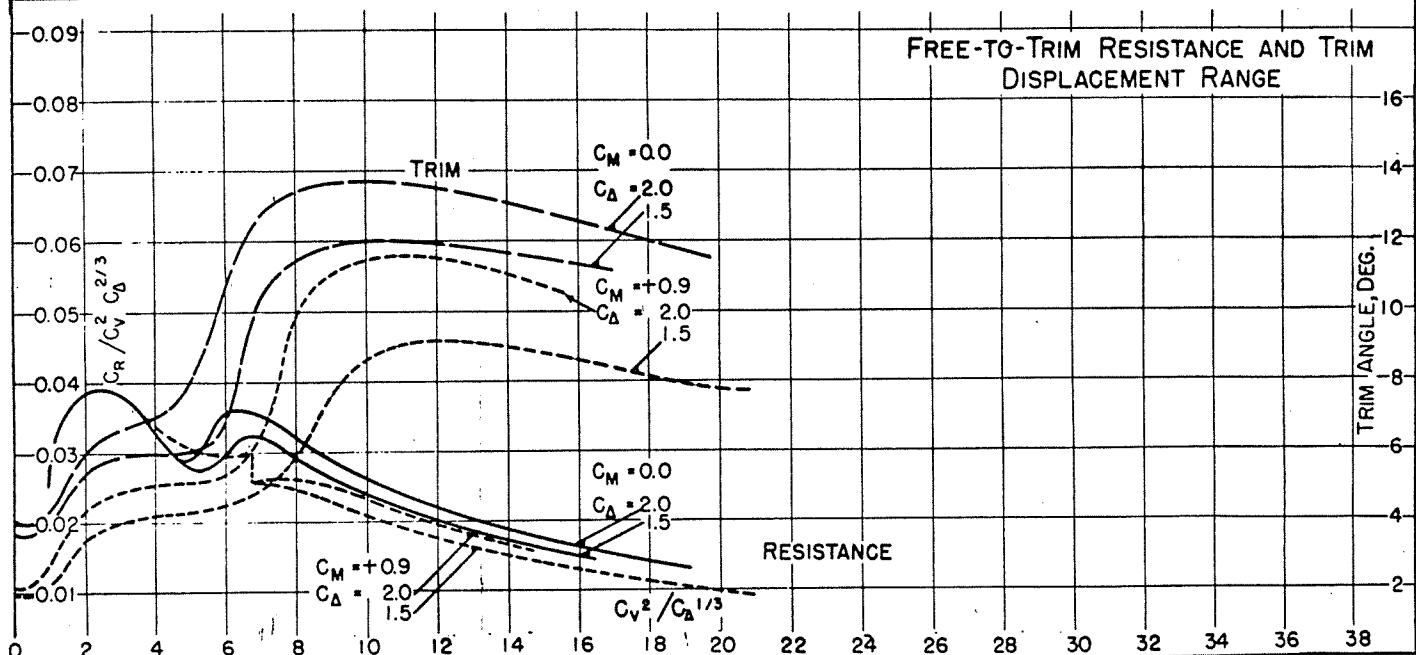
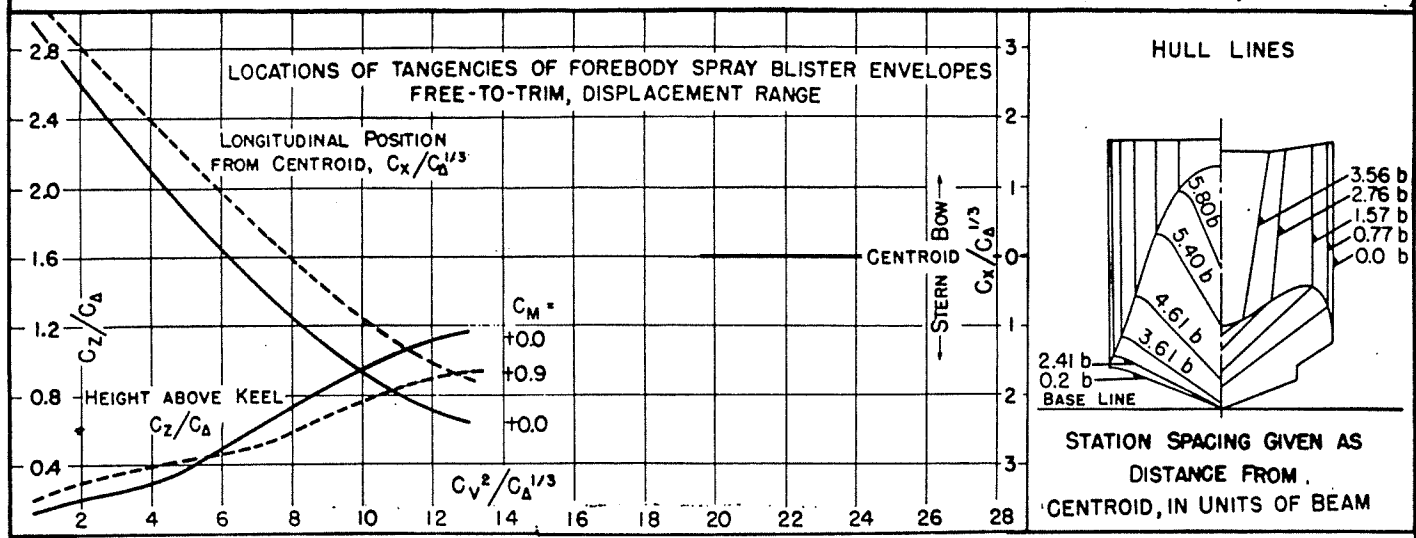


FIGURE 13

DESIGNATION: 6-4-0.80-22

MODEL NO. 1068-02-10 C.G. = 0.32 b FWD. OF CENTROID $C_a = 2.00$ (NOMINAL) TESTED AT E.T.T. NO. 3 TANK
 MODEL BEAM: 5.02" 1.29 b ABOVE KEEL $k/L =$ DATE: Nov. 10, 1951

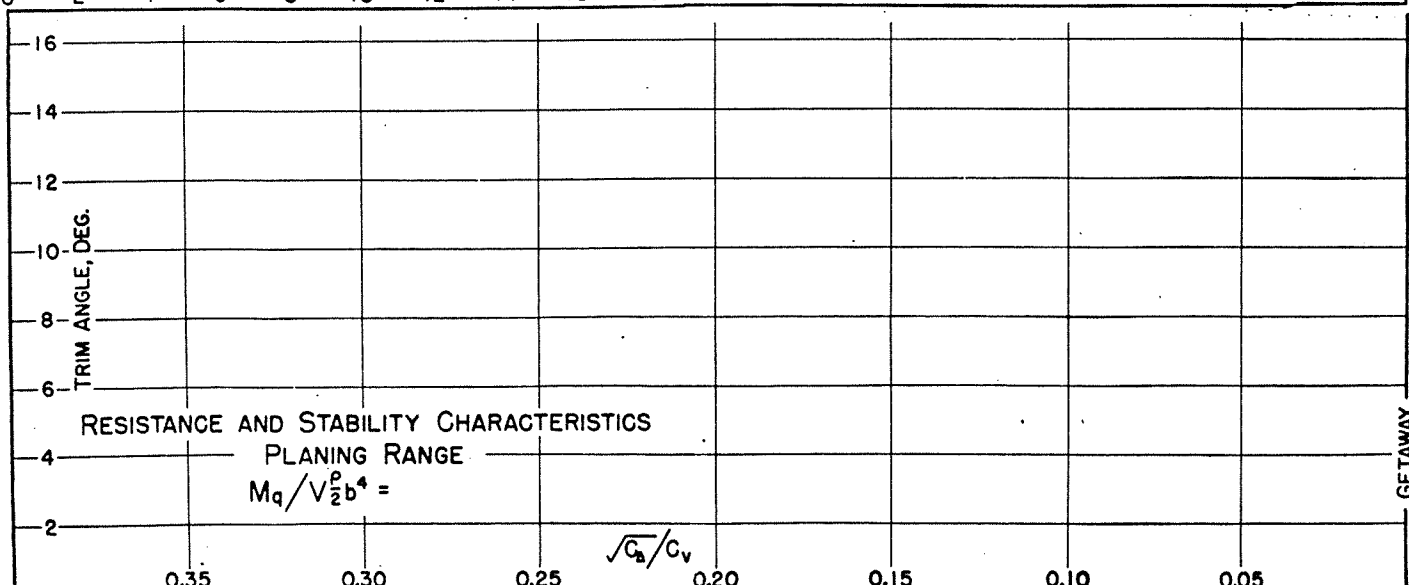
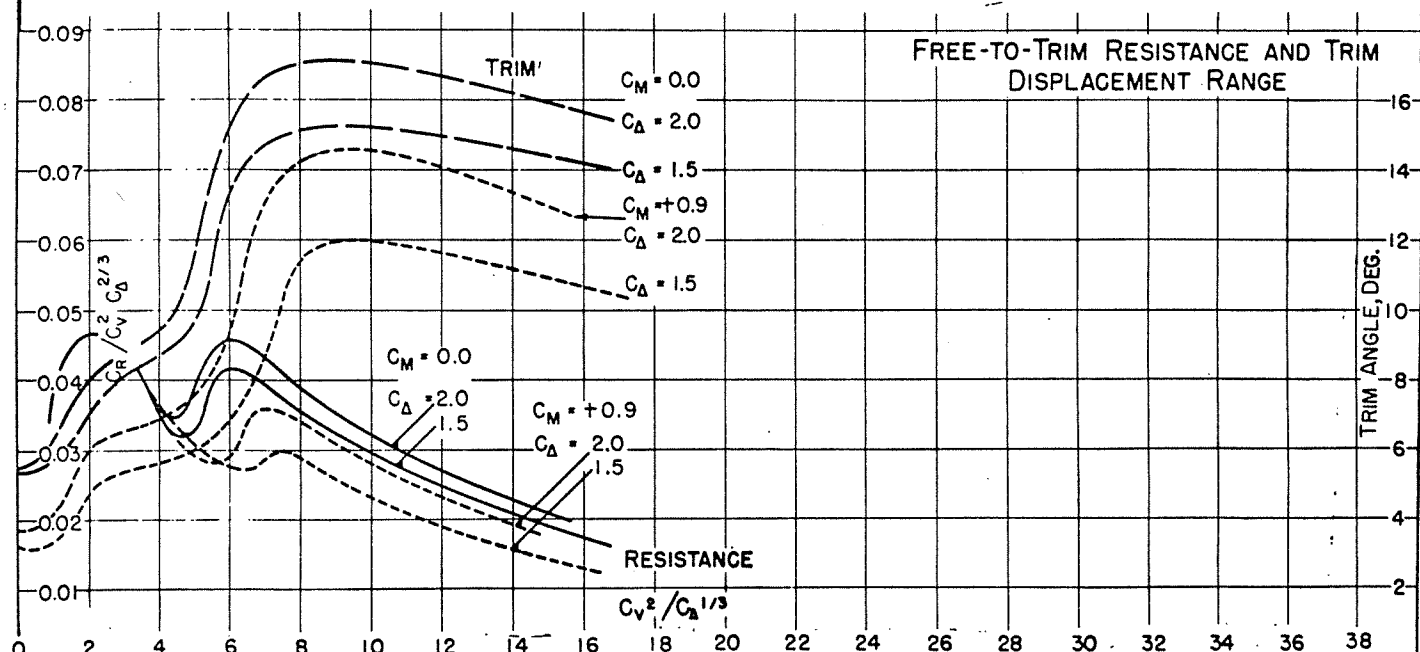
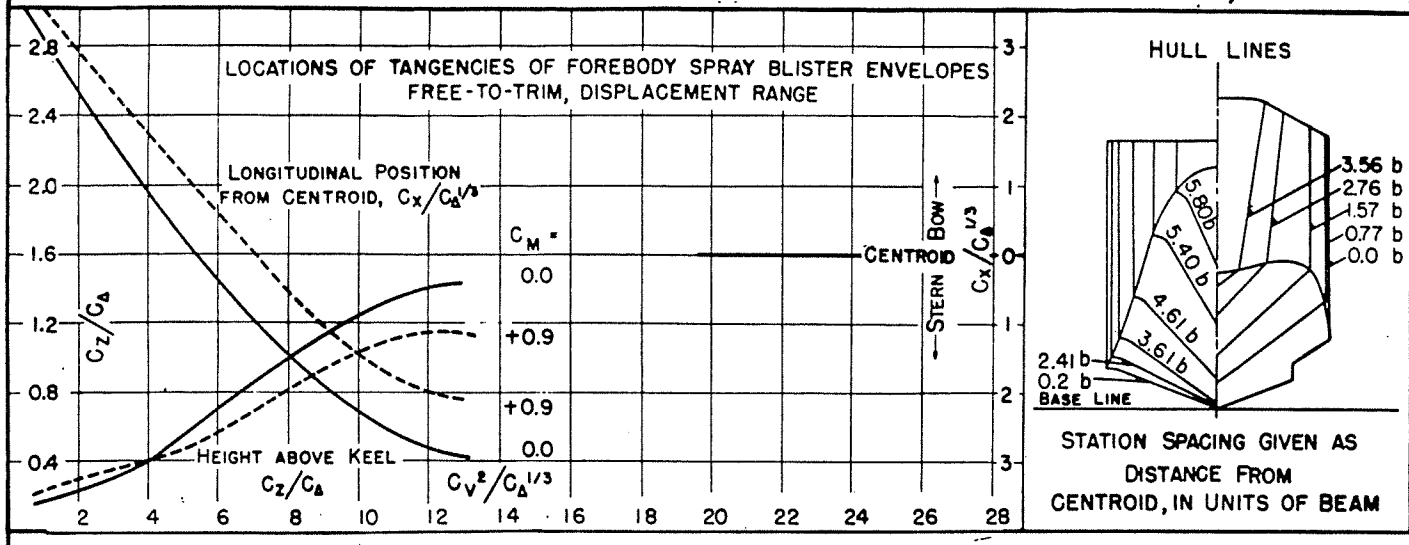


FIGURE 14

DESIGNATION: 6-6-1.33-22

MODEL NO. 1068-01-06 C.G. = 0.32 b FWD. OF CENTROID $C_d = 2.64$ (NOMINAL) TESTED AT E.T.T. No.3 TANK
 MODEL BEAM: 5.02" 1.29 b ABOVE KEEL $k/L =$ DATE: OCT. 17, 1951

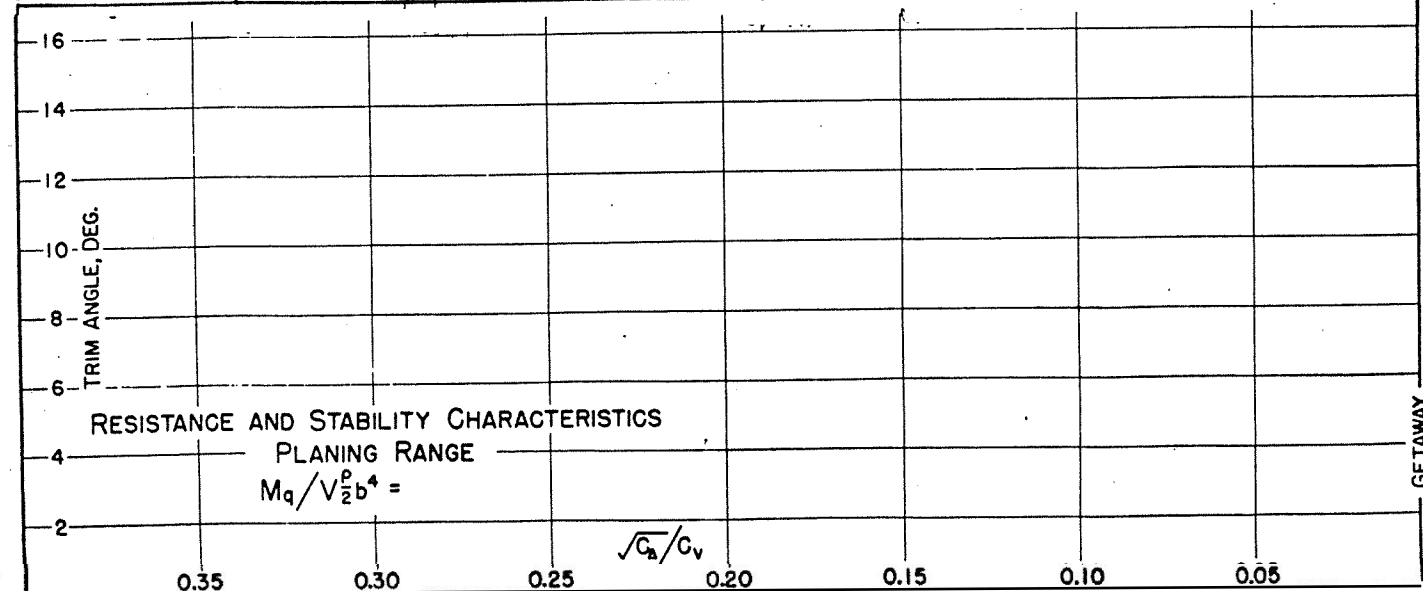
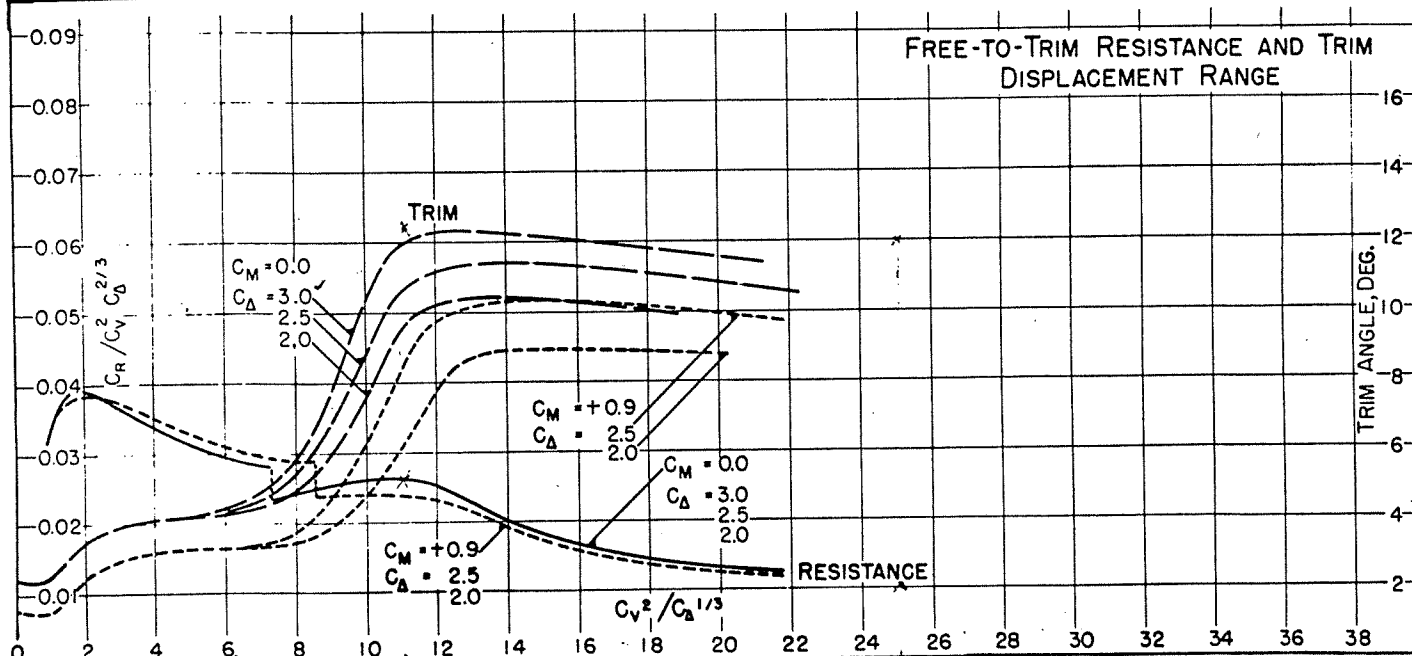
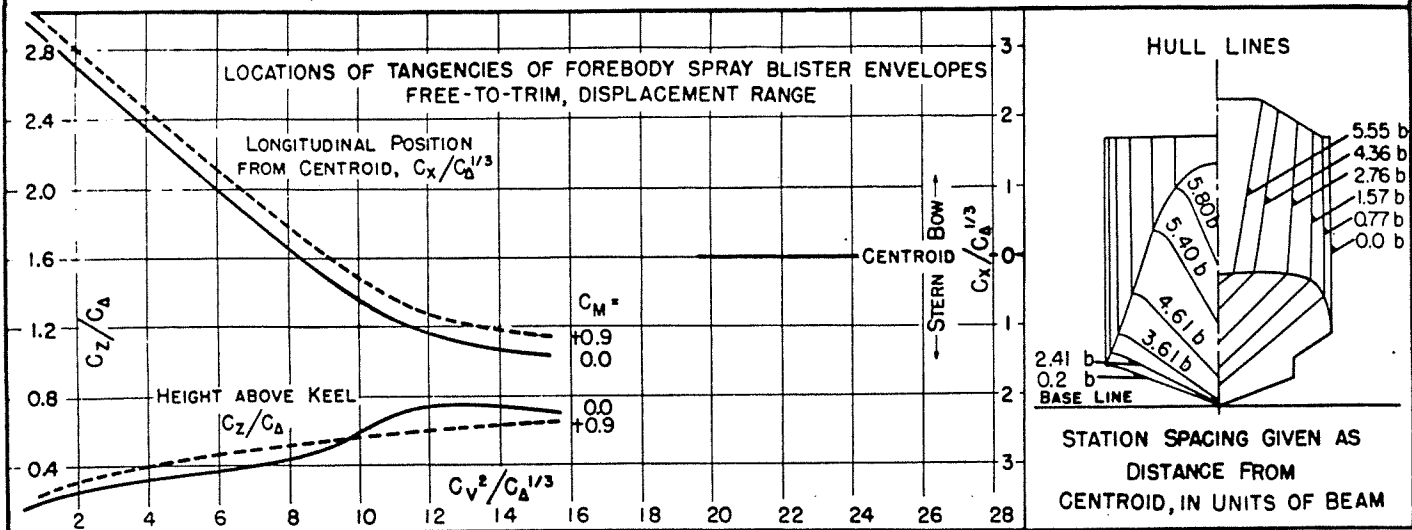


FIGURE 15

DESIGNATION: 6-6-0.80-22

MODEL NO. 1068-01-10 C.G. = 0.32 b FWD. OF CENTROID $C_b = 2.64$ (NOMINAL)
 MODEL BEAM: 5.02" 1.29 b ABOVE KEEL $K/L =$ TESTED AT E.T.T. NO. 3 TANK
 DATE: OCT. 9, 1951

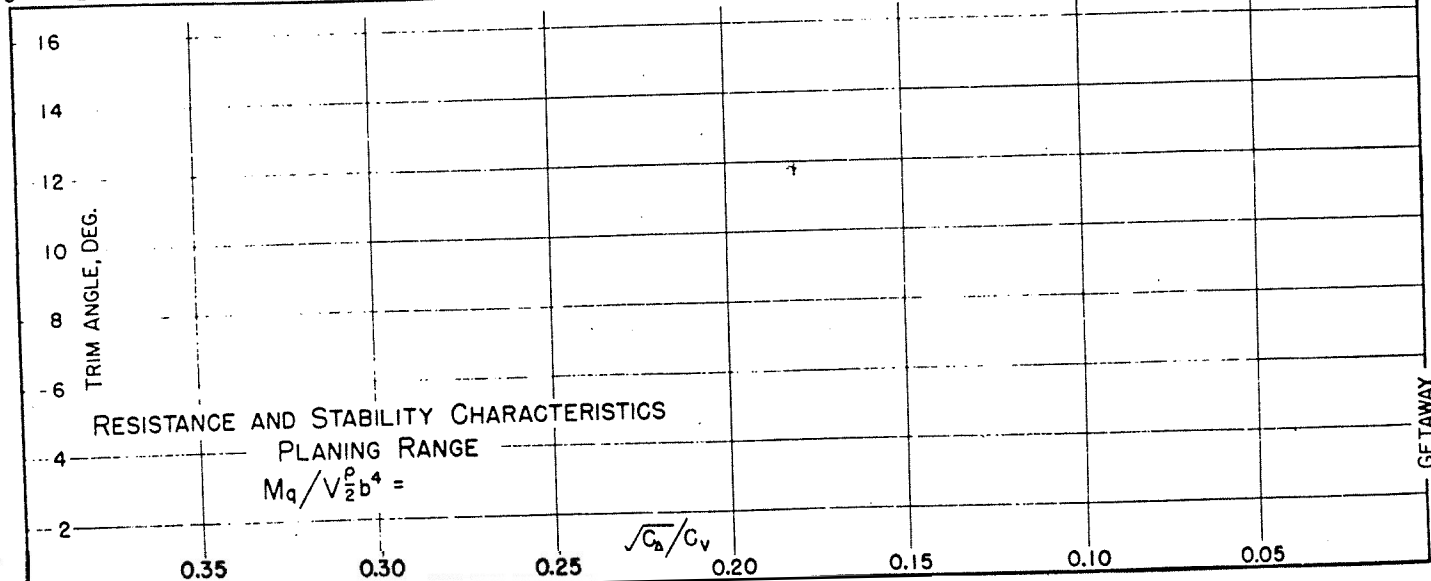
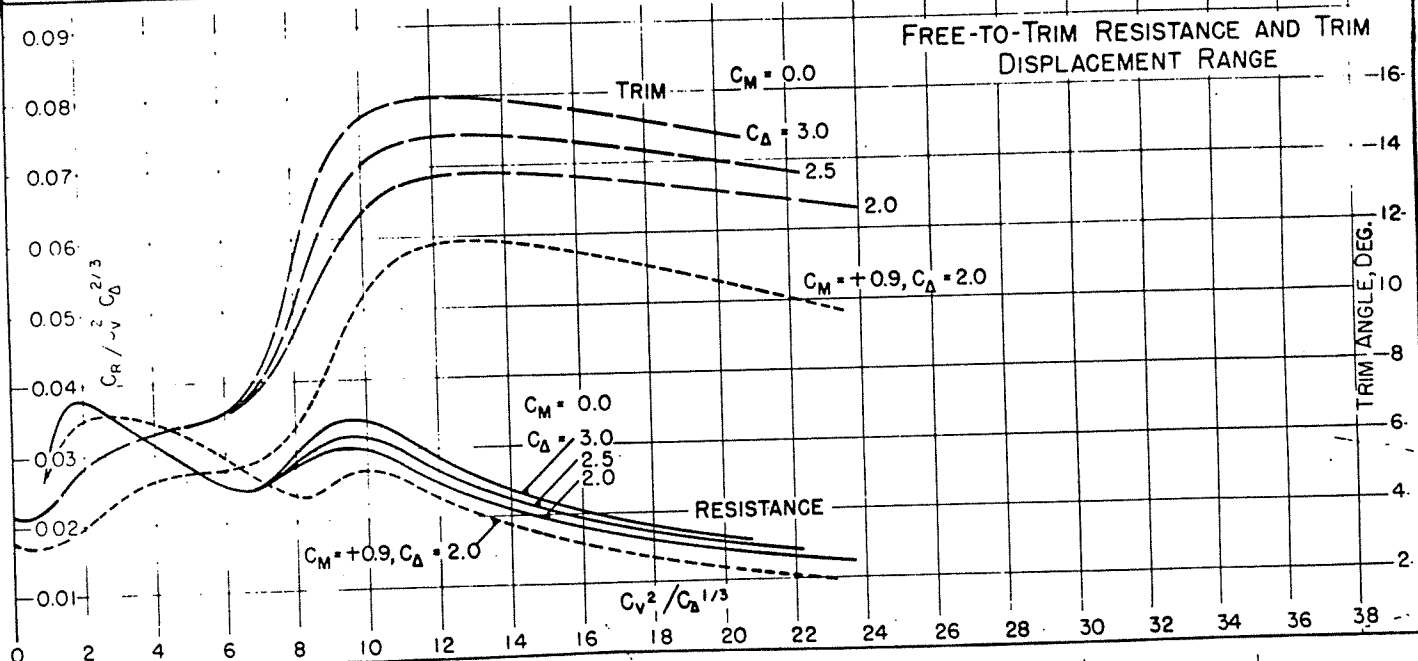
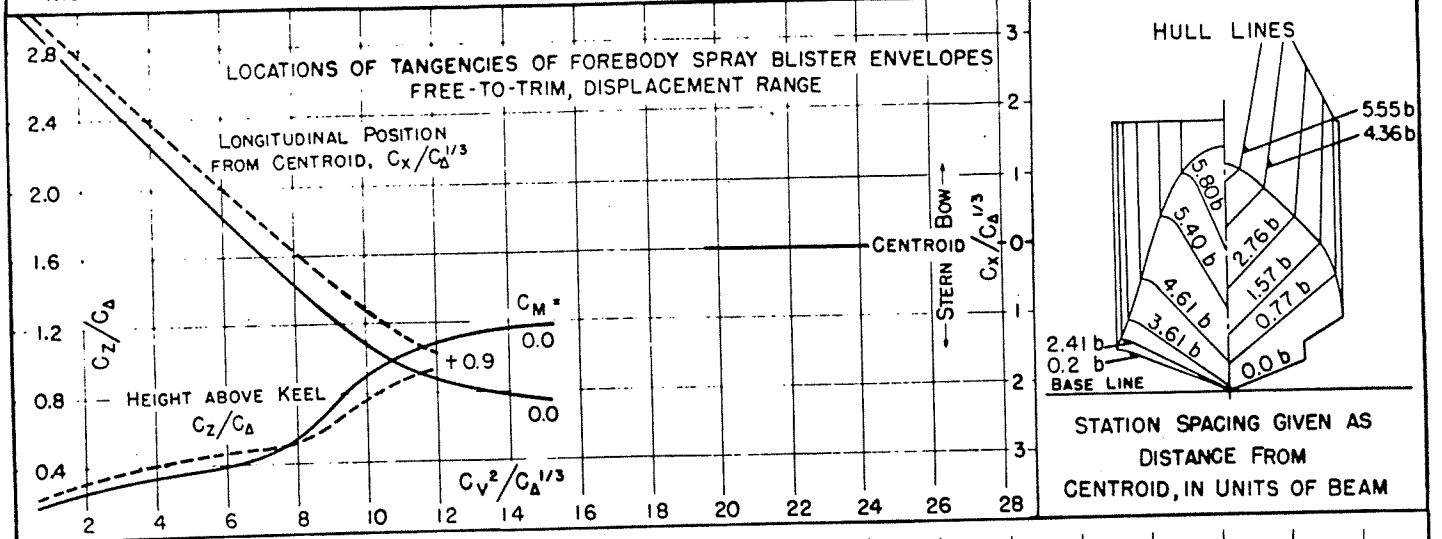


FIGURE 16

DESIGNATION: 6-10-1.33-22

MODEL NO. 1068-03-06 C.G. = 0.32 b FWD. OF CENTROID $C_A = 4.05$ (NOMINAL)
 MODEL BEAM: 5.02" 1.29 b ABOVE KEEL $k/L =$ TESTED AT E.T.T. NO. 3 TANK
 DATE: NOV. 9, 1951

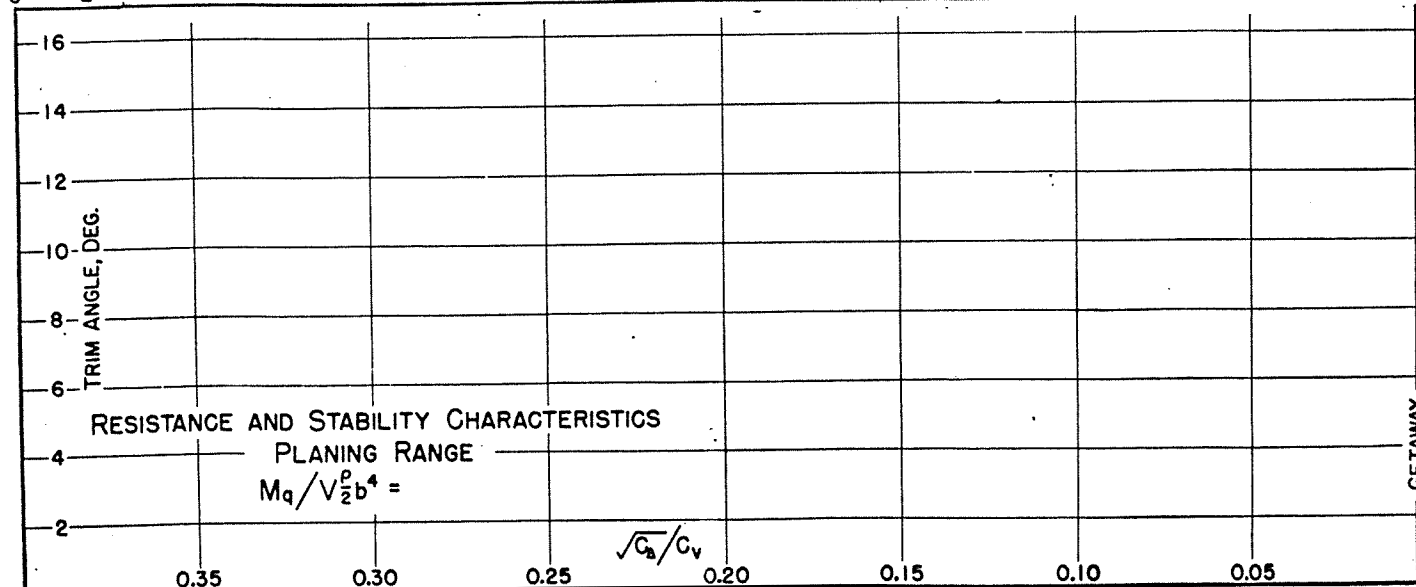
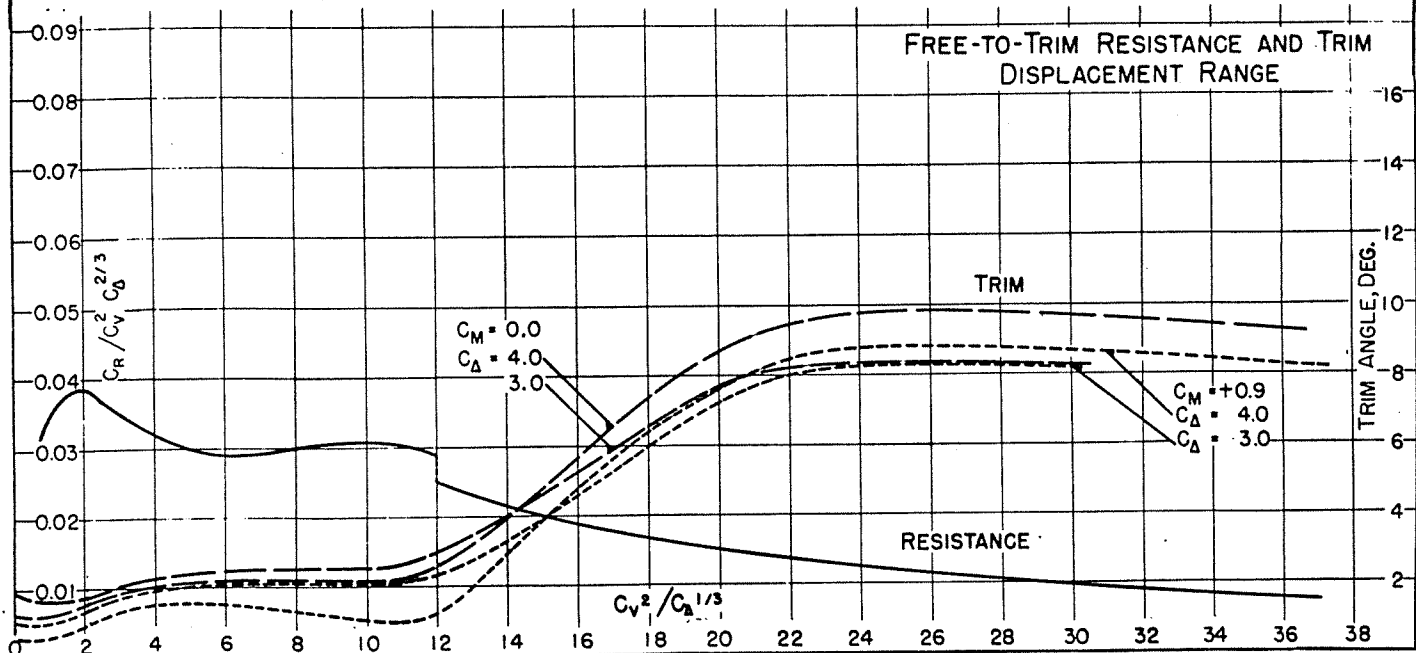
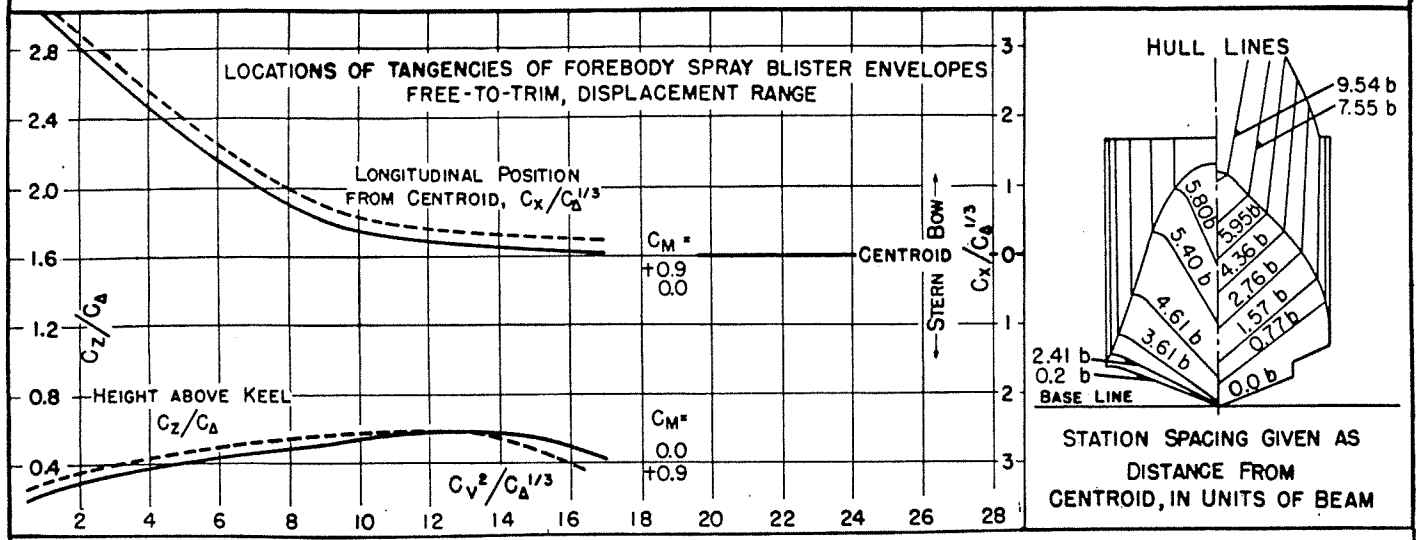


FIGURE 17

DESIGNATION: 6-10-0.80-22

MODEL NO. 1068-03-10 C.G. = 0.32 b FWD. OF CENTROID $C_d = 4.05$ (NOMINAL) TESTED AT E.T.T. NO. 3 TANK
MODEL BEAM: 5.02" 1.29 b ABOVE KEEL k/L = DATE: OCT. 22, 1951

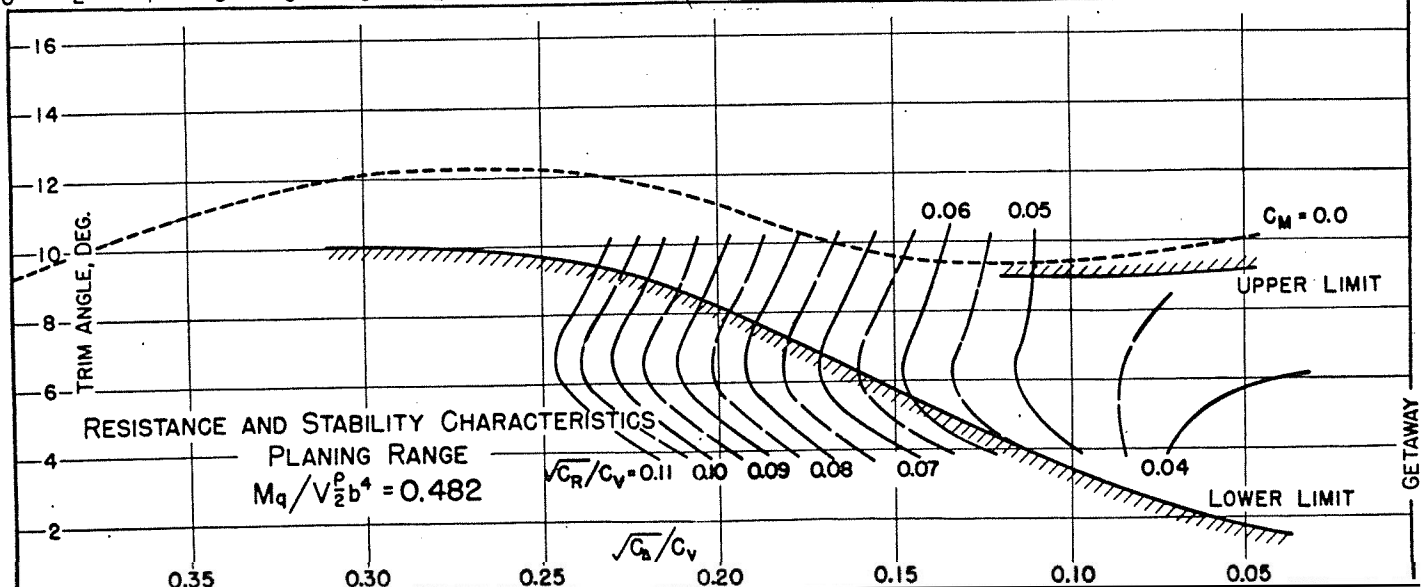
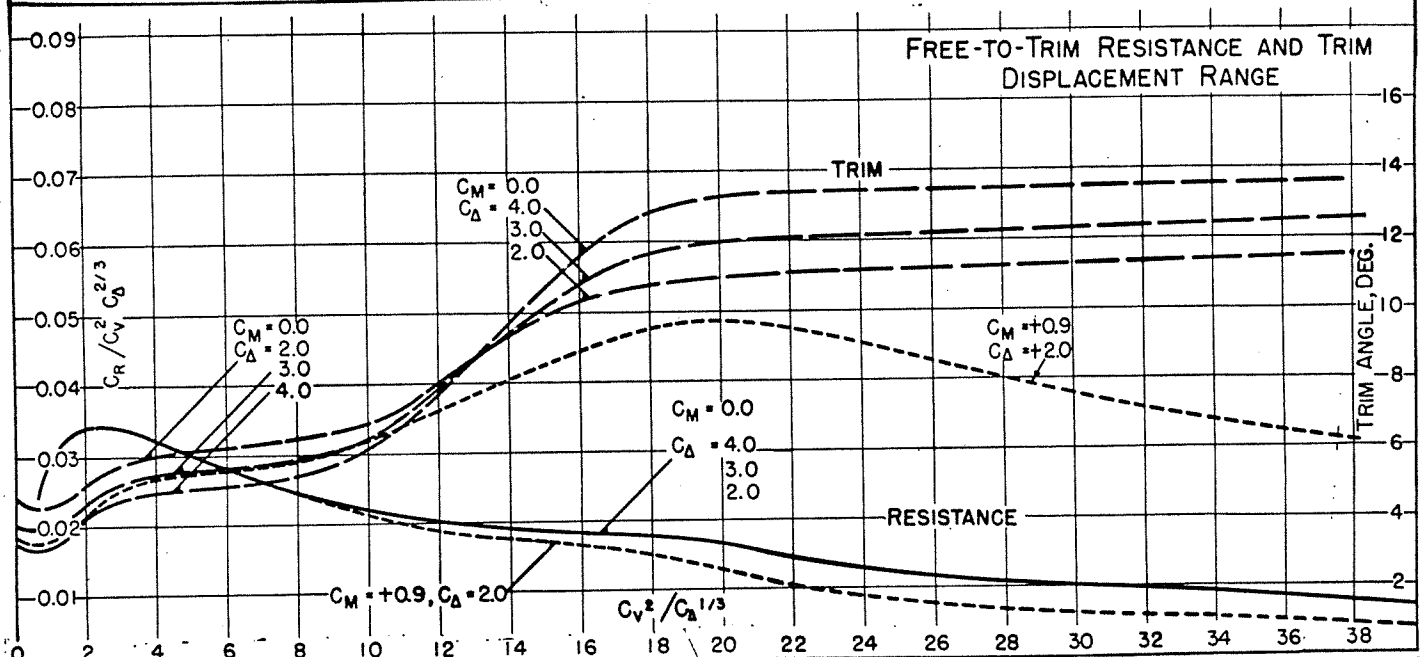
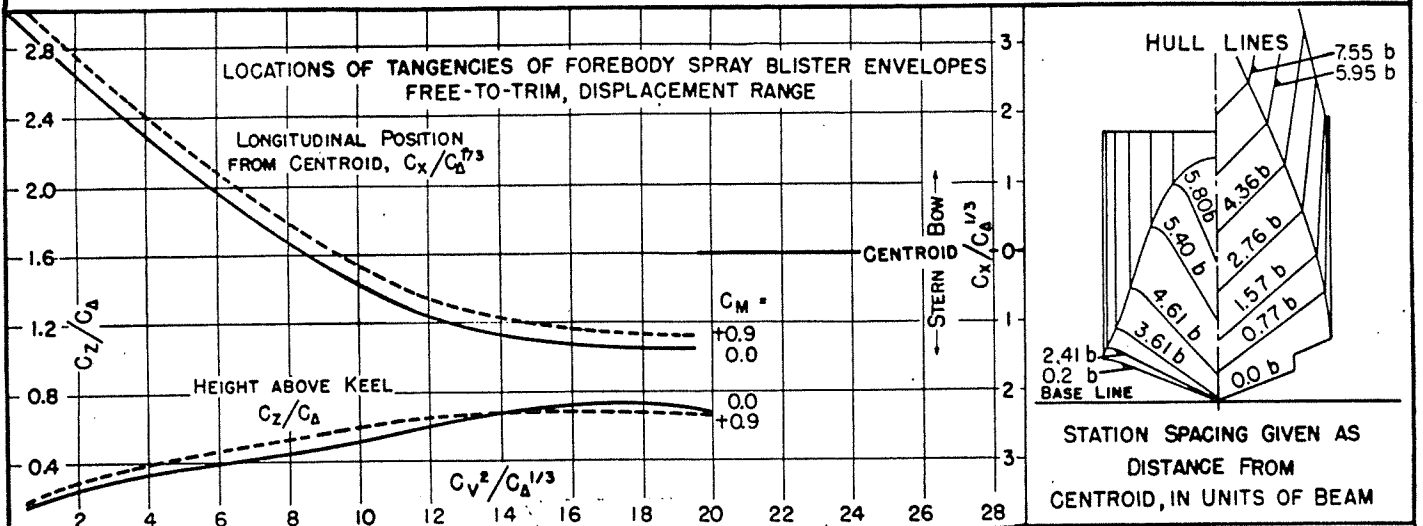


FIGURE 18

DESIGNATION: 8-6-112-22

MODEL NO. 1069-02-06 C.G. = 0.44 b FWD. OF CENTROID $C_{b_0} = 3.32$ (NOMINAL) TESTED AT E.T.T. NO. 3 TANK
 MODEL BEAM: 4.10" 1.59 b ABOVE KEEL $k/L =$ DATE: NOV. 21, 1951

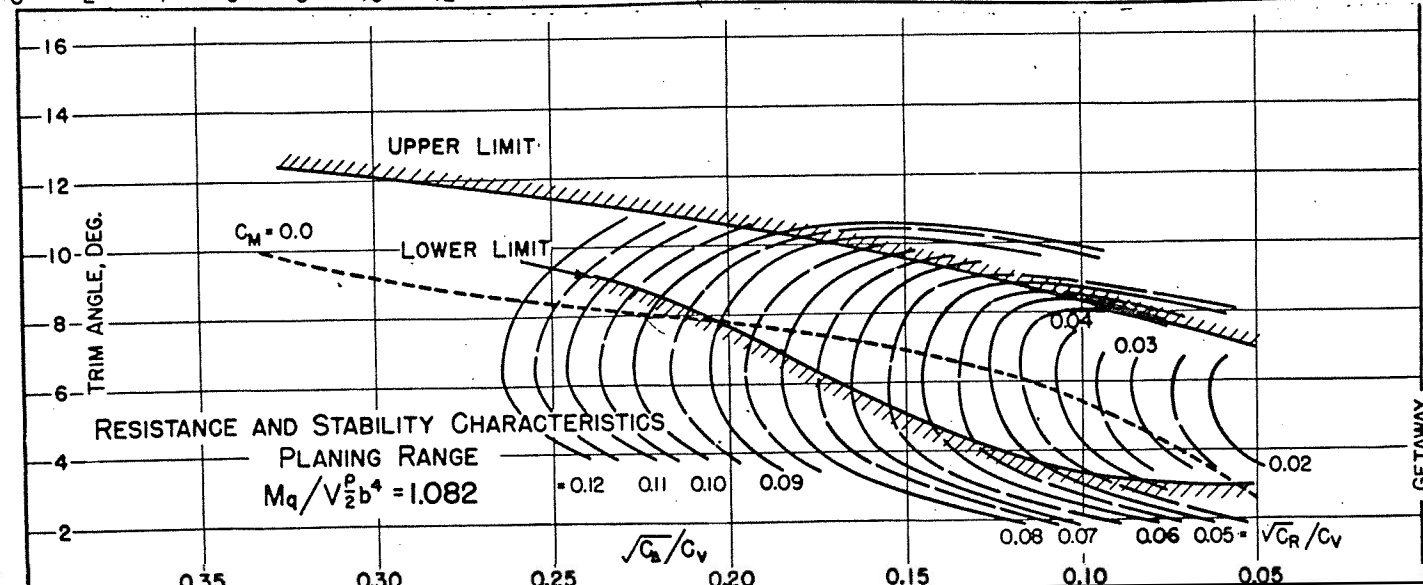
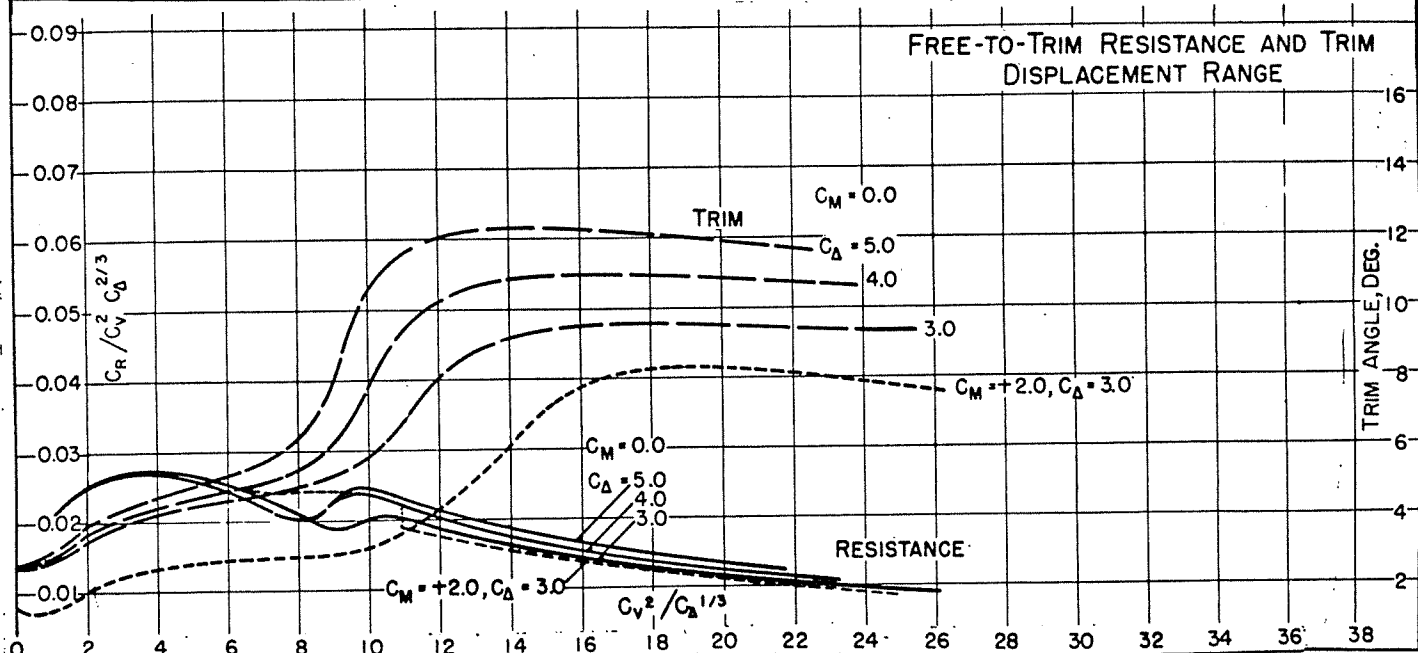
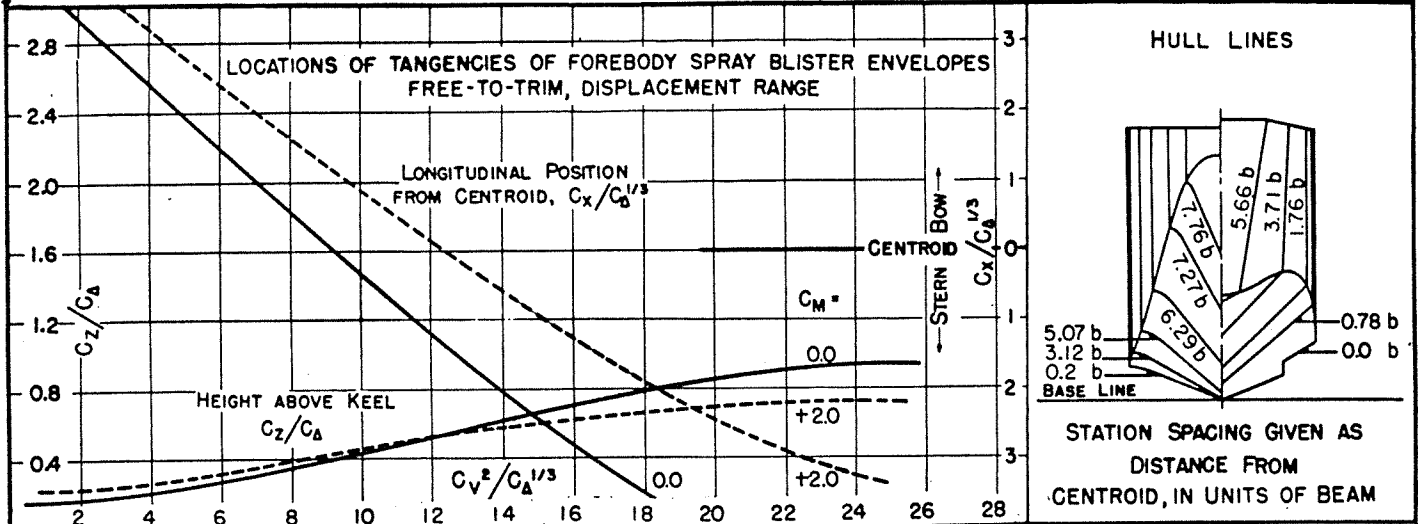


FIGURE 19

DESIGNATION: 8-6-0.67-22

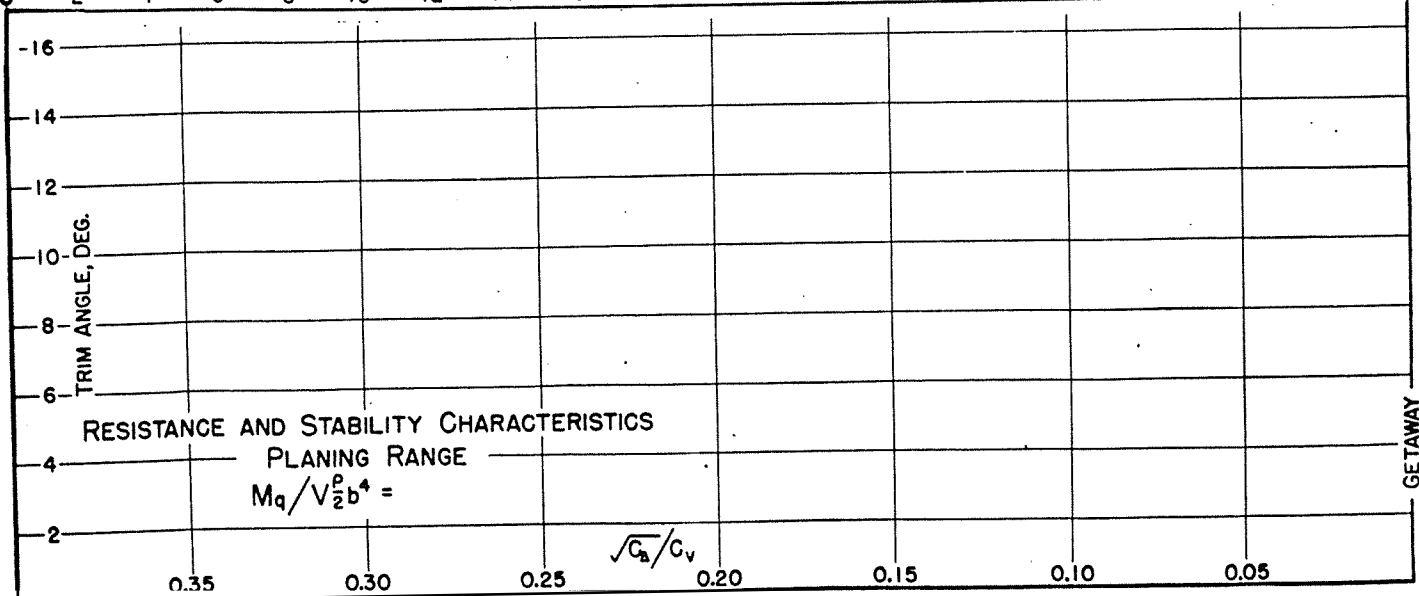
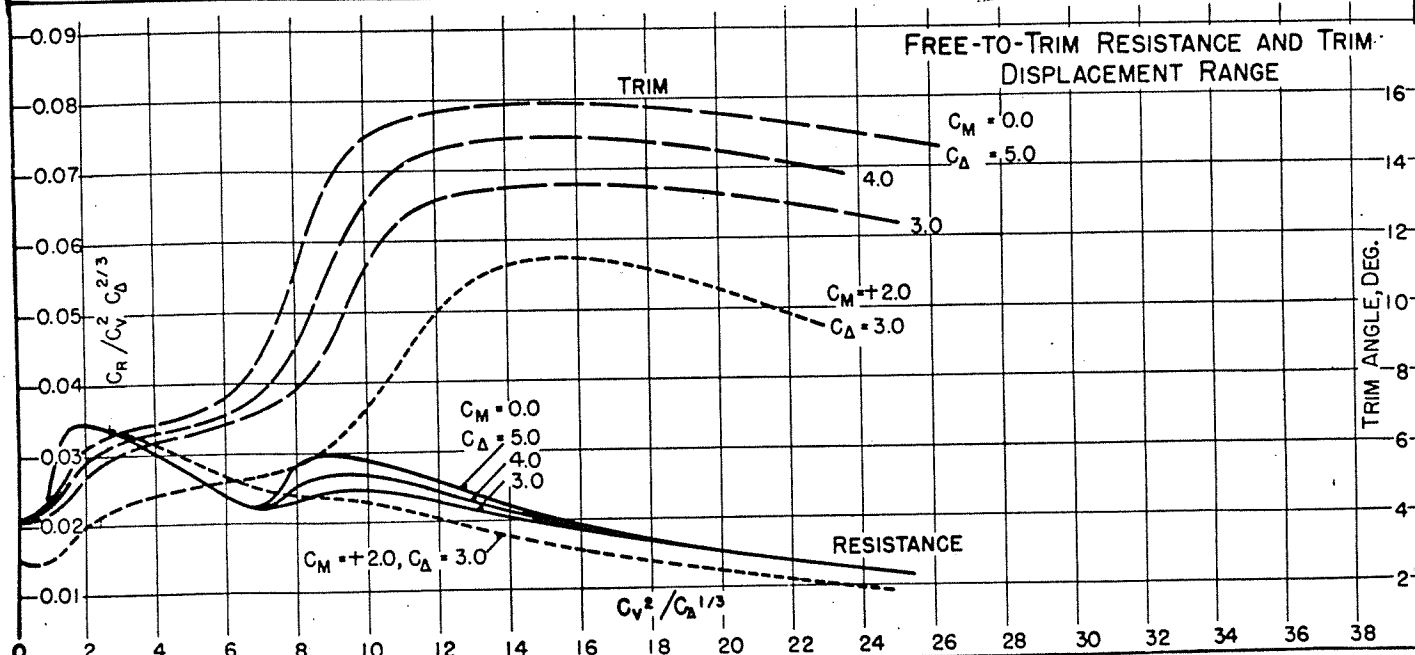
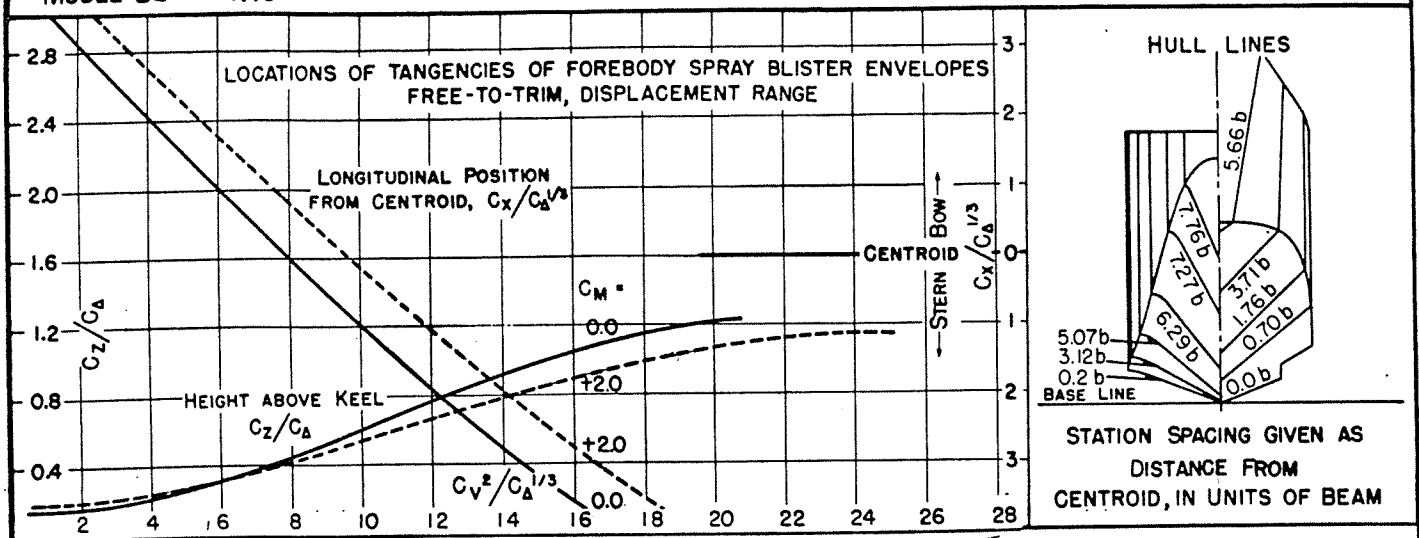
MODEL NO. 1069-02-10 C.G. = 0.44 b FWD. OF CENTROID $C_{\Delta} = 3.32$ (NOMINAL)
MODEL BEAM: 4.10" 1.59 b ABOVE KEEL $k/L =$ TESTED AT E.T.T. NO. 3 TANK
DATE: NOV. 15, 1951

FIGURE 20

DESIGNATION: 8-10-1.12-22

MODEL NO. 1069-01-06 C.G. = 0.44 b FWD. OF CENTROID $C_b = 4.84$ (NOMINAL) TESTED AT E.T.T. NO. 3 TANK
MODEL BEAM: 4.10" 1.59 b ABOVE KEEL $k/L =$ DATE: NOV. 22, 1951

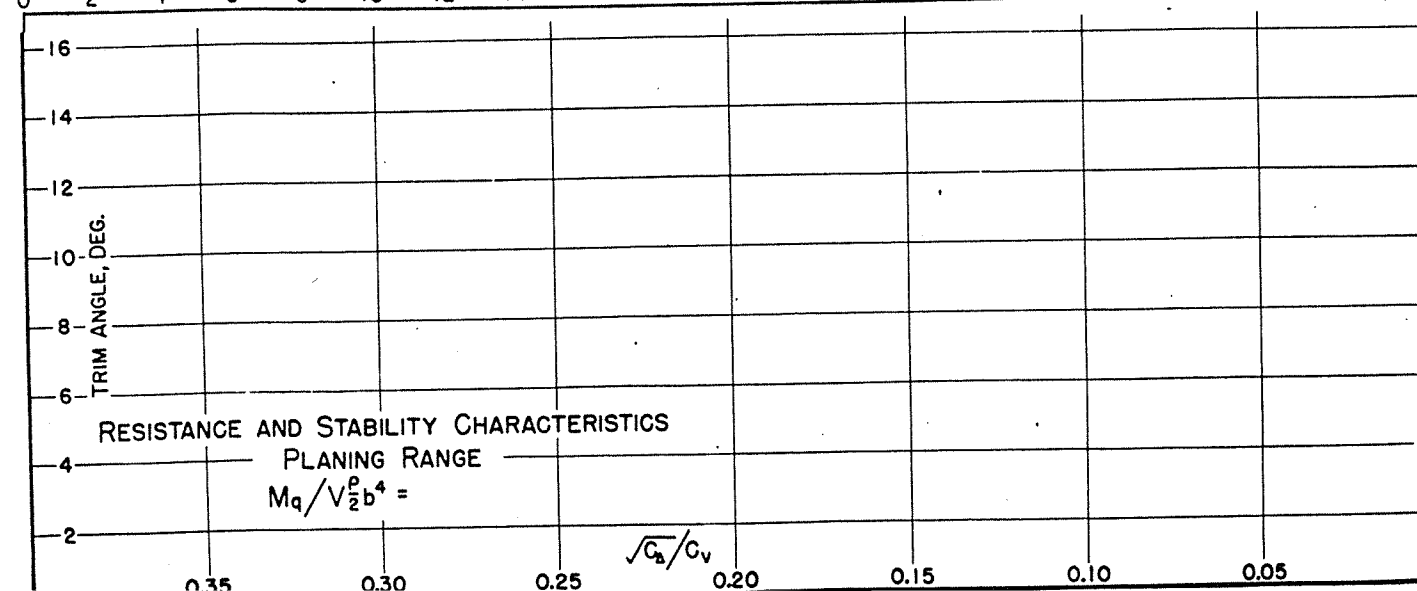
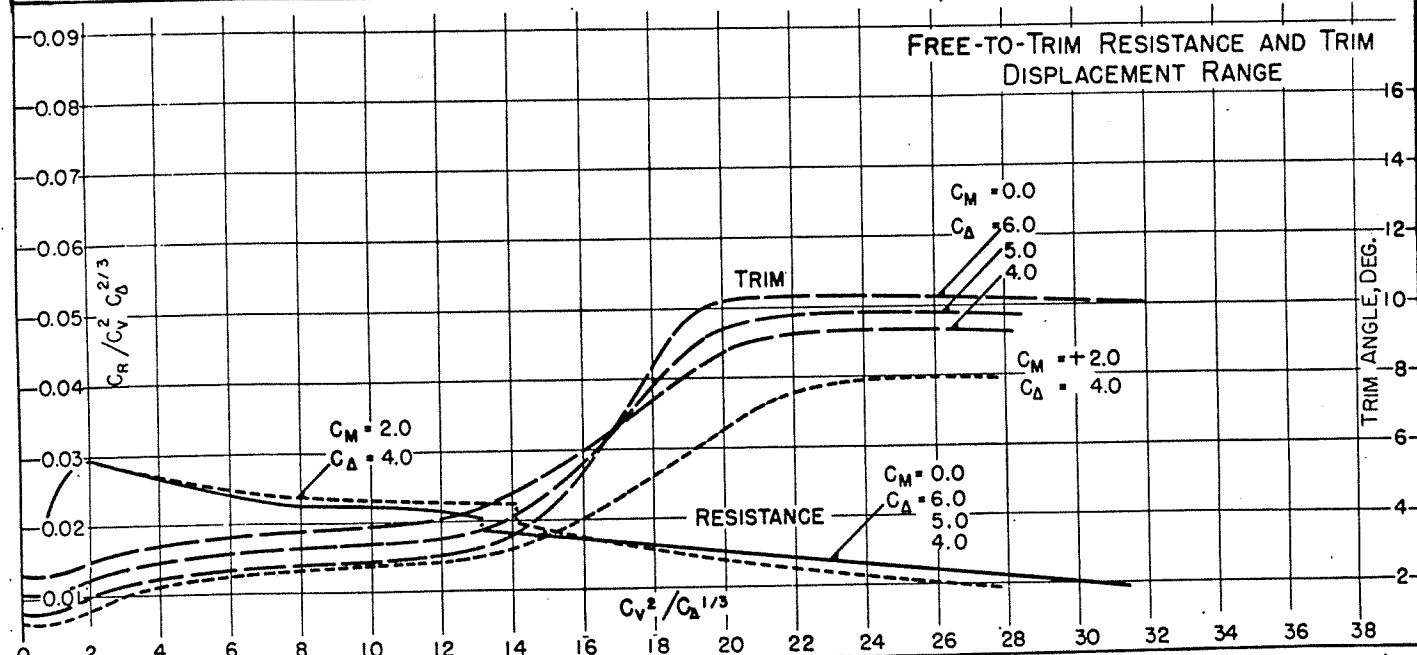
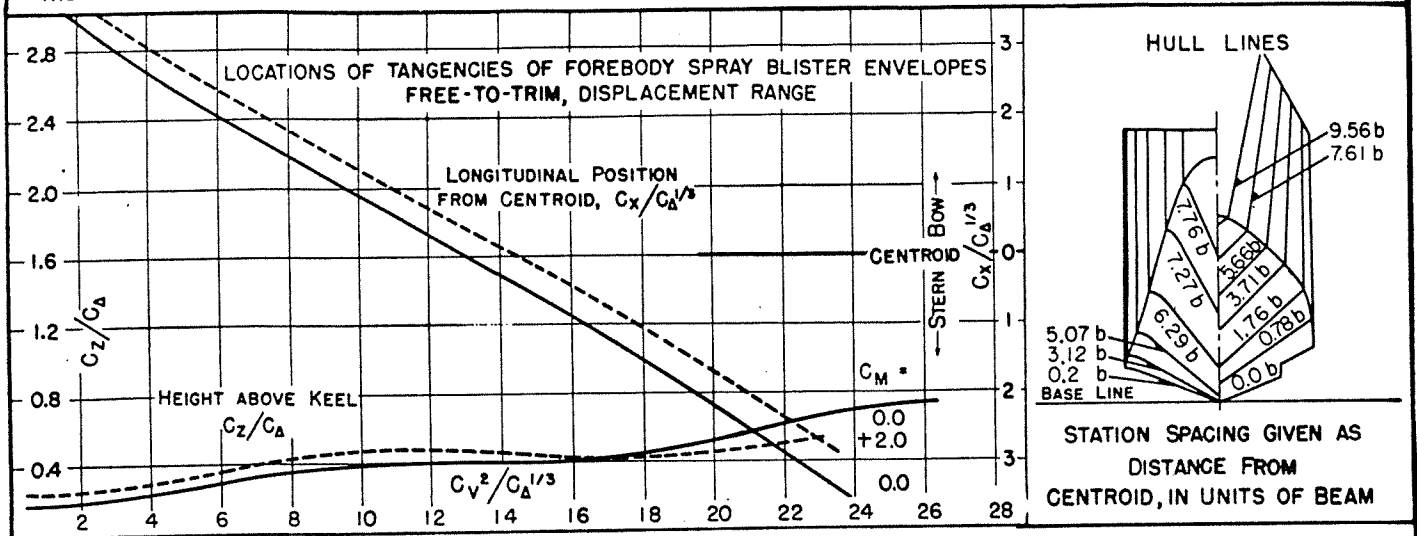


FIGURE 21

DESIGNATION: 8-10-0.67-22

MODEL NO. 1069-01-10
MODEL BEAM: 4.10"C.G. = 0.44 b FWD. OF CENTROID
1.59 b ABOVE KEELC_A = 4.84 (NOMINAL)

k/L =

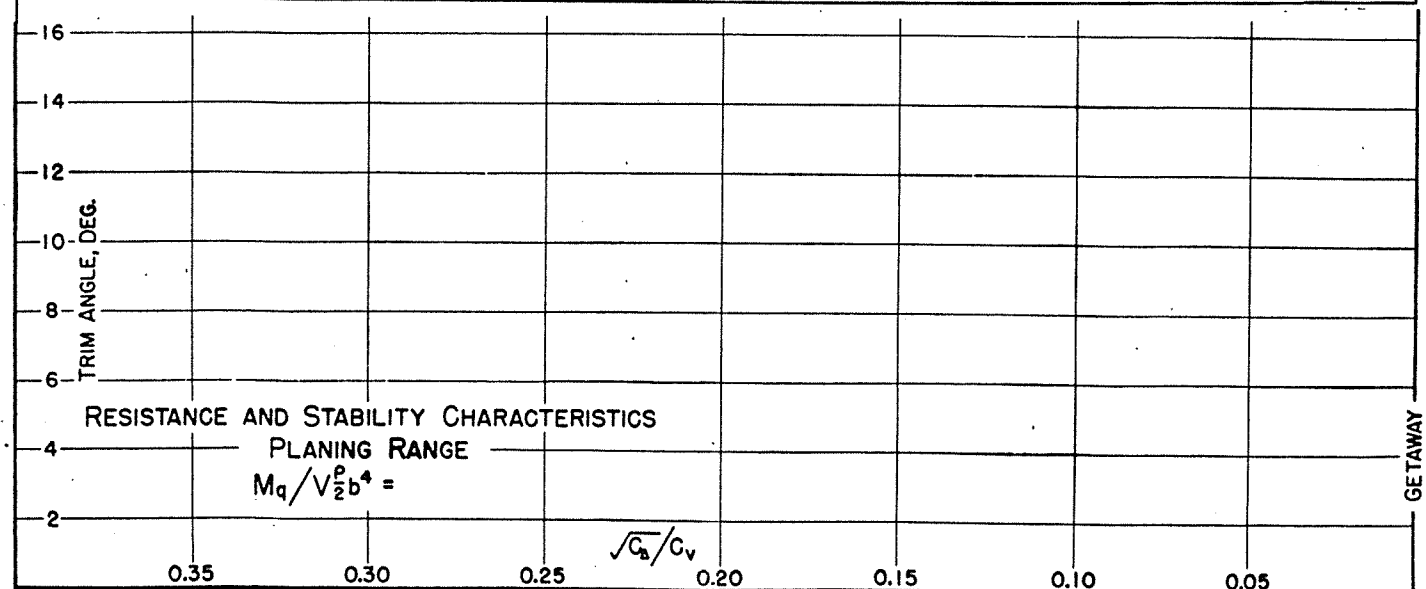
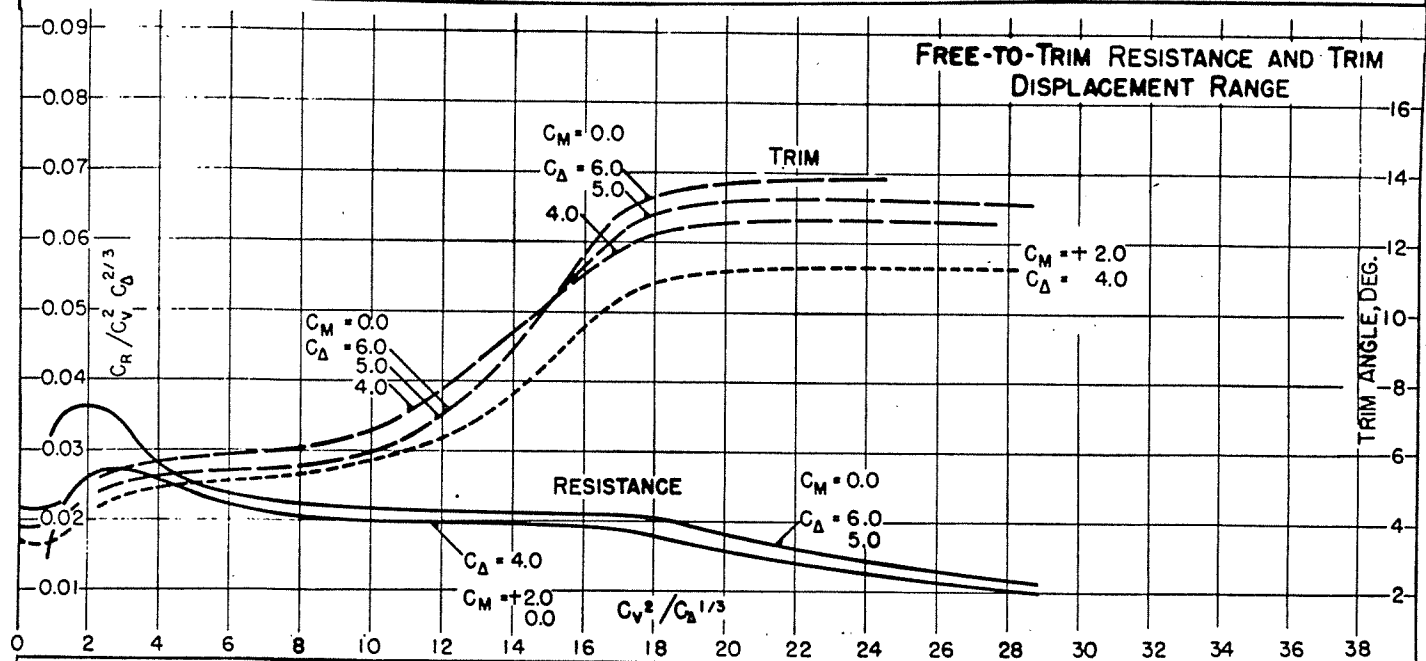
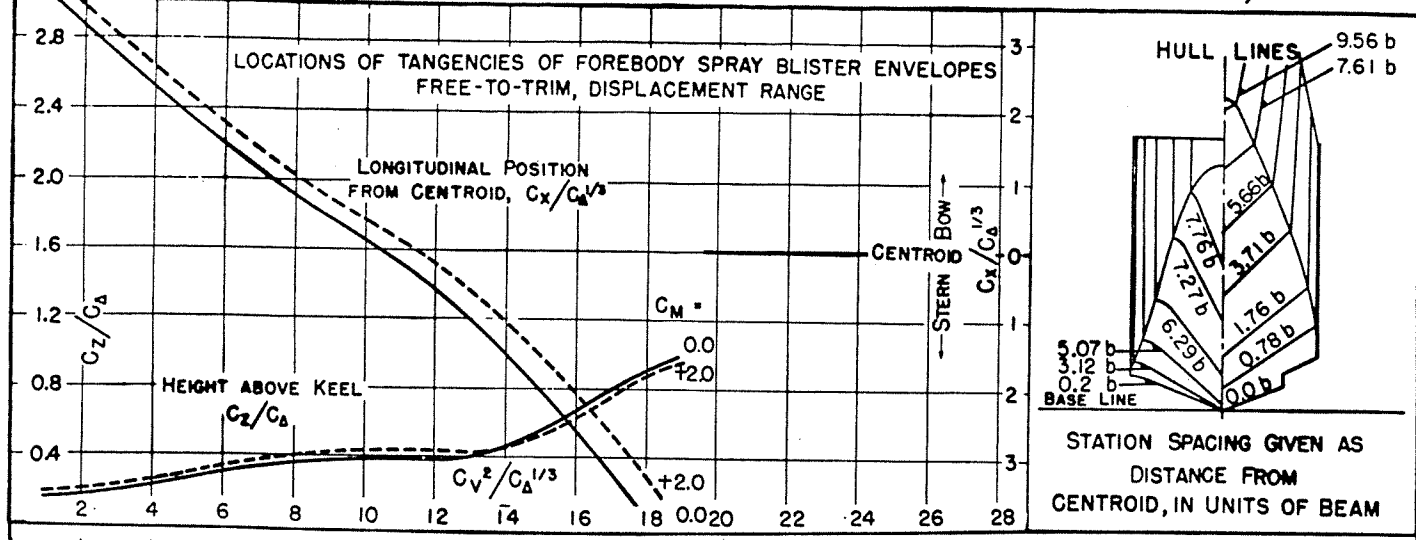
TESTED AT E.T.T. NO. 3 TANK
DATE: NOV. 20, 1951

FIGURE 22

DESIGNATION: 8-16-1.12-22

MODEL NO. 1069-03-06 C.G. = 0.44 b FWD. OF CENTROID $C_A = 7.44$ (NOMINAL)
 MODEL BEAM: 4.10" 1.59 b ABOVE KEEL $k/L =$ TESTED AT E.T.T. NO. 3 TANK
 DATE: NOV. 27, 1951

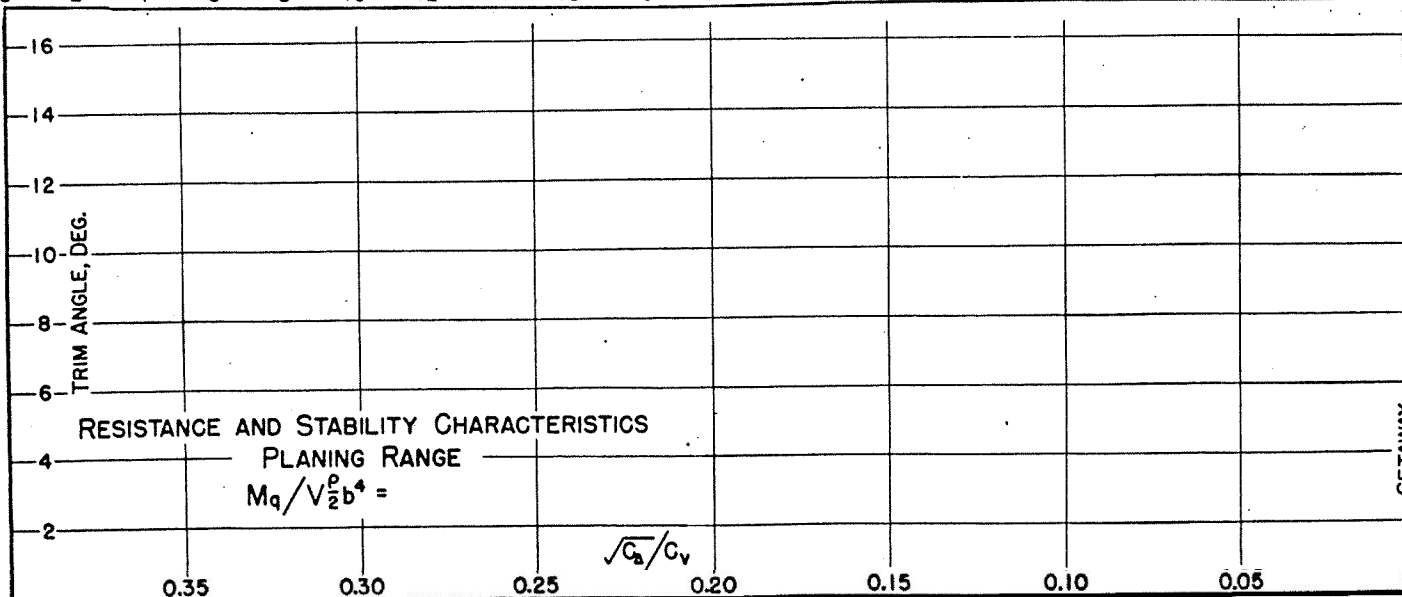
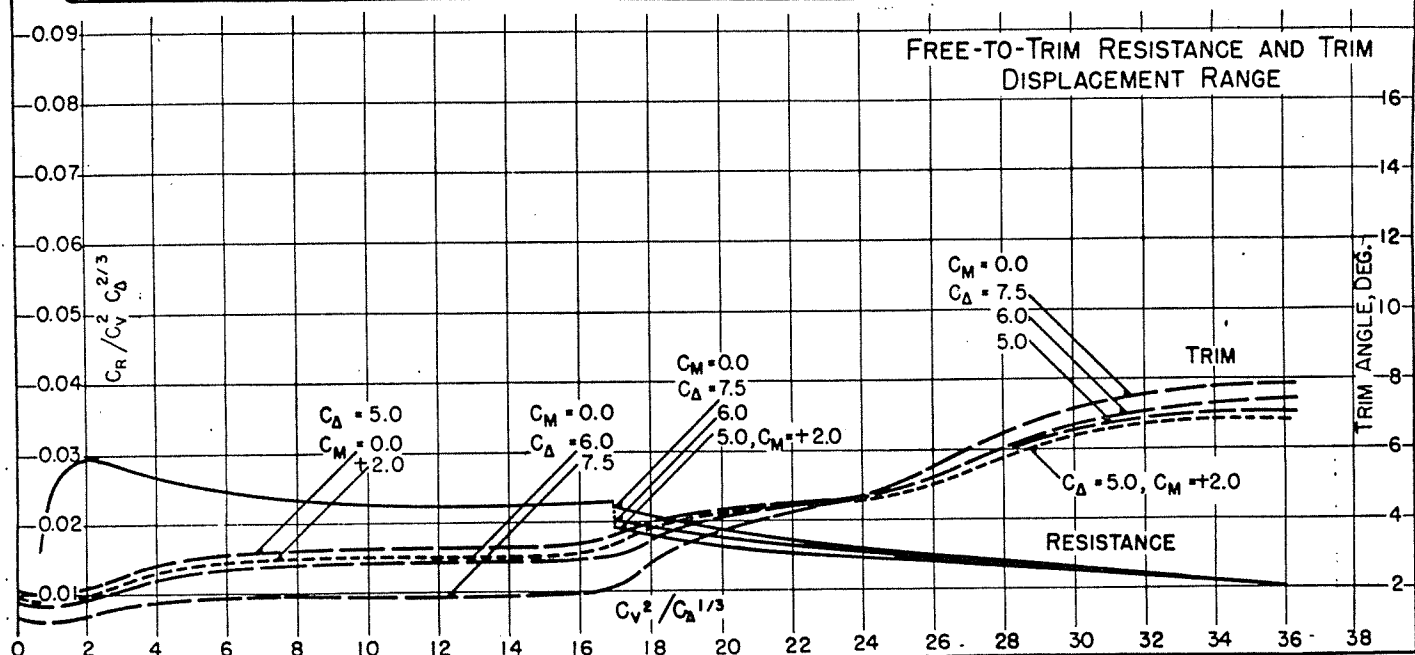
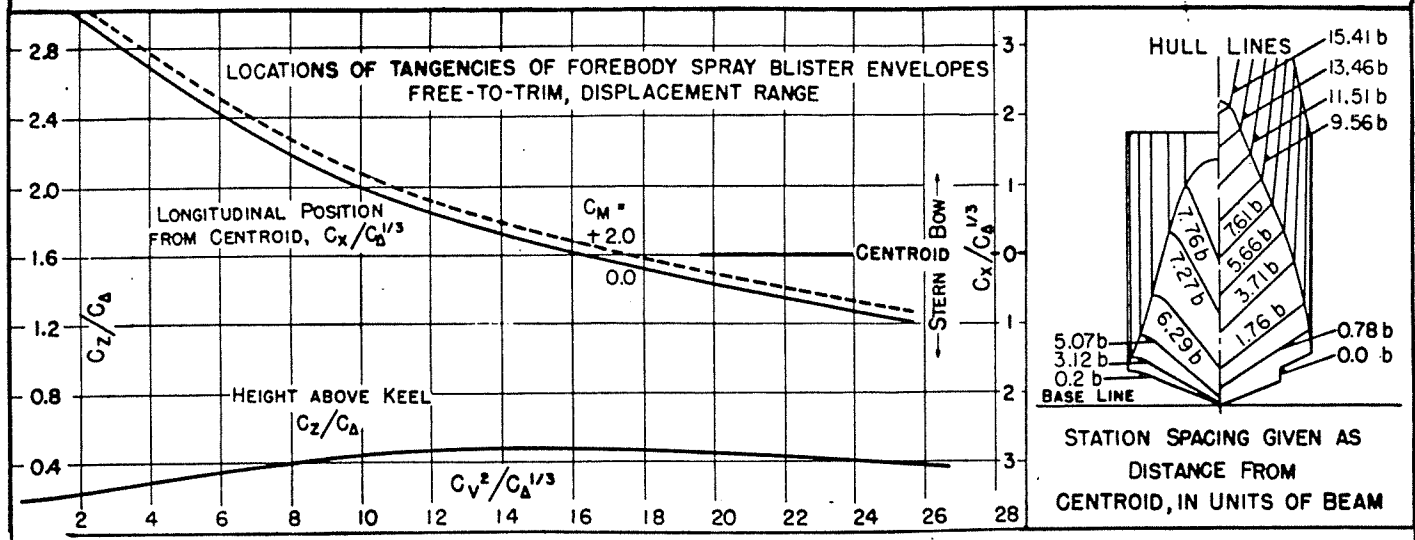
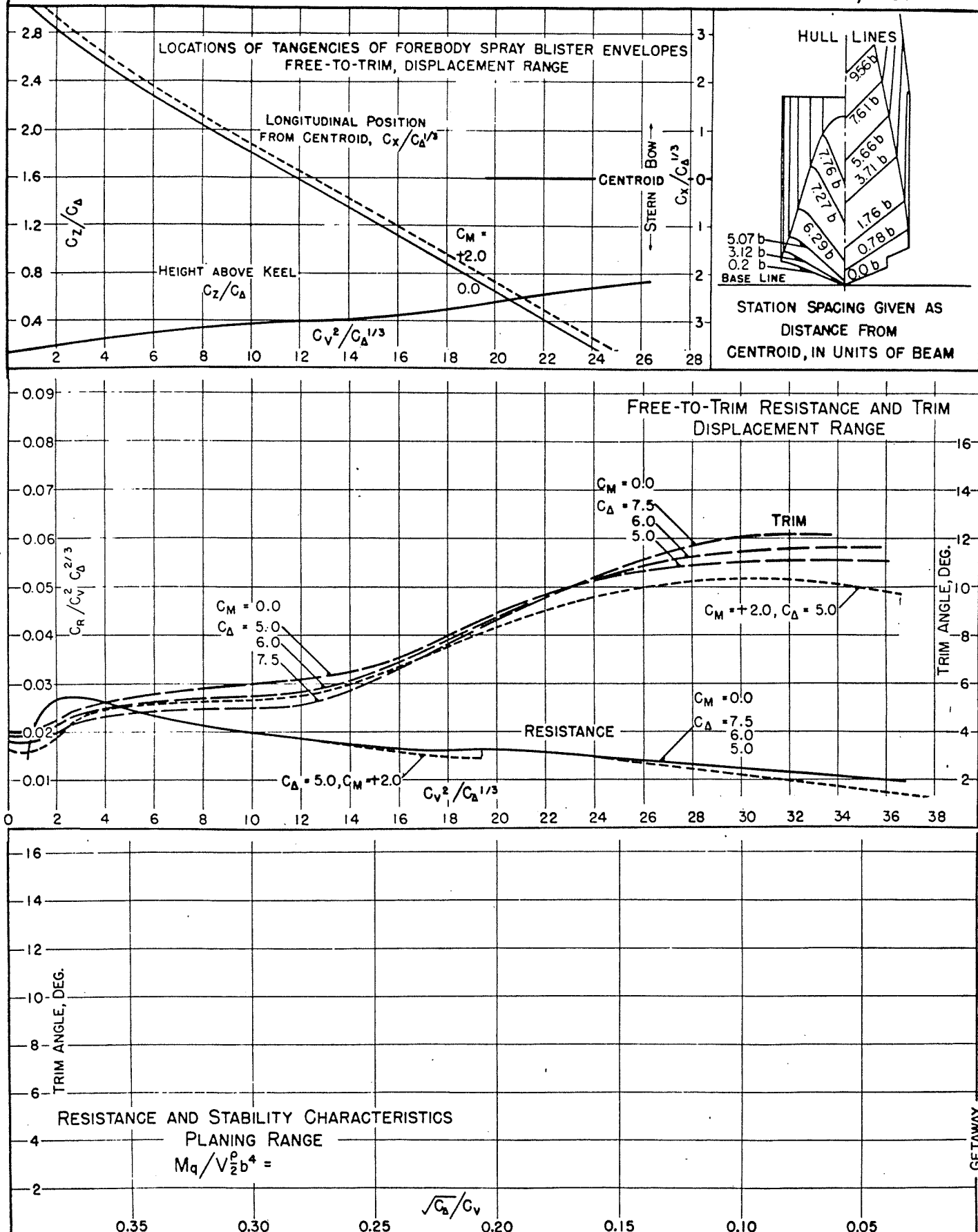


FIGURE 23

DESIGNATION: 8-16-0.67-22

MODEL NO. 1069-03-10 C.G. = 0.44 b FWD. OF CENTROID $C_d = 7.44$ (NOMINAL) TESTED AT E.T.T. No. 3 TANK
MODEL BEAM: 4.10" 1.59 b ABOVE KEEL $k/L =$ DATE: NOV. 14, 1951



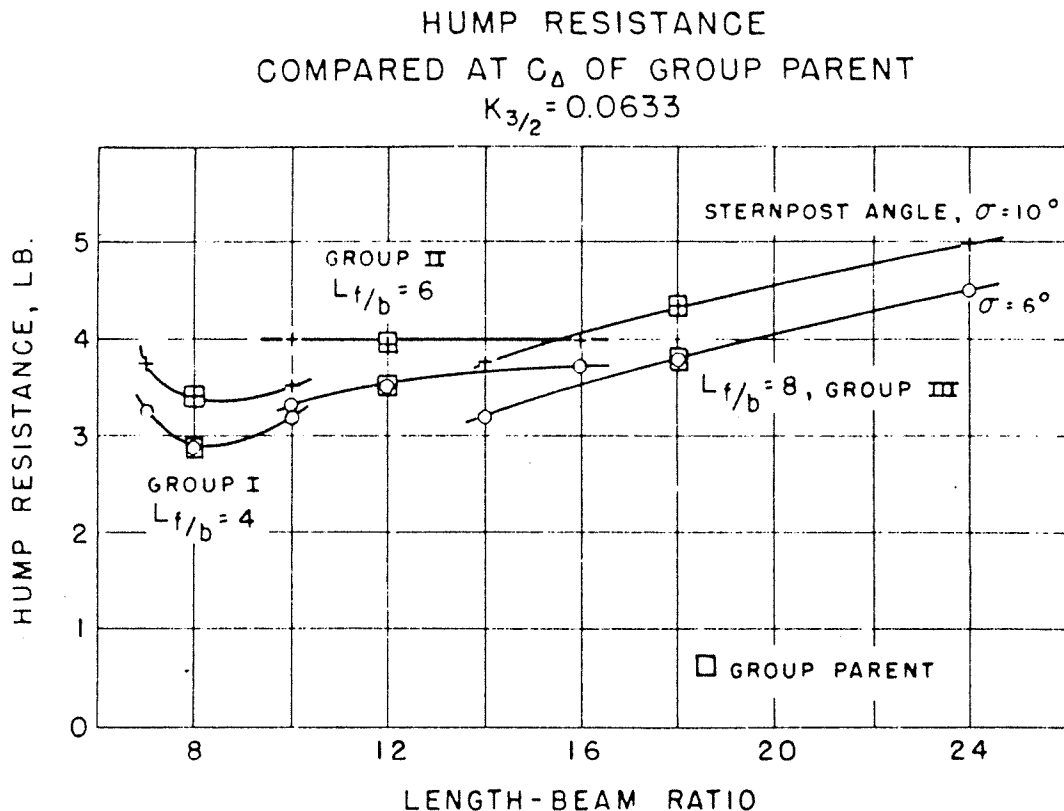


FIGURE 24

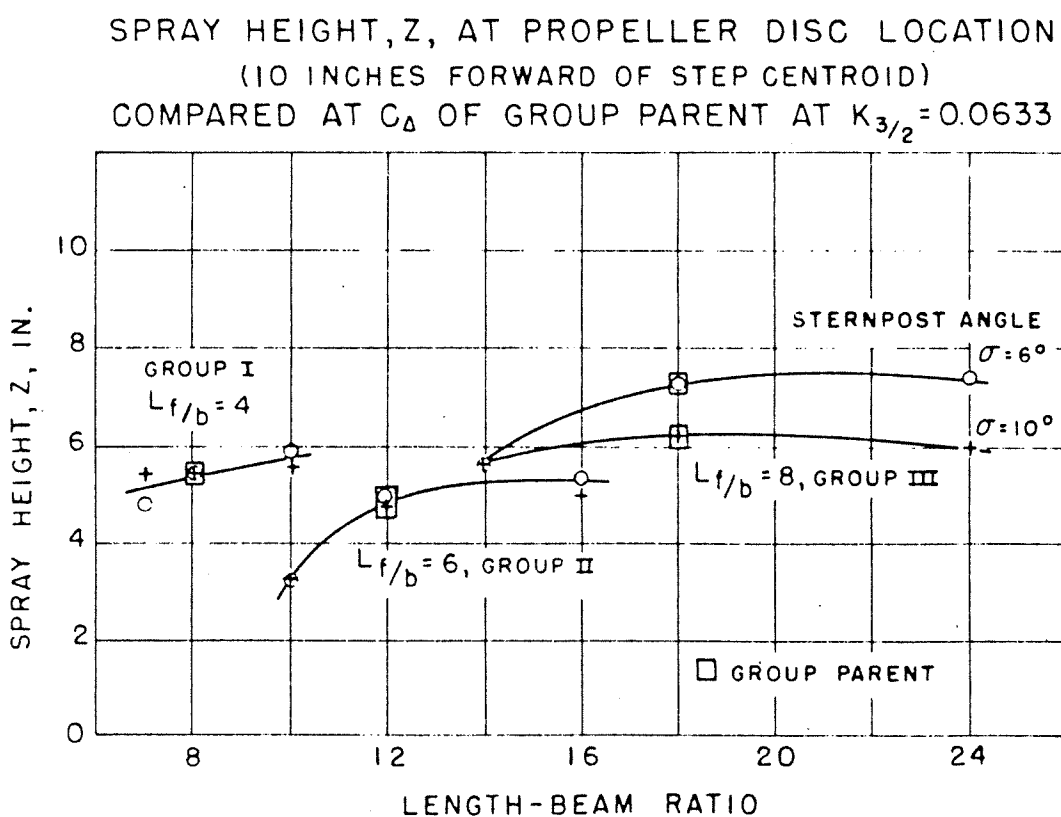


FIGURE 25

HUMP TRIM AT C_D OF GROUP PARENT

$$K_{3/2} = 0.0633$$

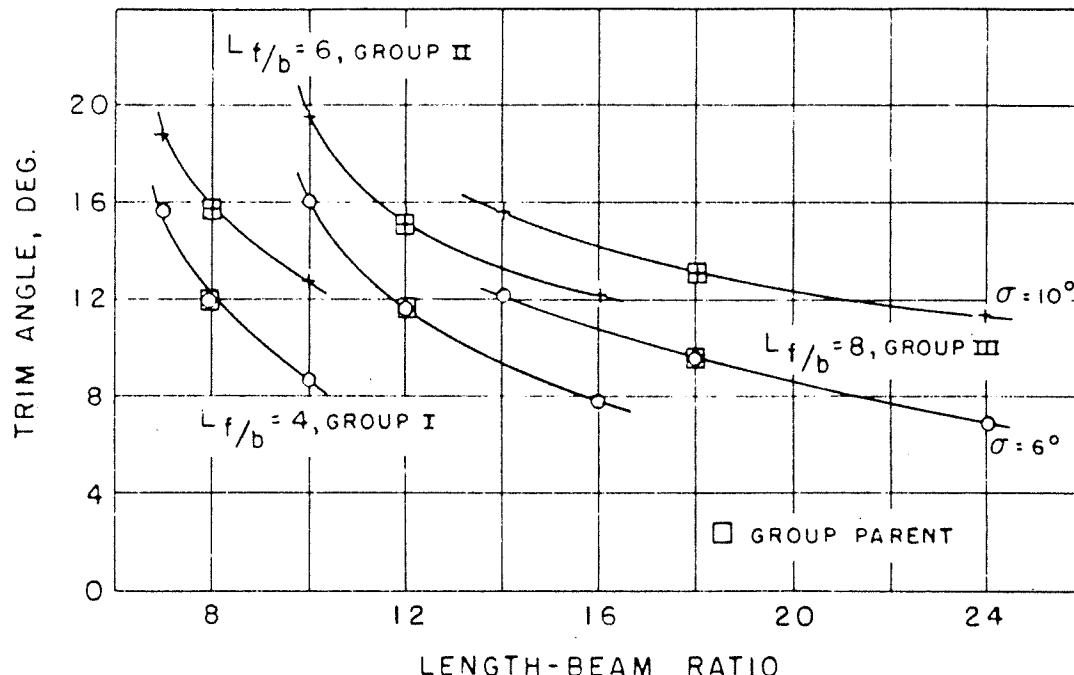


FIGURE 26

HUMP SPEED COEFFICIENT, C_v , AT C_D OF GROUP PARENT

$$K_{3/2} = 0.0633$$

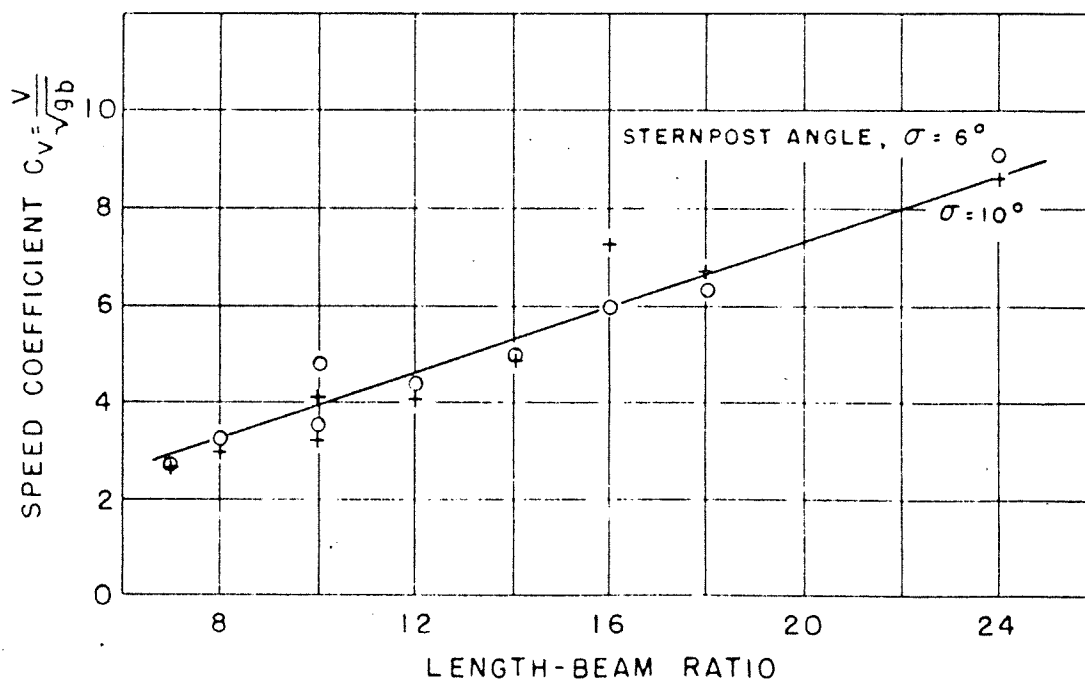


FIGURE 27

SPRAY HEIGHT COEFFICIENT, C_z , AT PROPELLER DISC LOCATION
(10 INCHES FORWARD OF STEP CENTROID)
COMPARED AT C_d OF GROUP PARENT AT $K_{3/2} = 0.0633$

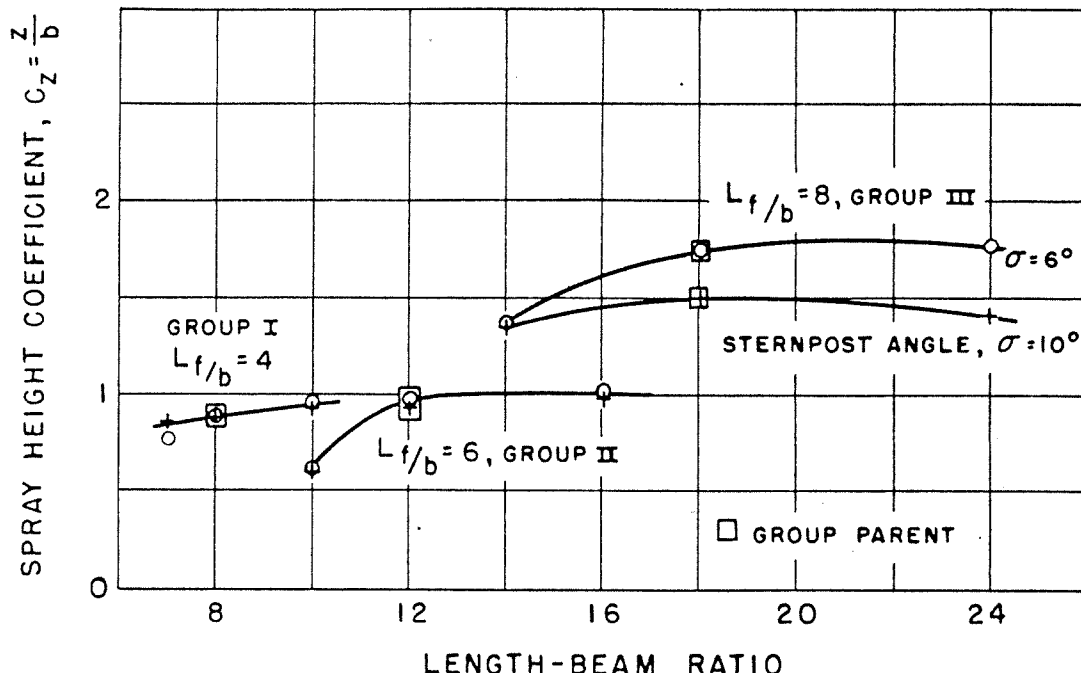


FIGURE 28

SPEED COEFFICIENT, C_v , FOR MAXIMUM SPRAY
AT PROPELLER DISC LOCATION
COMPARED AT C_d OF GROUP PARENT AT $K_{3/2} = 0.0633$

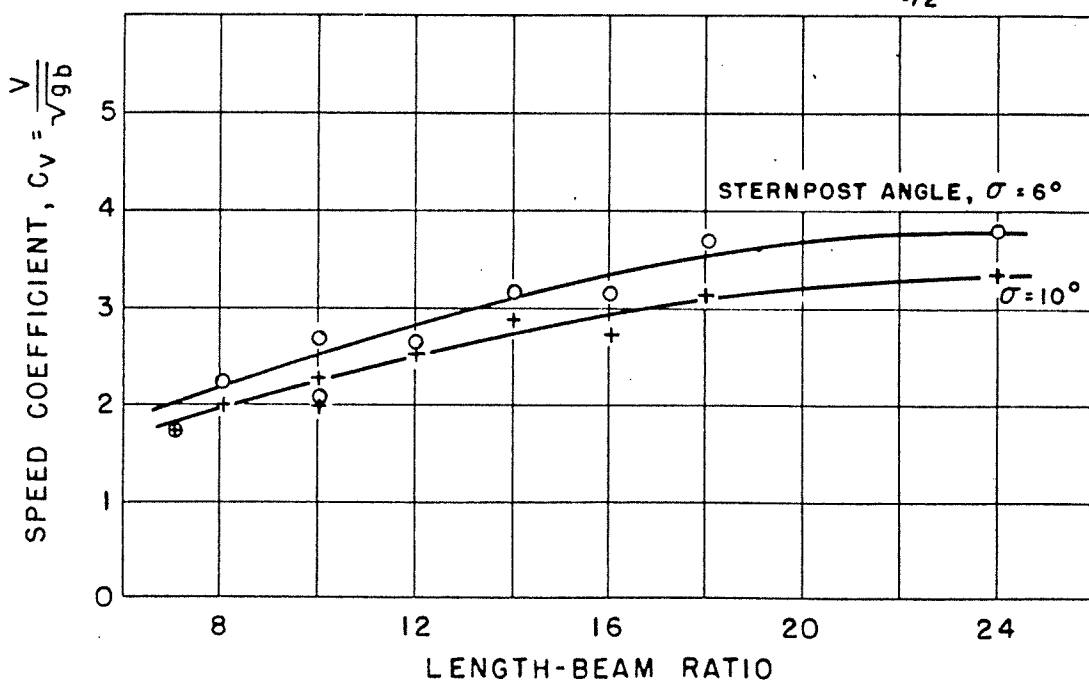


FIGURE 29

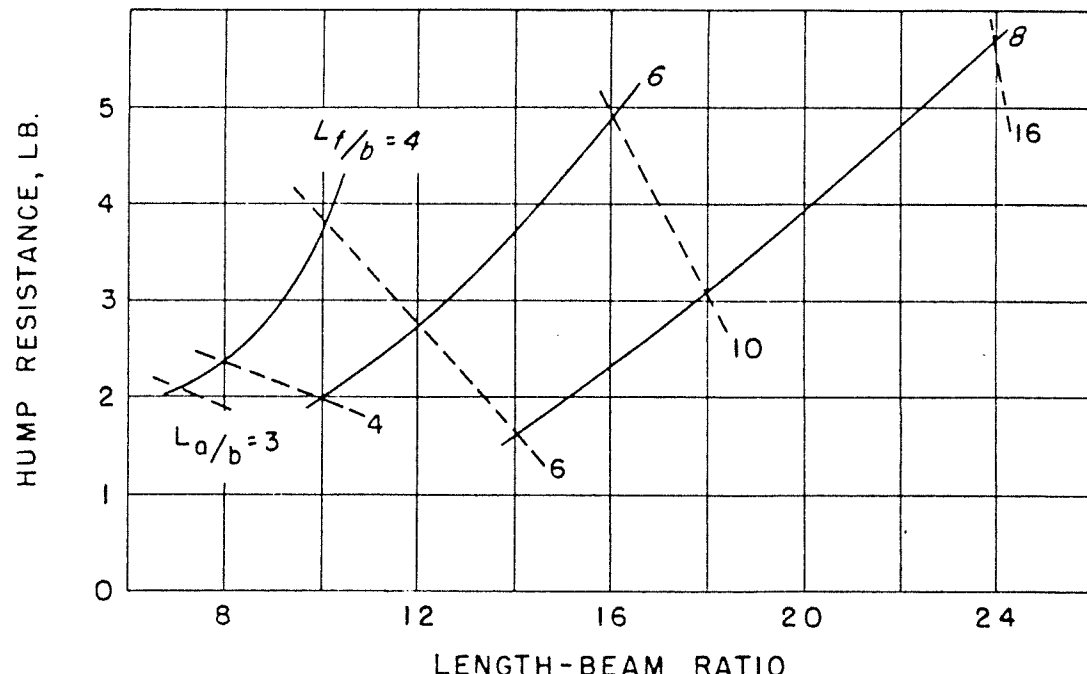
HUMP RESISTANCE AT $K_{3/2} = 0.05$ 

FIGURE 30

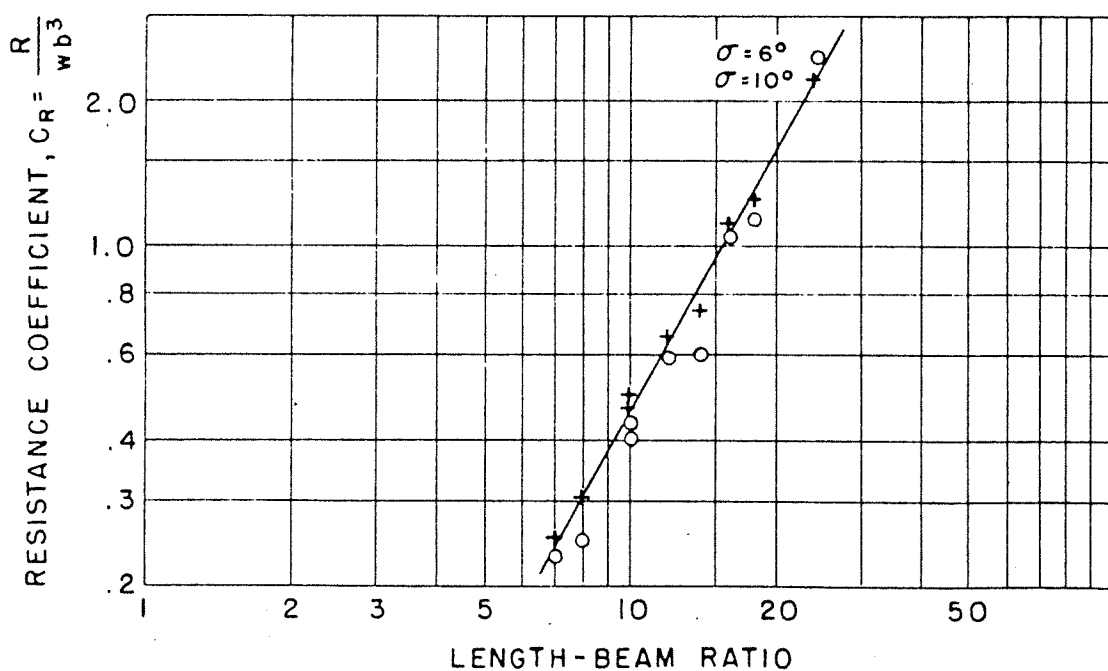
HUMP RESISTANCE COEFFICIENT, C_R AT $K_{3/2} = 0.05$ 

FIGURE 31

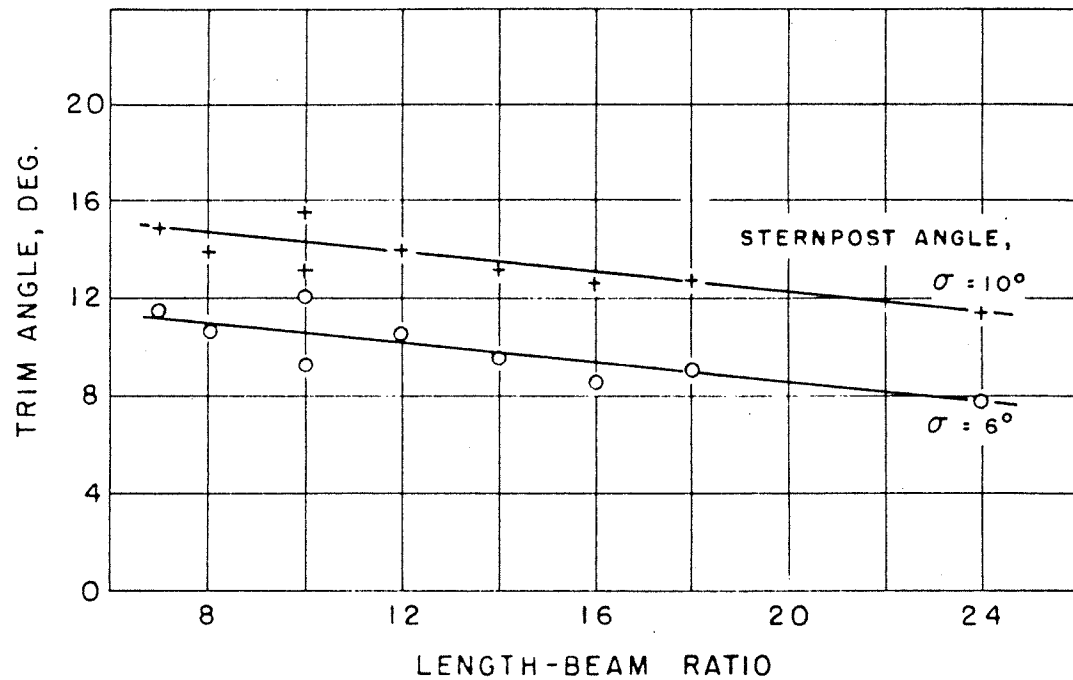
HUMP TRIM AT $K_{3/2} = 0.05$ 

FIGURE 32

SPRAY HEIGHT, Z, AT PROPELLER DISC LOCATION

(10 INCHES FORWARD OF STEP CENTROID)

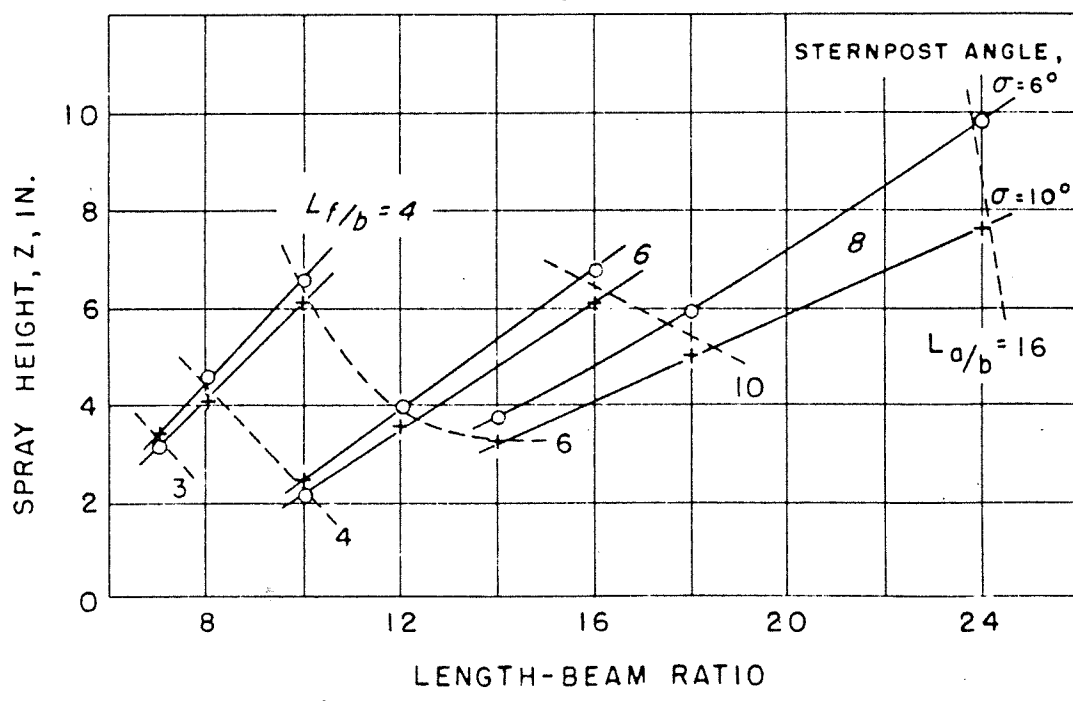
 $K_{3/2} = 0.05$ 

FIGURE 33

C_R/C_Δ AT ZERO MOMENT TRIM

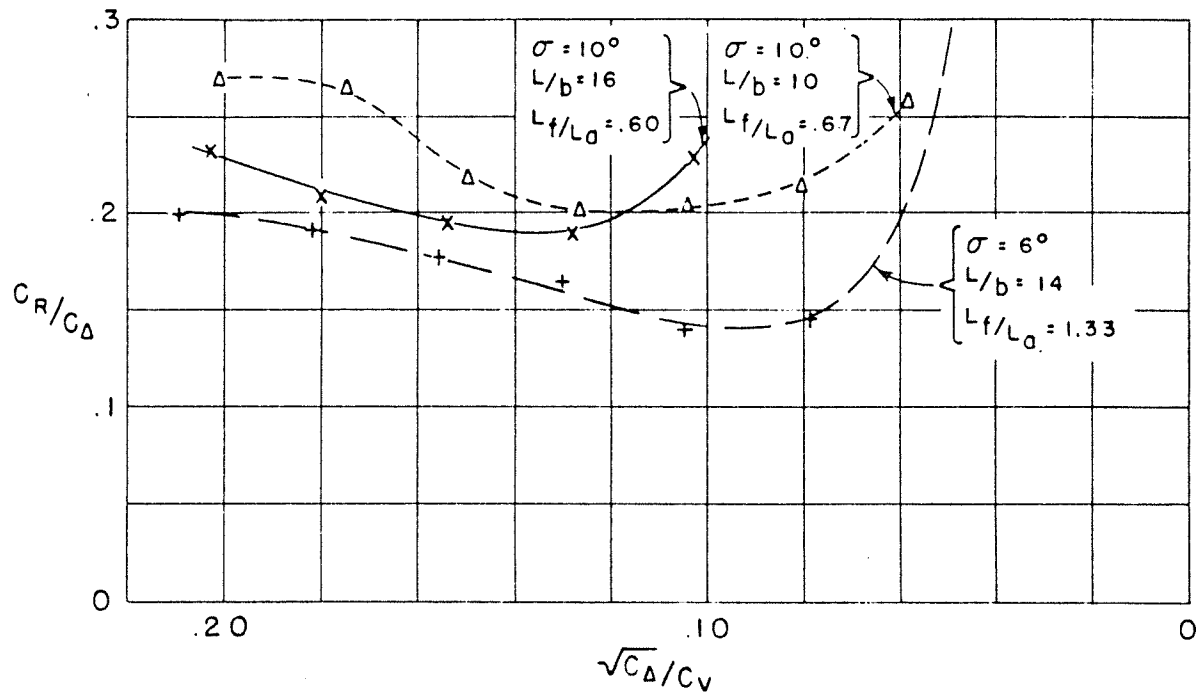


FIGURE 34A

C_R/C_Δ AT BEST TRIM

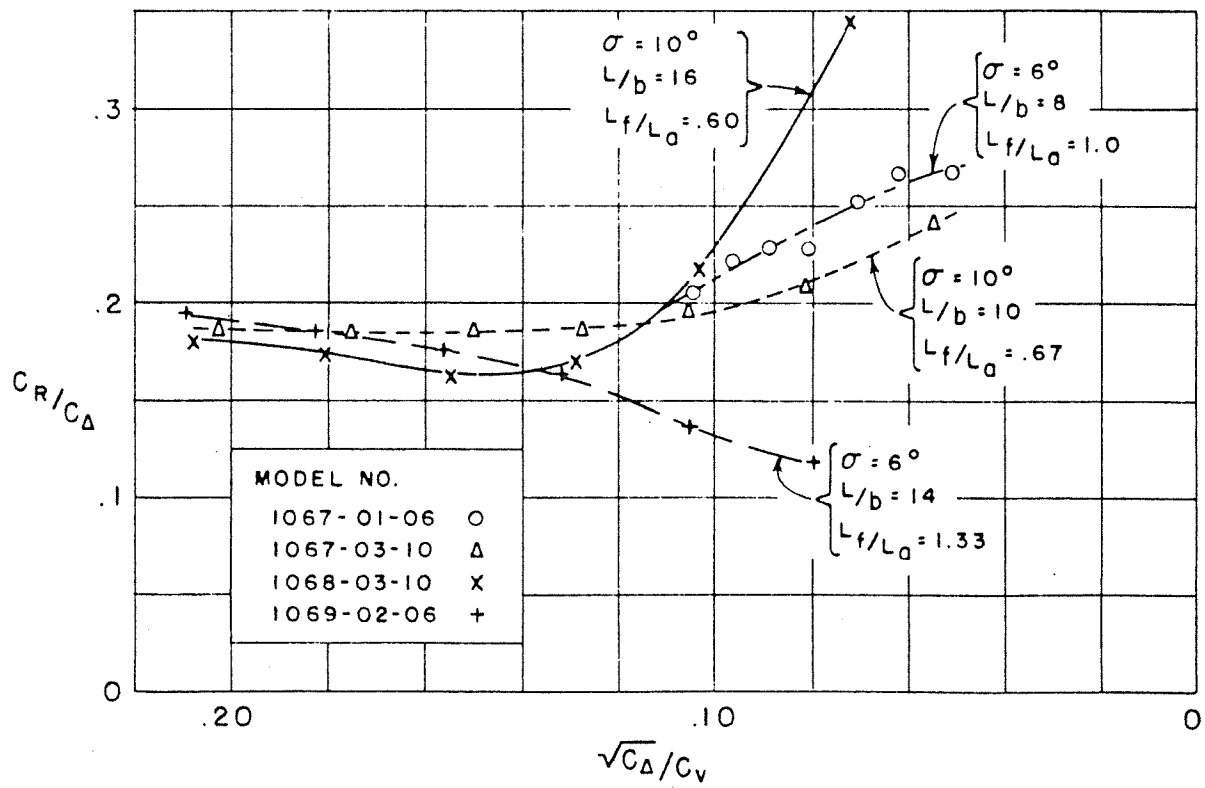
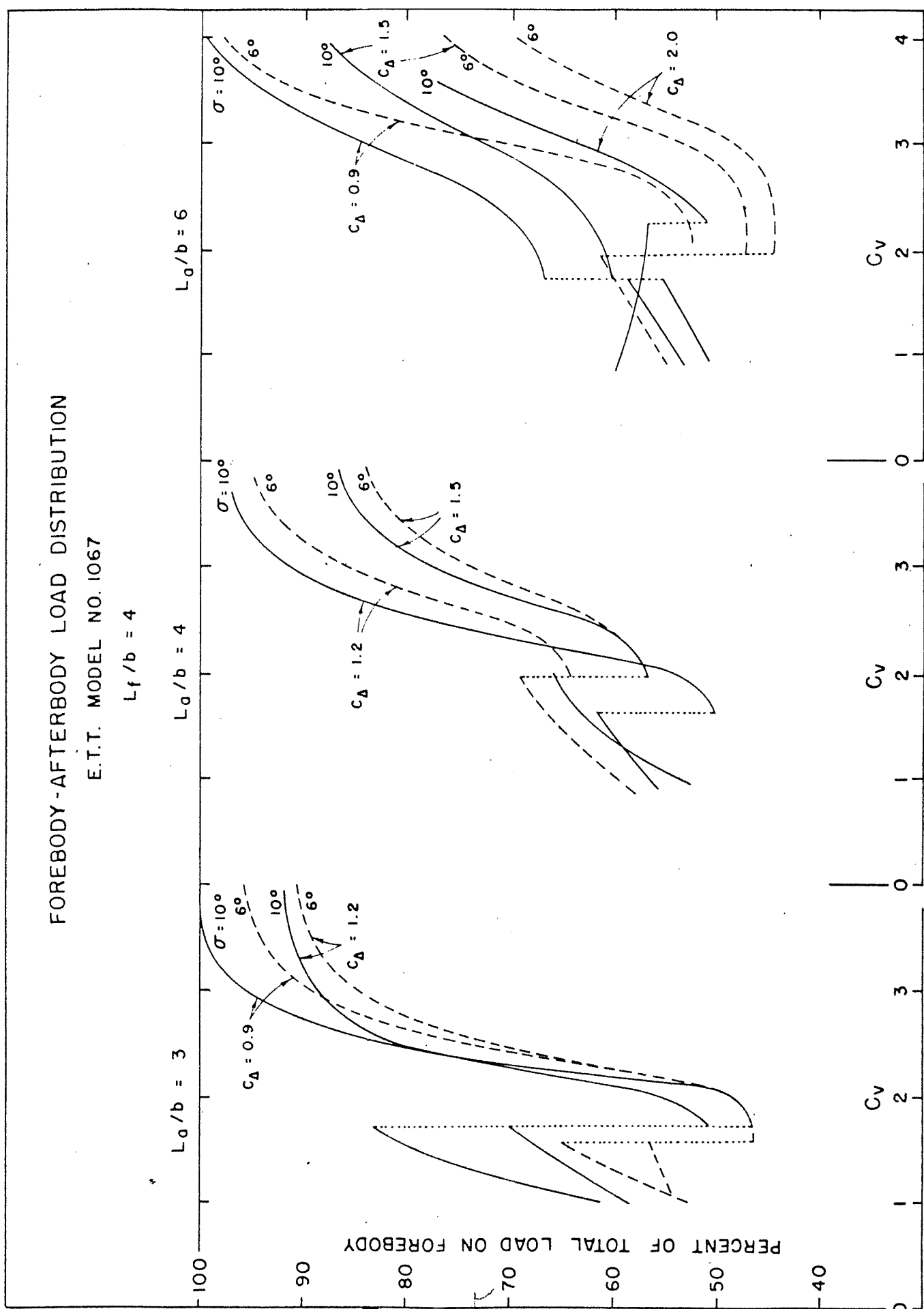
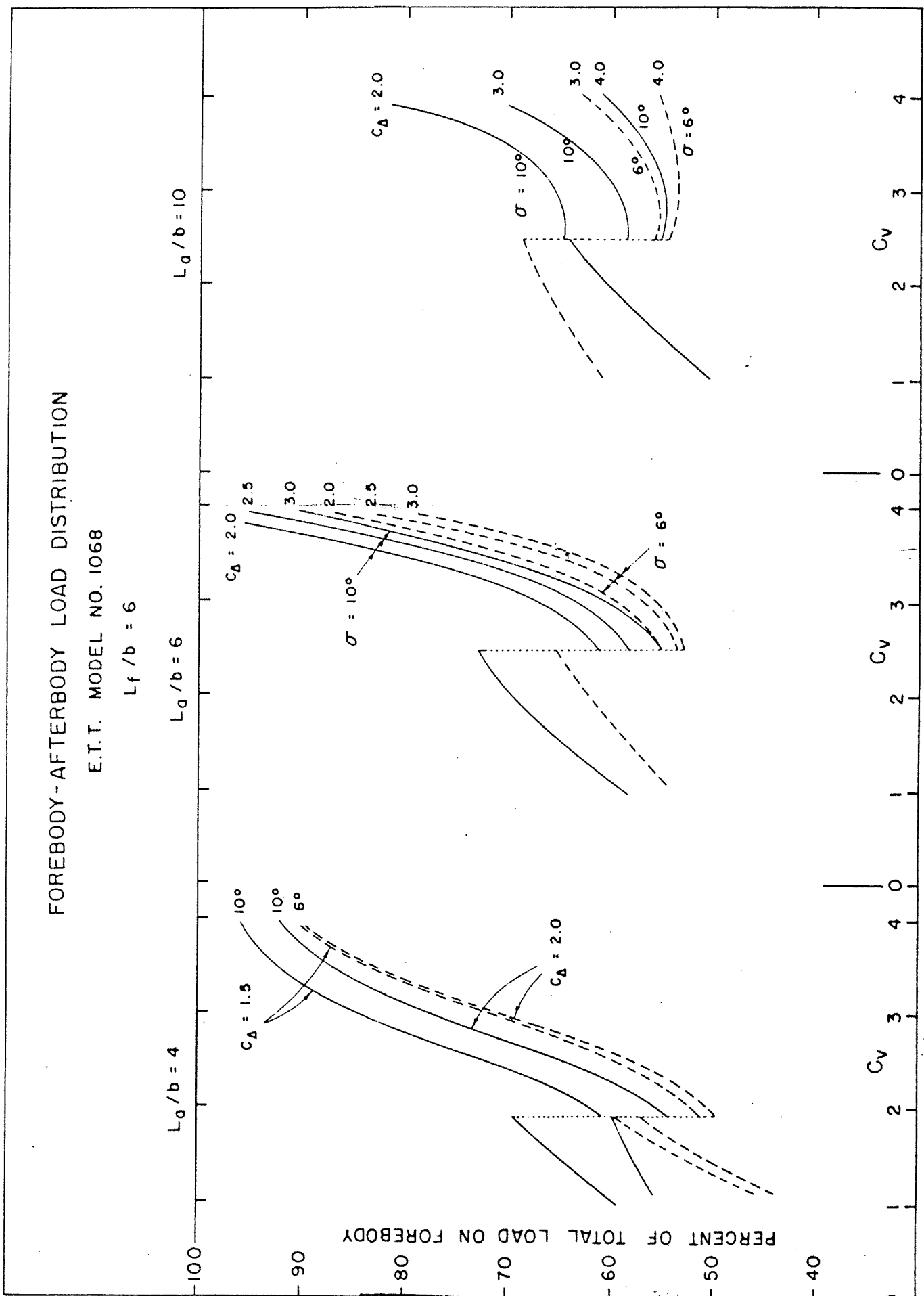
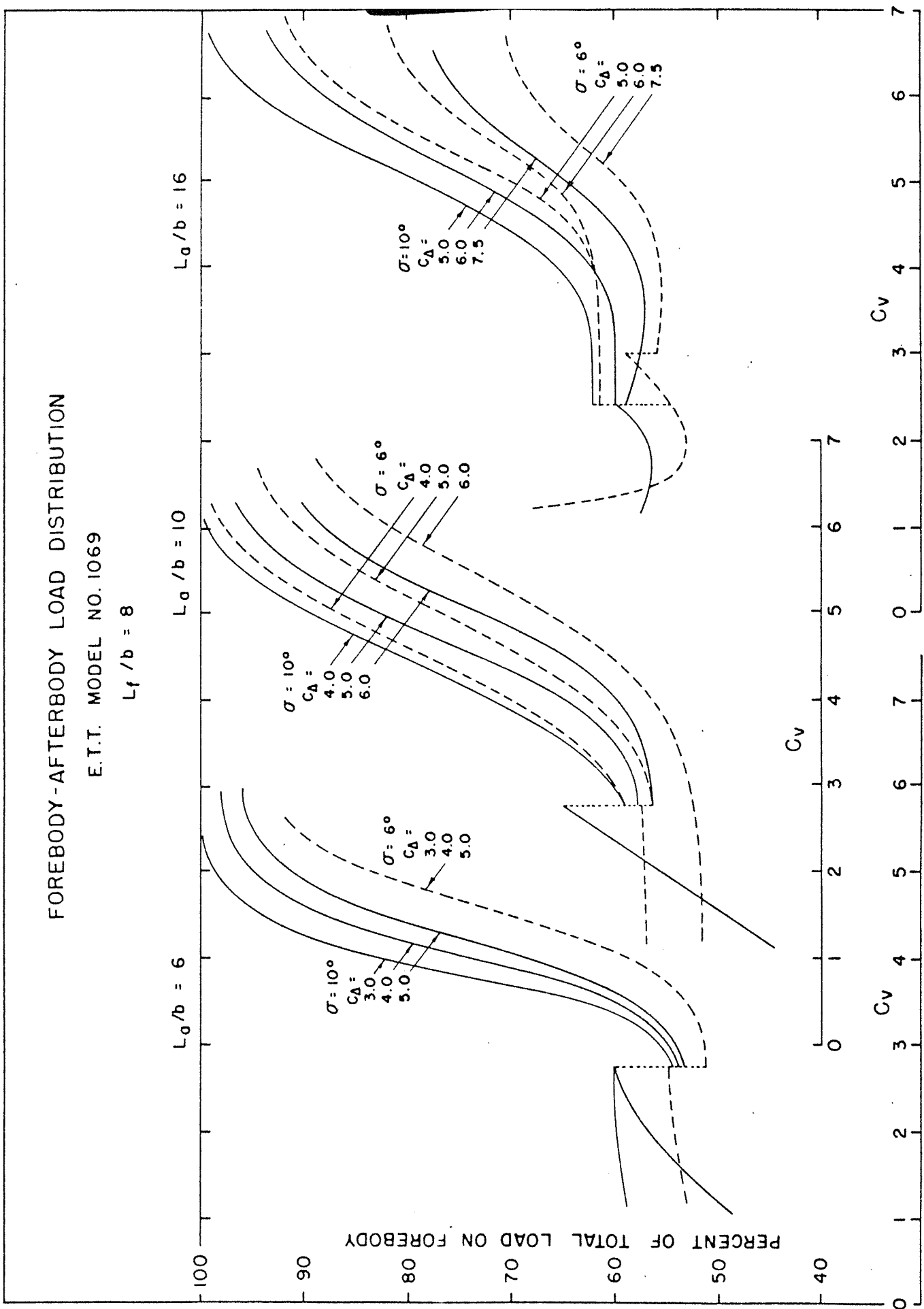
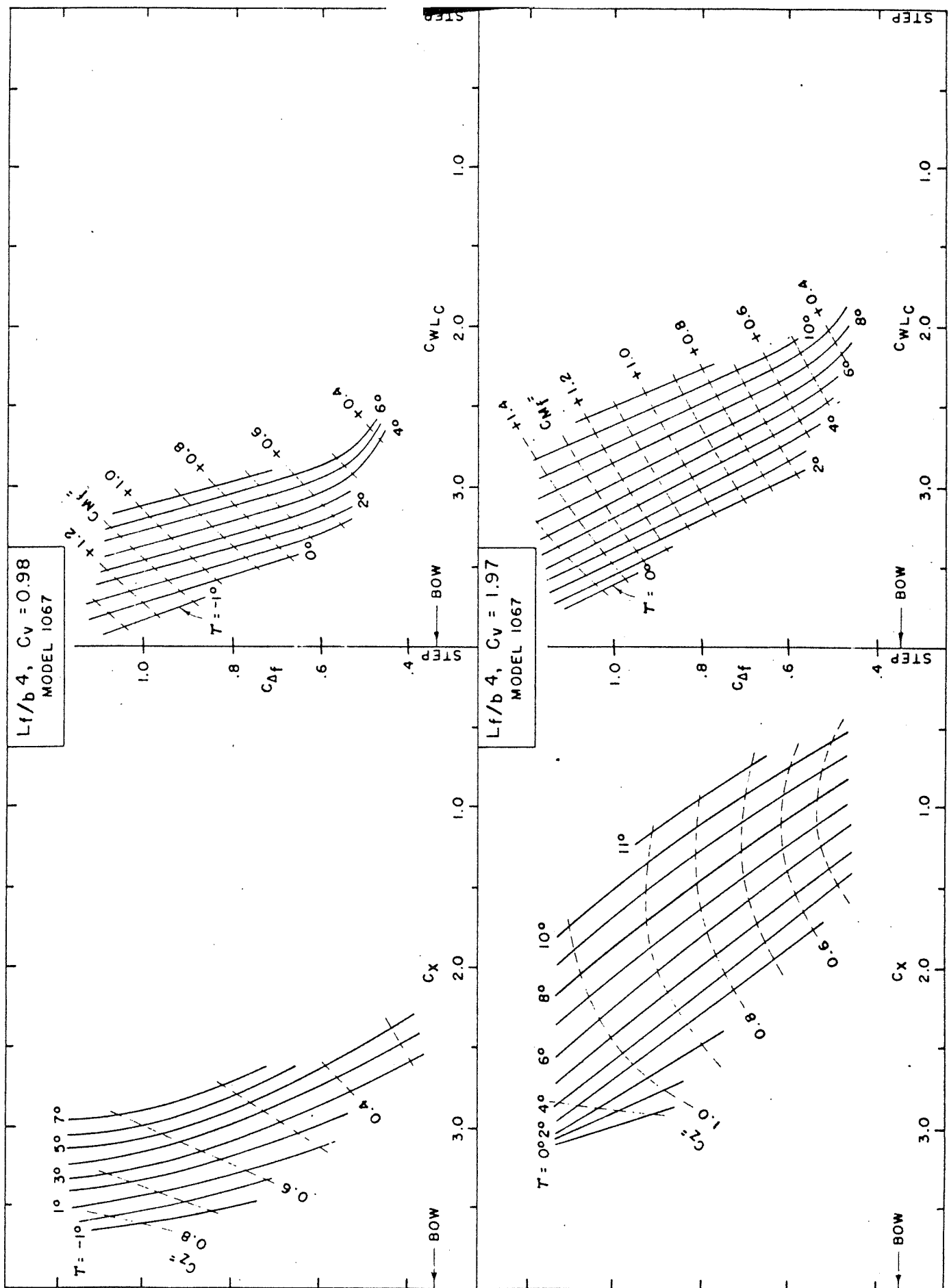


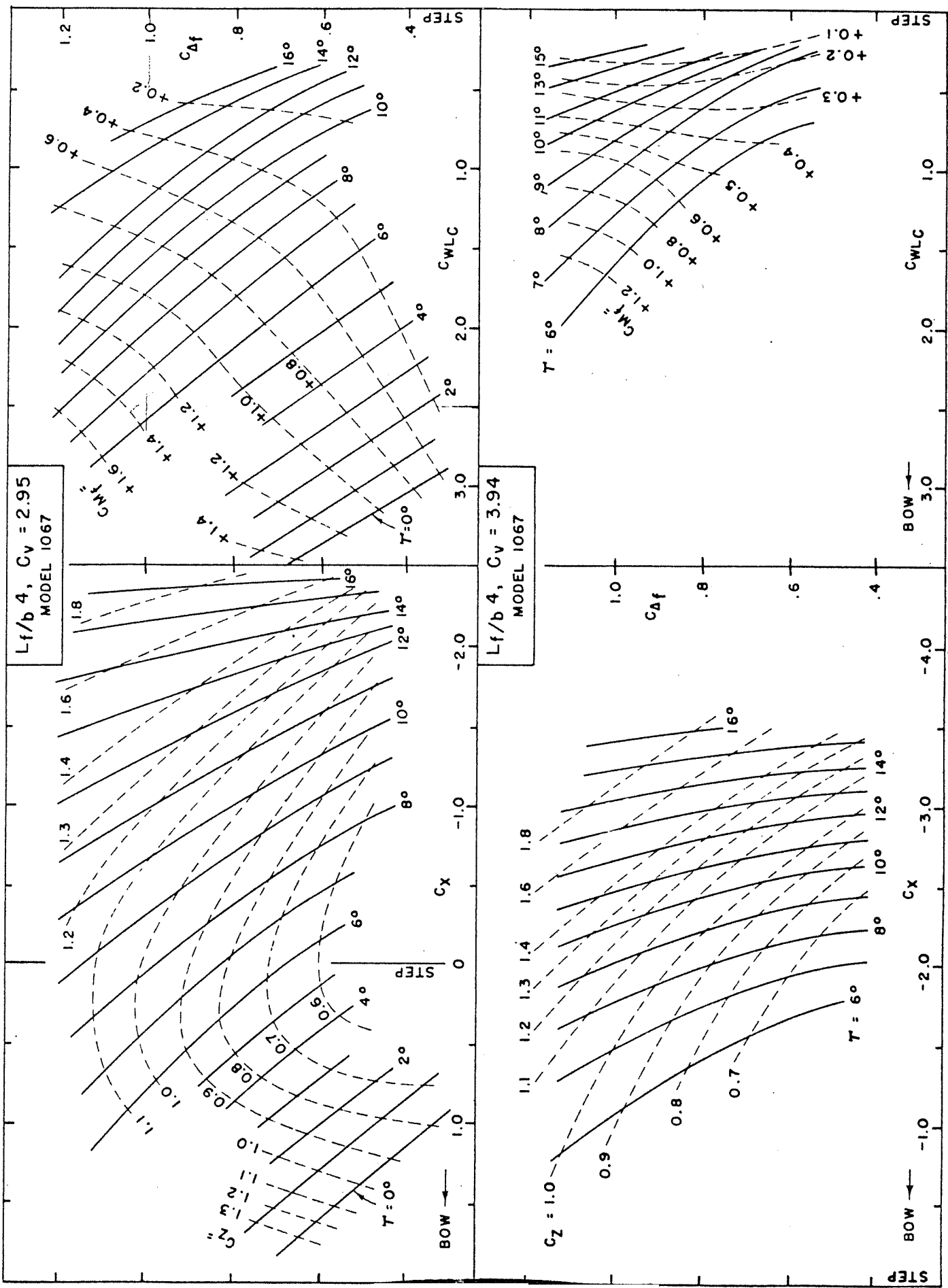
FIGURE 34B

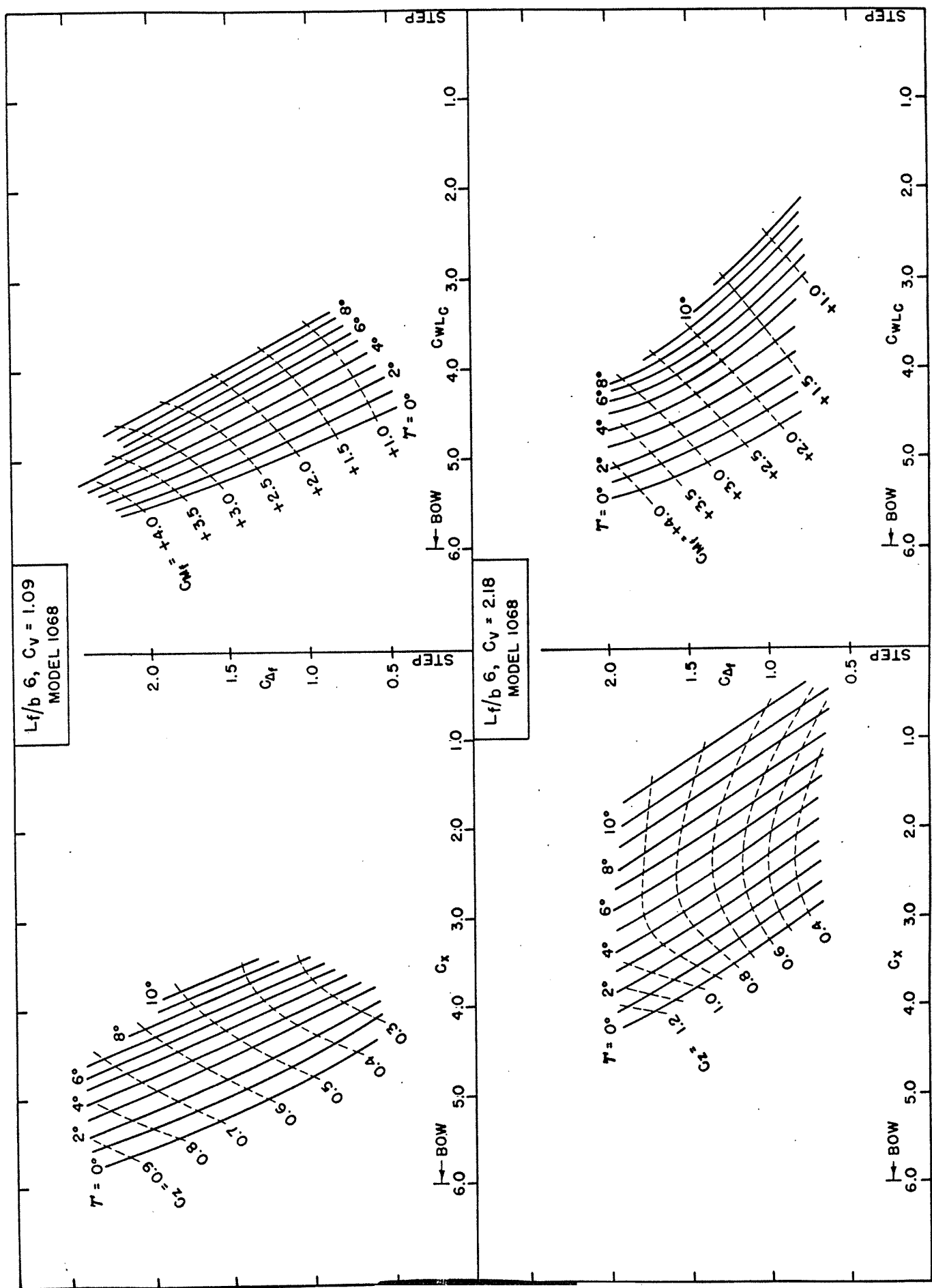


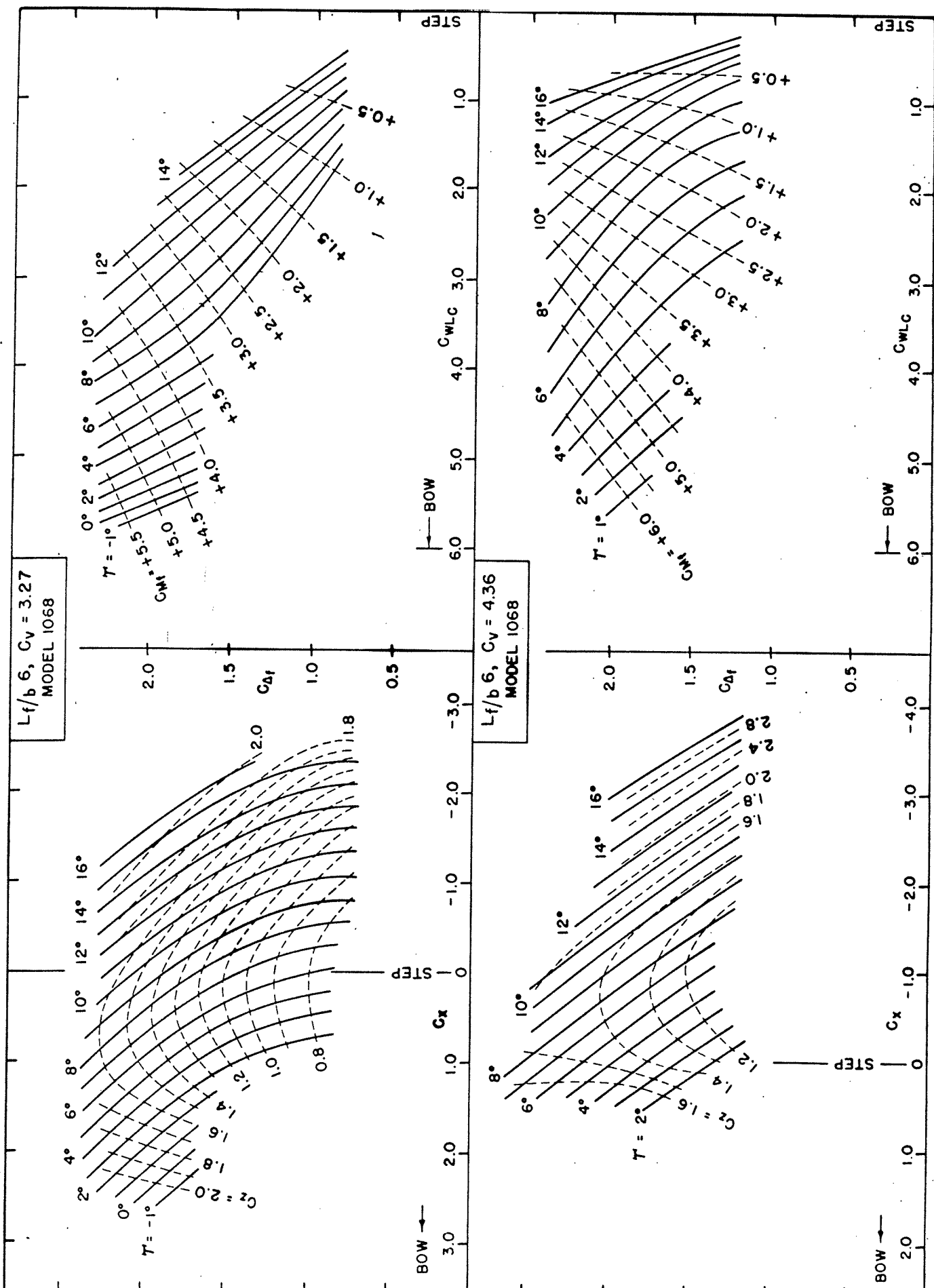


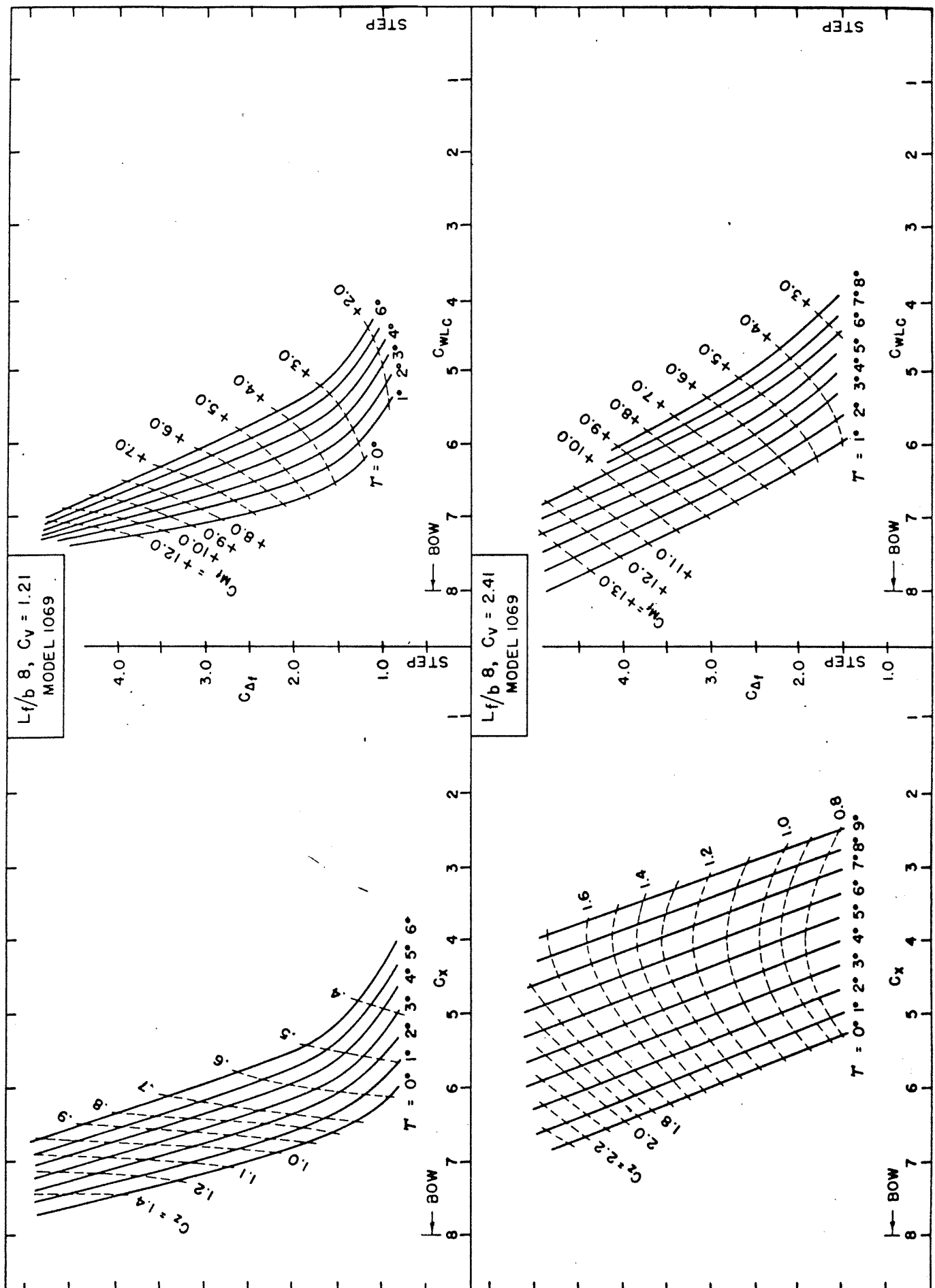


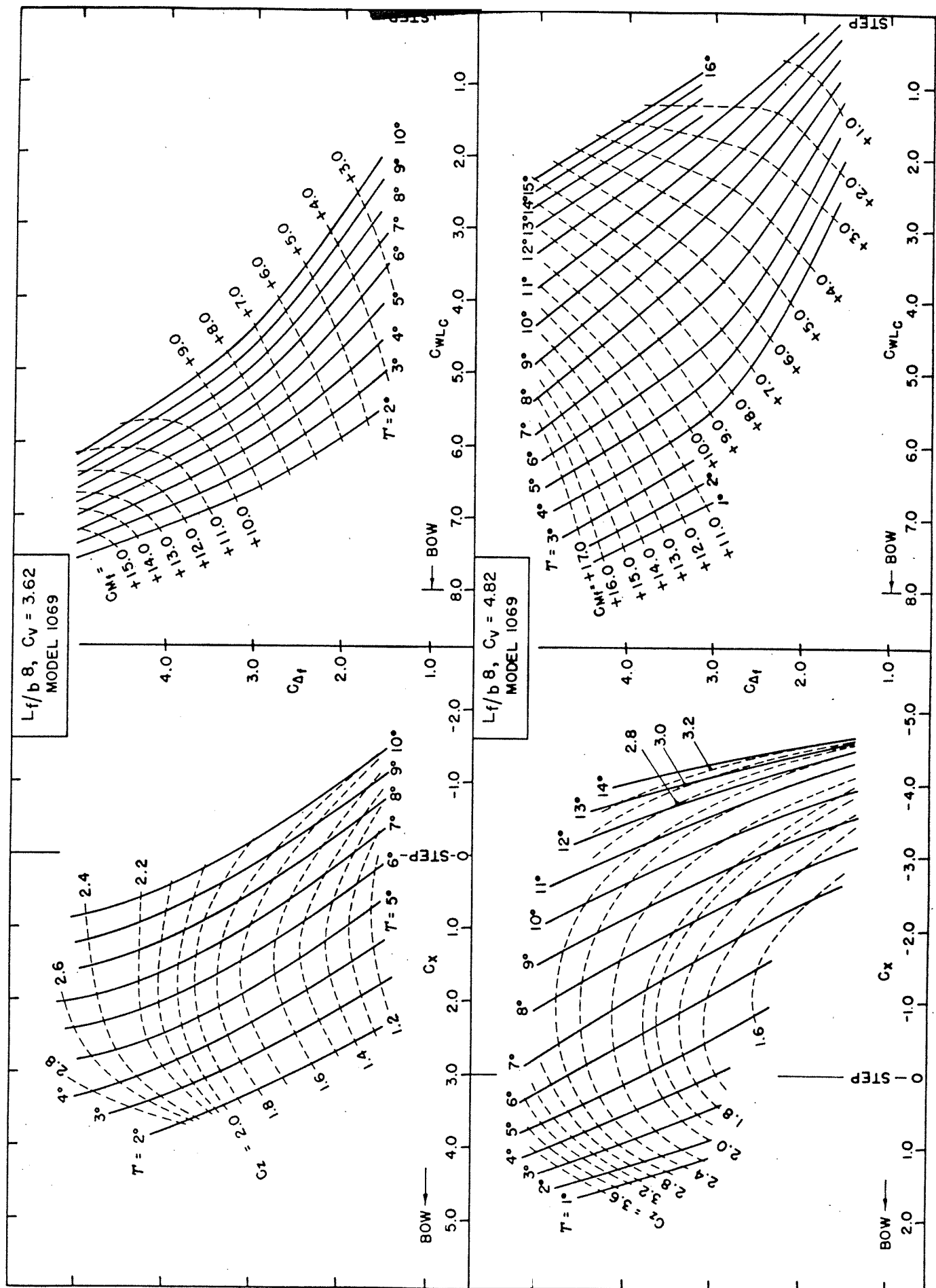












SPRAY HEIGHT COMPARISON
(DIRECT PHOTO AND CONTOUR DATA)
E.T.T. MODEL NO. 1067-01-06

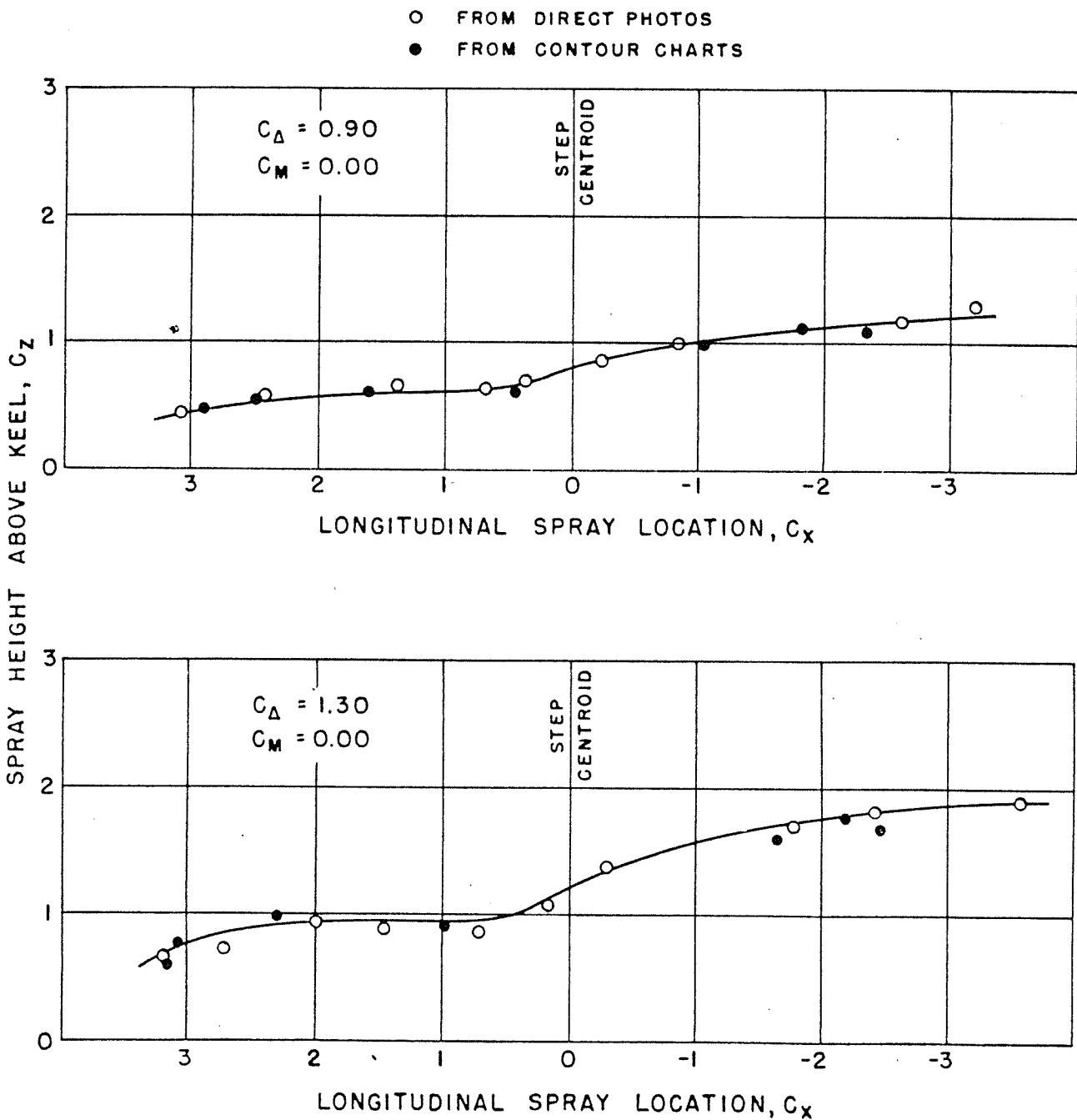


FIGURE 44

DESCRIPTION OF THE LINES OF THE PROPOSED FLYING-BOAT HULL MODELS

WITH

FOREBODY LENGTH-BEAM RATIO OF 4

Item 1(a) of Section A of ONR Contract N6onr-247, Task Order III

Introduction

The length-beam ratio of flying-boat hulls has gradually increased in recent years. No flying boat has yet been constructed with a hull having a length-beam ratio in excess of 10, but the aerodynamic and hydrodynamic characteristics of flying-boat models with length-beam ratios up to 16 have been investigated. These model investigations are of considerable interest to design and research groups working for high-performance water-based aircraft because they have shown that utilization of high length-beam ratio hulls will reduce aerodynamic drag, hull weight and landing impact loads in rough water without materially affecting the hydrodynamic qualities in smooth water.

The length-beam ratio investigations to date have all been conducted with groups of relative models, derived by expanding the station spacing of low length-beam ratio parent hulls. In order to isolate the effect of length-beam ratio, other changes in the hull proportions and in the hull shape of the parent were held to a minimum. Although the parent selected in these studies may have had optimum proportions and shape it is conceivable that the higher length-beam ratio hulls derived from this parent will not necessarily have optimum proportions and shape. In fact, there is some evidence that the forebody-to-afterbody-length ratio should decrease with increasing over-all length-beam ratio. The purpose of the present investigation -- Item 1(a), Section A, ONR Contract N6onr-247, Task Order III -- is to determine the influence of forebody-to-afterbody length ratio on the hydrodynamic characteristics of flying-boat hulls. The study will include tests of 9 models with over-all length-beam ratio varying from 7 to 24; the first group of three are the subject of this note.

Scope

The three hulls discussed below comprise the first of three groups of hulls being designed for the present investigation. Each group of three hull models will be made up of one forebody design and three afterbody designs of different length. Thus, in each group of hulls the forebody length-beam ratio will be constant and the afterbody length-beam ratio will vary. The length-beam ratios of the forebodies and afterbodies in the various groups are given in Table I. (Page 10).

In each group the hull with the intermediate afterbody length was arbitrarily chosen as the "parent" hull of the group, the other two hulls being considered as variations of the parent.

The true influence of length-beam ratio as such will not be brought out unless changes of size can be eliminated. Previous studies on series of hulls with varying length-beam ratio have indicated that by keeping the planform area of the hulls constant the effects of differences in size are most nearly eliminated. Consequently, the parent models in the present investigation are being designed to have equal length-beam products*.

This note presents the hull lines of the first group of models — the shortest ones — with a forebody length-beam ratio of 4. The various design features incorporated in these hull lines are discussed in turn.

General Remarks

Each hull, although separately designed, was considered as a variation of hull form to be substituted under one hypothetical airplane design. The hulls are not, therefore, related in the usual sense, since they cannot all be derived from a single parent.

Prior to the actual layout of the hull lines, values of hump speed, hump trim and waterborne load at hump speed were assigned for the

— — — — —
*It should be noted that the hydrodynamic characteristics of these hulls can be compared on bases other than constant planform area if the loadings vary over a sufficiently wide range.

"parent" or basic hull on the basis of previous experience. From these data, an estimation of the forebody wetted length was obtained which, in turn, enabled an estimation of the center of pressure and of the pitching moment due to resultant hydrodynamic force on the forebody to be made. This pitching moment has, then, to be balanced by a moment produced by a force on the afterbody near the second step.

To determine the moment produced by the afterbody, the wave profile in the wake of the forebody was plotted. By trial and error a location of the afterbody was chosen such that the resulting position of the center of pressure -- determined from the wetted length of the afterbody -- produced the necessary moment to balance the moment due to the hydrodynamic force acting on the forebody. In this manner, the sternpost angle was determined for a given afterbody length.

An attempt has been made to design these hulls analytically. In so doing, the results of previous model tests on flying-boat hulls and on planing surfaces have been utilized to the fullest extent possible. Unfortunately, the data available are not sufficient to completely design the hulls by analytic methods, making it necessary to resort to straightforward comparisons with previous designs in many instances. Whether the design is based on previous experience or on analytical methods, there is a certain amount of flexibility in the choice of several design parameters. While these were chosen as judiciously as possible, the merits of the proposed designs cannot be fully determined without model tests.

Main Dimensions of Models

	<u>Short Afterbody</u>	<u>Basic*</u>	<u>Long Afterbody</u>
Forebody length, inches	24.60	24.60	24.60
Afterbody length, inches	18.45	24.60	36.90
Beam-Maximum, inches	6.15	6.15	6.15
Forebody deadrise at step centroid, degrees	22.00	22.00	22.00
Afterbody deadrise at step centroid, degrees	29.70	30.24	32.62
Step height at centroid, inches	0.418	0.434	0.491
Afterbody angle, degrees	5.7	7.1	8.4
Sternpost angle, degrees	7.0	8.0	9.0
Forebody length-beam ratio	4.0	4.0	6.0
Afterbody length-beam ratio	3.0	4.0	6.0
Over-all length-beam ratio	7.0	8.0	10.0

*The basic hull of the group is the so-called "parent" hull.

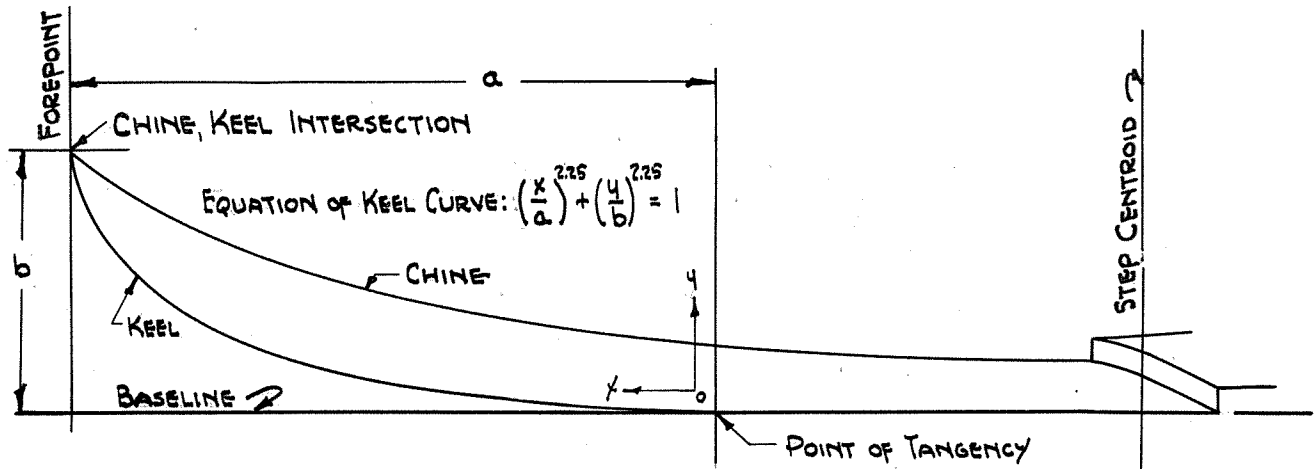
Forebody

Wherever practicable, the hull lines chosen are made up from readily computable curves -- a process which easily permits the scaling up or down of the lines. In addition, this procedure has construction advantages since it facilitates the accurate joining of component portions.

The "forebody flat" -- the region in which the deadrise increases linearly with the distance forward of the step centroid -- is 37.5 percent of the forebody length. It is sufficiently long to satisfy the need of planing area at the hump, and yet short enough to obtain easy buttock lines. A slight increase of the deadrise has been introduced in this portion of the forebody to ease the buttock lines further. Easy buttock lines are considered important since diving and spray characteristics are affected by curvature of the buttocks.

The keel curvature, starting at the forward end of the flat, is of essentially elliptical form with somewhat more fullness than a true

ellipse as shown by the sketch below.



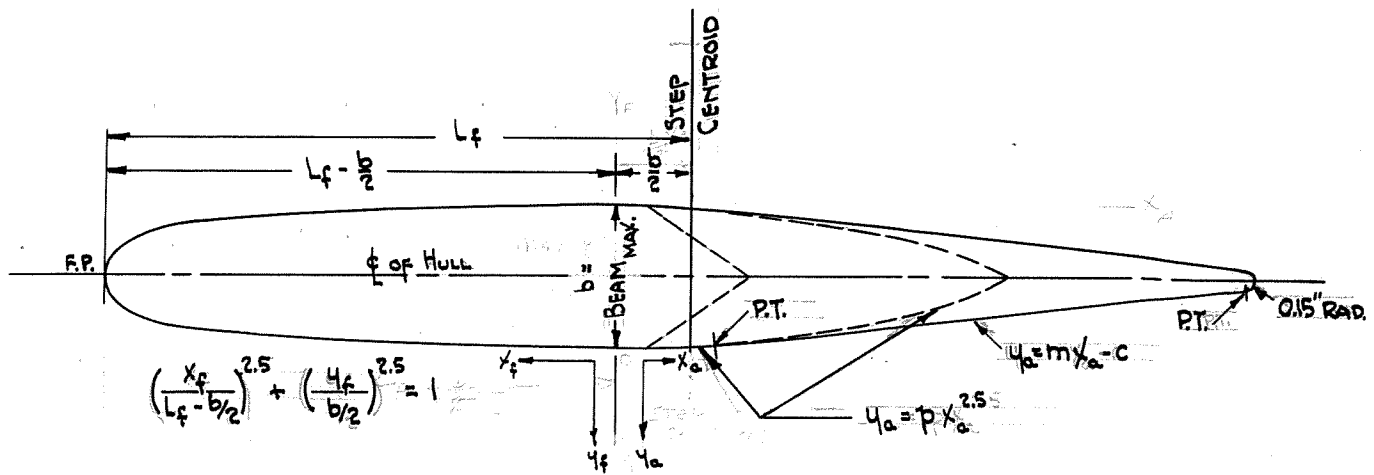
FOREBODY KEEL AND CHINE PROFILES

The variation in deadrise angle with forebody length is shown by Figure 1. As can be seen on this chart, the variation in deadrise is linear over the region of the forebody flat and parabolic over the region forward of the forebody flat. The deadrise at the step centroid is 22 degrees, while the deadrise at the bow is 70 degrees.

It is believed that the combination of keel curvature and deadrise distribution chosen for the proposed design will be less likely to produce high speed diving than is the more conventional hull design which has a longer length of straight keel and more rapid curvature near the bow.

The intersection of the keel and chine lines at the bow was placed 5.41 inches (approximately 90 percent of the beam) above the baseline. This height should insure satisfactory operation in waves up to five feet in height (full scale).

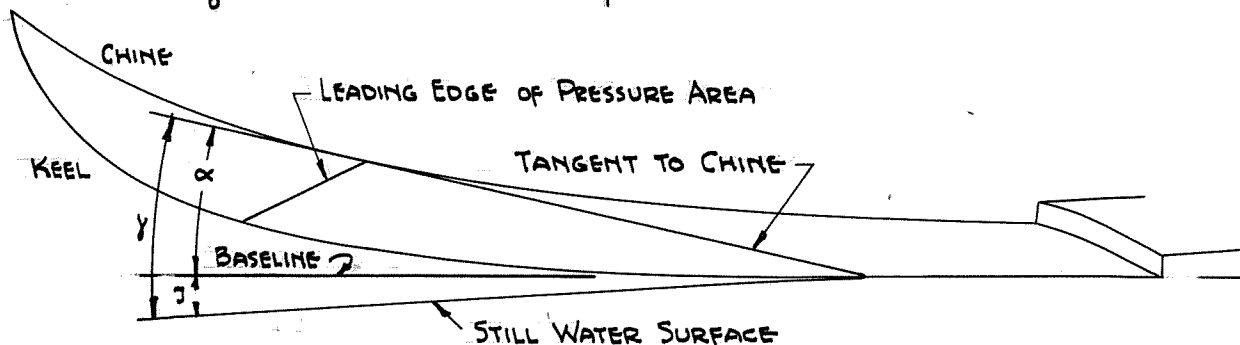
The plan of the forebody chine from bow to the maximum beam is of essentially elliptical form with somewhat more fullness than the true ellipse as shown by the sketch below.



FOREBODY AND AFTERBODY CHINE PLANFORMS

The profile of the forebody chine line was first obtained for the case of no chine flare from the keel line, the deadrise distribution and the plan of the chine line. This chine line has been designated the theoretical chine line. The chine flare shown on the proposed forebody lines was obtained by the method outlined below. First, a trim track up to hump speed was estimated for the model. From this and the unloading curve, the forebody wetted lengths could be determined. These data enabled a determination of the local angles of attack at theoretical chine to be made. (The local angle of attack at the chine is defined as the angle -- measured in a plane parallel to the plane of symmetry -- between the still water surface and tangent to the chine at the point of intersection of the leading edge of the pressure area and the chine line.)

$$\gamma = \alpha + \beta = \text{LOCAL ANGLE OF ATTACK}$$



SKETCH DEFINING LOCAL ANGLE OF ATTACK

The theoretical chine heights were then adjusted where necessary to keep the local angles of attack at the chine below 16 degrees at every point. A line was smoothed through the adjusted chine heights to make the actual profile of the forebody chine line. The chine-flare radius was then added.

Beam

A maximum beam of 6.15 inches, occurring 3.075 inches forward of the main step centroid, was selected for the proposed forebody. Placing the maximum beam forward of the step yields the maximum wetted area for a given wetted length — a condition desired at hump speeds. As the speed increases and the wetted area diminishes, the wetted length becomes excessively short for a given beam and it is, therefore, of advantage to have a smaller beam at the step. In addition, this expedient provides for finer lines aft, thus reducing afterbody interference and also reduces the skin area of the hull which would reduce the weight.

Main Step

Essentially, a step of a flying-boat hull is the juncture between two discontinuous surfaces. In the case of a "V"-planform step, the two discontinuous surfaces need not have the same deadrise angles in order to obtain a uniform depth of step. The proposed hull utilizes a 50° V-step to allow the joining of the forebody with lower deadrise angles with an afterbody of higher deadrise without obtaining an excessive depth of step at the chines. This is fortunate because the high afterbody deadrise angles, occurring at about 50 percent of the afterbody length, need not be fully reduced to those of the forebody at the main step.

The landing stability and the high-speed resistance characteristics for flying-boat hulls with moderate step depths are known to be improved by the use of V-steps. The increase in hump trim and planing resistance anticipated with a V-step has been shown to be small when the V-step is used in combination with a long afterbody.

The step depth at the centroid for the proposed design is 7 percent of the maximum beam.

Afterbody

Three afterbodies, differing mainly in length, were designed for the one forebody design described above. These afterbodies together with the forebody make three hulls -- comprising group I -- of varying overall length-beam ratio, but of constant forebody length-beam ratio.

The lengths of the afterbodies, in terms of the beam, are given in Table I. The variation in afterbody length is believed sufficient to cover the range from "short" to "long" afterbodies. Short afterbody lengths have been used on the majority of flying boats now in service, but recent model studies have shown that the rough-water landing behavior of flying boats with short afterbody lengths can be considerably improved by increasing the afterbody length.

The afterbody of a flying-boat hull is needed for static buoyancy and for trim control to speeds just beyond hump speed, while at high speeds the presence of the afterbody results in increased resistances. Furthermore, on landing the afterbody must also bear a portion of the impact loads. For trim control, only the rearward portion of the afterbody is necessary, but almost the entire bottom area of the afterbody may be subject to impact loads in rough water. Since an increase in the deadrise will reduce bottom pressures, and hence impact loads, all portions of the afterbody not utilized for trim control should have as high deadrise angle as possible.

Consequently, the deadrise angles of the three proposed afterbodies are increased behind the step to a maximum over the middle portion and are then reduced to effective planing sections in the vicinity of the second step. The variation in deadrise angle with afterbody length, for each of the three afterbodies, is shown by Figure 2.

In the vicinity of the main step, the afterbody deadrise angles are greater than those of the forebody thus providing greater clearance for spray thrown up by the step at high speeds.

Hull Lines

The lines of the forebody and of the three afterbodies of Group I, derived in the manner outlined above, are shown in Figure 3. note.

Concluding Remarks

The development of the hull lines -- discussed in the body of the report -- was governed by the following principles. Wetted area of forebody flat sufficient to support the waterborne load at hump speed, rearward portion of the afterbody supporting a small percentage of the waterborne load at hump speed, details of forebody designed for definite control of spray, and, finally, utilizing geometrical curves to the fullest extent possible.

The tank tests will show to what extent this procedure was successful, and will provide an opportunity to check the assumptions that had to be made in order to design the hulls.

W. C. Hugli, Jr.

W. C. Hugli, Jr.
5 October 1948

References

1. Korvin-Kroukovsky, B. V., Savitsky, Daniel and Lehman, William F.: "Wave Contours in the Wake of a 20° Deadrise Planing Surface", Experimental Towing Tank Report No. 337, June 1948.
2. Locke, F. W. S., Jr.: "An Empirical Study of Low Aspect Ratio Lifting Surfaces with Particular Regard to Planing Craft", Bureau of Aeronautics D. R. Report No. 1043, January 1948.
3. Hugli, W. C., Jr.: "Data Report on the Preliminary Tank Tests of a Flying-Boat Model with a Planing-Tail Hull", Experimental Towing Tank Note No. 60, September 1947.

TABLE I

FOREBODY AND AFTERBODY PROPORTIONS FOR THE VARIOUS GROUPS OF HULLS

<u>Group Number</u>	<u>Forebody Length-Beam Ratio L_f/b</u>	<u>Afterbody Length-Beam Ratio L_a/b</u>
I	4.0	3.0 4.0 6.0
II	6.0	4.0 6.0 10.0
III	8.0	6.0 10.0 16.0

TABLE II

STATIC LOAD COEFFICIENTS FOR THE VARIOUS GROUPS OF HULLS

<u>Group Number</u>	<u>Over-All Length-Beam Ratio L/b</u>	<u>Static Load Coefficient C_{A_0}</u>
I	7.0 8.0 10.0	1.0 -- 2.0
II	10.0 12.0 16.0	2.0 -- 4.0
III	14.0 18.0 24.0	4.0 -- 8.0

EXPERIMENTAL TOWING TANK
STEVENS INSTITUTE OF TECHNOLOGY
HOBOKEN, NEW JERSEY

N-90
Fig. 1

DATE _____ INITIALS _____ FILE _____

FOREBODY DEADRISE DISTRIBUTION
OF
PROPOSED FOREBODY WITH A LENGTH-BEAM RATIO OF 4
(E.T.T. MODEL NO. 1067-01)

70

60

50

50

40

30

20

10

0

DEADRISE ANGLE, DEG.

100
90
80
70
60
50
40
30
20
10
0
STEP
CENTROID

FOREBODY LENGTH, PERCENT

EXPERIMENTAL TOWING TANK
STEVENS INSTITUTE OF TECHNOLOGY
HOBOKEN, NEW JERSEY

N-90
Fig. 2

AFTERTBODY DEADRISE DISTRIBUTION
OF
PROPOSED AFTERTBODIES TO BE USED WITH
A FOREBODY OF LENGTH / BEAM RATIO OF 4

DATE _____ INITIALS _____ FILE _____

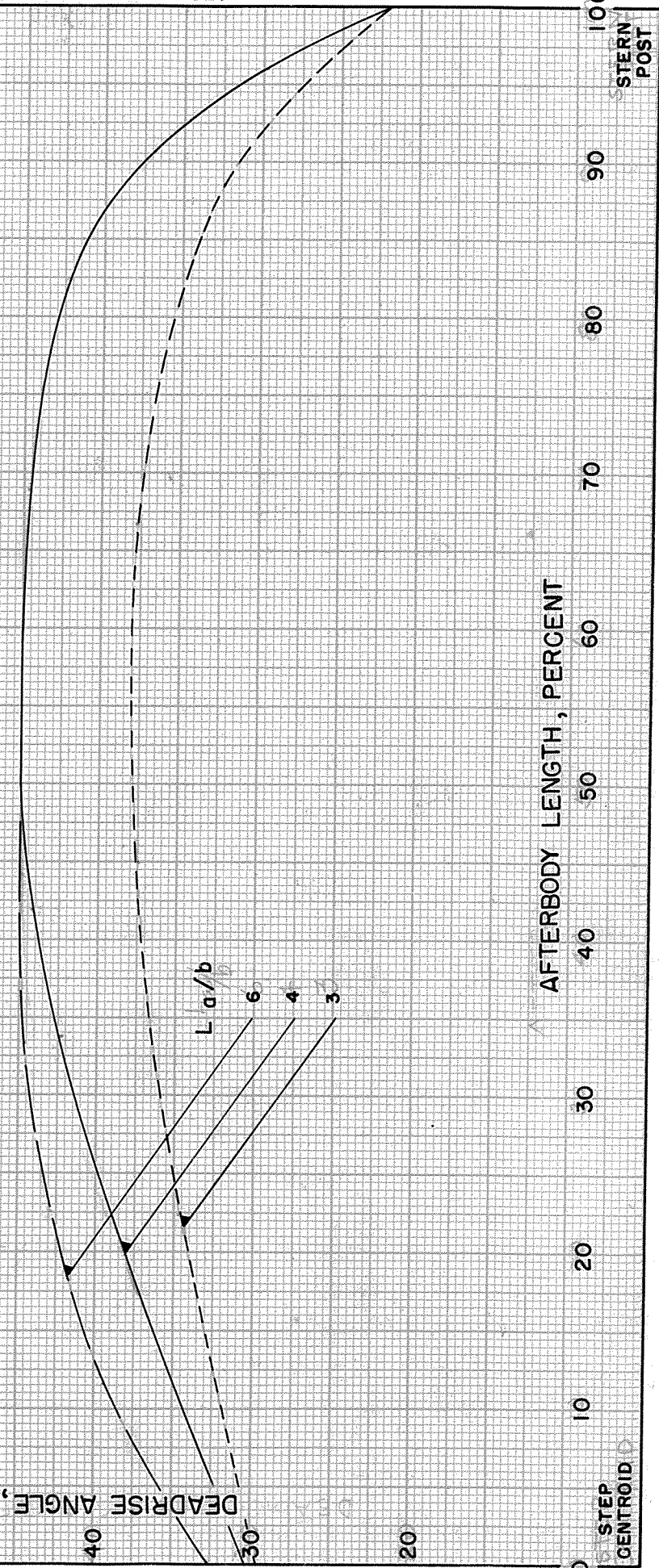
E.T.T. MODEL NO. L_a/b

1067-01 4

1067-02 3

1067-03 6

50
40
30
20
DEADRISE ANGLE, DEG.



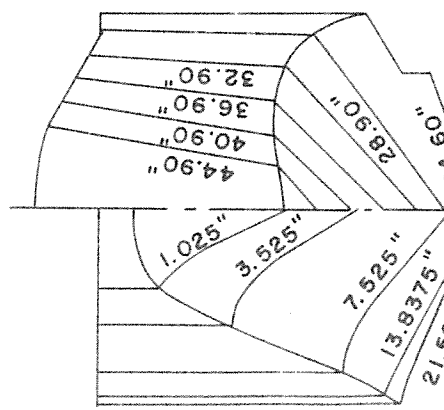
EXPERIMENTAL TOWING TANK
STEVENS INSTITUTE OF TECHNOLOGY
HOBOKEN, NEW JERSEY

N-90
FIG. 3

HULL MODELS

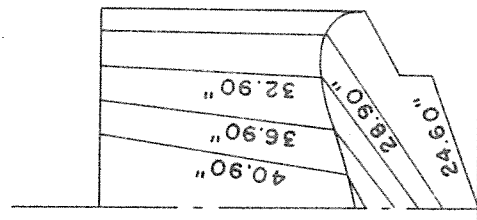
GROUP I MAX. BEAM = 6.15" ; $L_f/b = 4$

MODELS NO.	DES.	L_a/b
1067-01	6.15-4-4	4
1067-02	6.15-4-3	3
1067-03	6.15-4-6	6

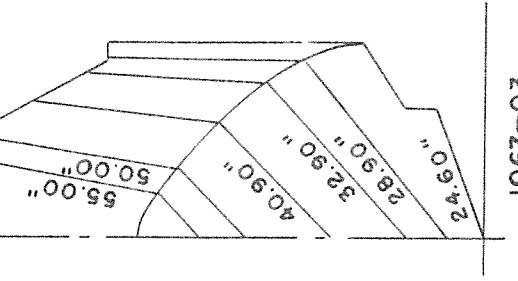


1067-01

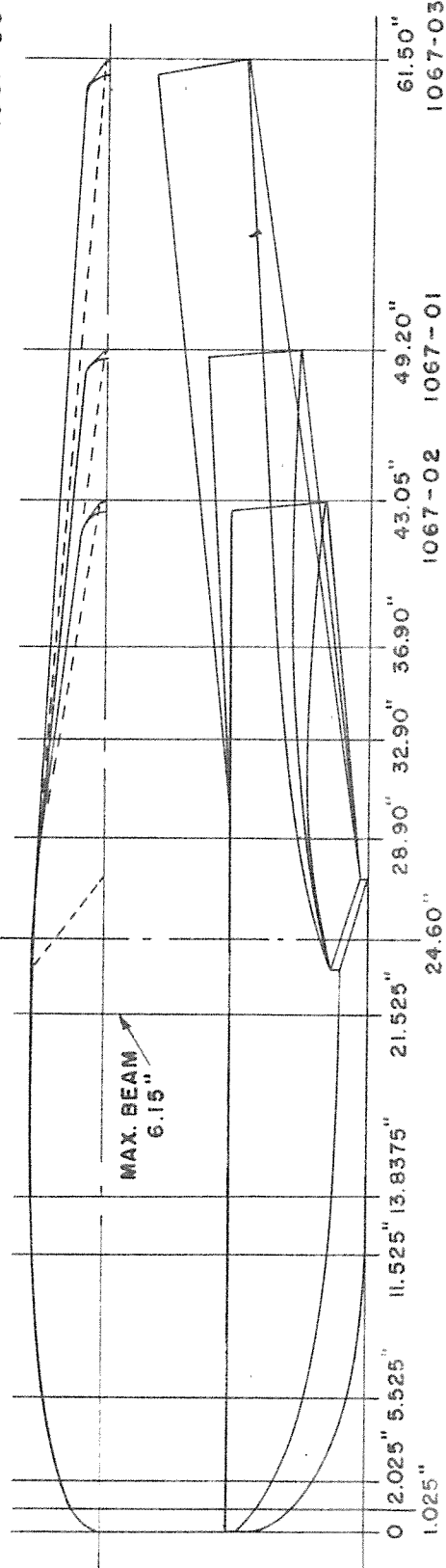
MAX. BEAM
6.15"



1067-02



1067-03



1067-03

0 2.025" 5.525" 11.525" 13.8375" 21.525" 24.60" 1.025" 1.025" 6.15" 49.20" 43.05" 36.90" 32.90" 28.90" 24.60" 1067-02 1067-01 1067-03